AD-A139 358 FUNDAMENTAL PROPERTIES OF SOILS FOR COMPLEX DYNAMIC LOADINGS; DYNAMIC CON..(U) APPLIED RESEARCH ASSOCIATES INC ALBUQUERQUE NM D H MERKLE ET AL. 01 DEC 83 1/2

UNCLASSIFIED AFOSR-TR-84-0166 F49620-80-C-0088 F/G 8/13 NL

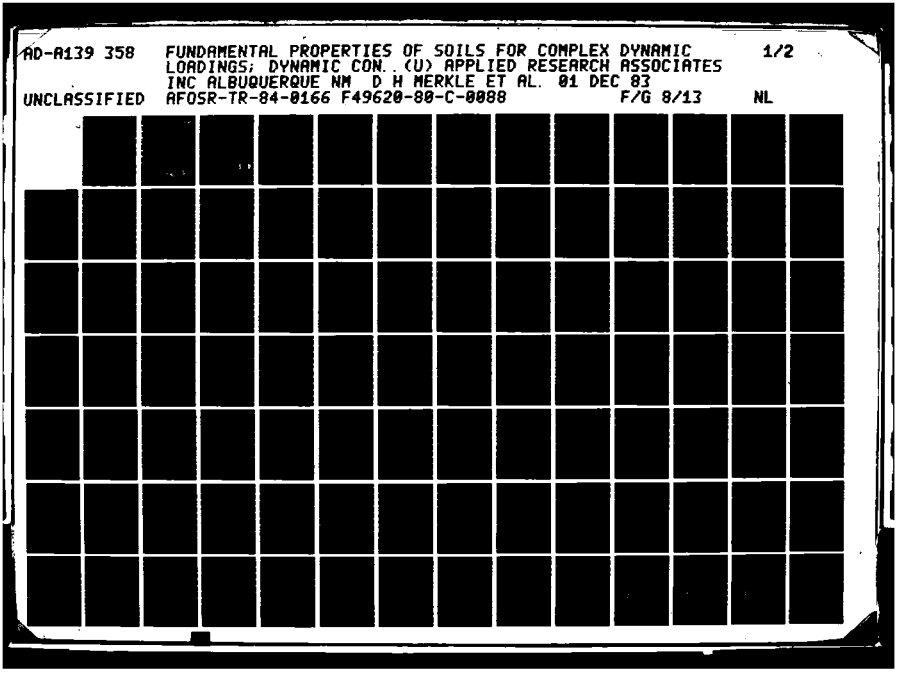

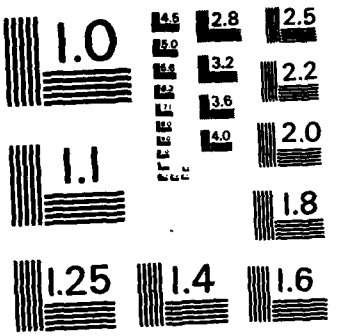

12

L

FUNDAMENTAL PROPERTIES OF SOILS FOR COMPLEX DYNAMIC LOADINGS:

ANNUAL TECHNICAL REPORT NO. 3

"Dynamic Constitutive Model Fundamentals"

APPLIED RESEARCH ASSOCIATES, INC.
Engineering and Applied Science

FUNDAMENTAL PROPERTIES OF SOILS FOR COMPLEX DYNAMIC LOADINGS:

ANNUAL TECHNICAL REPORT NO. 3

"Dynamic Constitutive Model Fundamentals"

by

Douglas H. Merkle
William C. Dass

December 1983

Applied Research Associates, Inc.
2101 San Pedro, N.E., Suite A
Albuquerque, NM 87110

Prepared for

Air Force Office of Scientific Research
Bolling Air Force Base
Washington, DC 20332

Contract No. F49620-80-C-0088

UNCLASSIFIED

SECURITY CLASSIFICATION OF THIS PAGE *(When Data Entered)*

REPORT DOCUMENTATION PAGE		READ INSTRUCTIONS BEFORE COMPLETING FORM
1. REPORT NUMBER AFOSR-TR- 84-0166	2. GOVT ACCESSION NO. AD A139 355	3. RECIPIENT'S CATALOG NUMBER
4. TITLE *(and Subtitle)* FUNDAMENTAL PROPERTIES OF SOILS FOR COMPLEX DYNAMIC LOADINGS; Dynamic Constitutive Model Fundamentals		5. TYPE OF REPORT & PERIOD COVERED ANNUAL 1 Aug 82 - 31 Jul 83 6. PERFORMING ORG. REPORT NUMBER
7. AUTHOR(s) DOUGLAS H MERKLE WILLIAM C DASS		8. CONTRACT OR GRANT NUMBER(s) F49620-80-C-0088
9. PERFORMING ORGANIZATION NAME AND ADDRESS APPLIED RESEARCH ASSOCIATES, INC. 2101 SAN PEDRO, N.E., SUITE A ALBUQUERQUE, NM 87110		10. PROGRAM ELEMENT, PROJECT, TASK AREA & WORK UNIT NUMBERS 61102F 2307/C1
11. CONTROLLING OFFICE NAME AND ADDRESS AIR FORCE OFFICE OF SCIENTIFIC RESEARCH/NA BOLLING AFB, DC 20332		12. REPORT DATE 1 December 1983 13. NUMBER OF PAGES 125
14. MONITORING AGENCY NAME & ADDRESS*(if different from Controlling Office)*		15. SECURITY CLASS. *(of this report)* UNCLASSIFIED 15a. DECLASSIFICATION DOWNGRADING SCHEDULE

16. DISTRIBUTION STATEMENT *(of this Report)*

Approved for public release; distribution unlimited.

17. DISTRIBUTION STATEMENT *(of the abstract entered in Block 20, if different from Report)*

18. SUPPLEMENTARY NOTES

19. KEY WORDS *(Continue on reverse side if necessary and identify by block number)*

EFFECTIVE STRESS
SOIL DYNAMICS
STRESS-STRAIN BEHAVIOR
SHEAR STRENGTH
MATERIAL MODELING

20. ABSTRACT *(Continue on reverse side if necessary and identify by block number)*

This report discussed the physical basis for the equations describing the dynamic response of a saturated soil. Next, the principal stress-strain features which a soil constitutive model may have to reproduce are reviewed. Finally, the basic equations of elastoplasticity are derived, existing failure criteria are reviewed, and a new failure criterion is presented.

DD FORM 1 JAN 73 1473

UNCLASSIFIED

SECURITY CLASSIFICATION OF THIS PAGE *When Data Entered)*

Conditions of Reproduction

FUNDAMENTAL PROPERTIES OF SOILS FOR COMPLEX DYNAMIC LOADINGS:

ANNUAL TECHNICAL REPORT NO. 3

"Dynamic Constitutive Model Fundamentals"

TABLE OF CONTENTS

TABLES

FIGURES

FIGURES, Continued

FIGURES, Continued

1.0 INTRODUCTION

This is the Third Annual Technical Report under Air Force Office of Scientific Research Contract F49620-80-C-0088, "Fundamental Properties of Soils for Complex Dynamic Loadings". The report covers the contractual period 1 August 1982 through 31 July 1983, but the work discussed was mostly accomplished after submission of the Second Annual Technical Report in April, 1983 [Dass, Merkle, and Bratton (1983)].

The FY 1983 modification to the basic contract statement of work contains three tasks:

E.1.e. Response of a Clay and Silt to Laboratory Boundary Conditions

E.1.f. Soil Element Model (SEM) Analysis of Laboratory Test Data

E.1.g. Theoretical Development/Modification of Constitutive Model

The first two tasks depend on laboratory test data not yet available, and will be reported separately. The third task reads as follows:

> Results of the previous work will establish a framework within which the material models can be evaluated, and illustrate the limitations of existing models. The theoretical development of improved constitutive models can develop along one of two paths. The first involves the development of a new model. The second involves modification to existing models to include effects not currently present. The selection of the preferred technical approach will be made and preliminary work begun on the new modeling procedure. The work begun last year on pore pressure, rate effects, and shear behavior will be continued and new aspects of soil modeling which come to light will be reviewed. Where inconsistencies arise the emphasis will be placed on matching insitu behavior as opposed to laboratory behavior. The initial theoretical development work will be checked in an ongoing fashion utilizing the Soil Element Model and CIST calculations.

This report contains three major sections. The first section deals with the general equations for dynamic response of a saturated soil, which establish the mathematical and computational framework into which any soil

constitutive model must fit. The second section deals with those aspects of soil stress-strain behavior which a soil constitutive model may have to reproduce. The third and final section presents the equations of elastoplasticity needed for model development, and then discusses the initial phase of that development, viz the shear failure criterion. The proposed shear failure criterion has several convenient features:

1. It is related to stress through the first total stress invariant and the second and third deviator stress invariants, each of which has a simple physical interpretation.
2. Its parameters can be determined from simple linear plots.
3. The model can match unequal friction angles in triaxial compression and extension.
4. The ratio of octahedral shear to octahedral normal stress can be calculated directly (without iteration) when the value of Lode's parameter is known.

Other features of the model are yet to be determined.

2.0 DYNAMIC RESPONSE OF SATURATED SOIL

2.1 Effective Stress

In a saturated soil having discrete grains with negligible intergranular contact areas each grain is completely surrounded by pore fluid. Therefore the pore pressure acts throughout a soil element, in both the pore fluid and the solid grains. Superimposed on the hydrostatic intragranular stress acting within each solid grain due to the pore pressure is the additional intragranular stress due to intergranular forces. A plane section through soil will generally cut through both solid grains and fluid-filled pore space. The intragranular stress acting on the solid portion of the section must balance the pore pressure acting on the cut grain surfaces on one side of the section, plus the intergranular forces acting on the same cut grain surfaces. The pore pressure acting on one side of the fluid portion of the section simply balances the pore pressure acting on the fluid portion on the other side of the section. This situation is shown in Figure 2.1. Summing forces in the vertical direction yields

$$\Sigma F_v \overset{+}{\uparrow} = (\Sigma C_{iv} + pA_t) - (pA_t + \bar{\bar{\sigma}}A_s) = 0 \qquad (2.1)$$

so that the intragranular normal stress component, $\bar{\bar{\sigma}}$, equals the sum of normal components of intergranular forces divided by the area of solids.

$$\bar{\bar{\sigma}} = \frac{\Sigma C_{iv}}{A_s} \qquad (2.2)$$

It turns out to be more convenient to normalize the sum of normal components of intergranular forces with respect to A_t, rather than with

respect to A_s, so we define the effective normal stress, $\bar{\sigma}$, by the equation

$$\bar{\sigma} = \frac{\Sigma C_{iv}}{A_t} \tag{2.3}$$

Comparison of Equations (2.2) and (2.3) shows that

$$\bar{\bar{\sigma}} = \frac{A_t}{A_s}\bar{\sigma} = \frac{\bar{\sigma}}{1 - n} \tag{2.4}$$

Returning to Equation (2.1), if we define the total normal stress, σ, by the equation

$$\sigma A_t = pA_t + \bar{\bar{\sigma}}A_s = (p + \bar{\sigma})A_t \tag{2.5}$$

then

$$\sigma = p + \bar{\sigma} \tag{2.6}$$

so that

$$\bar{\sigma} = \sigma - p \tag{2.7}$$

Summing forces in the horizontal direction in Figure 2.1 yields

$$\overset{+}{\rightarrow} \quad \Sigma F_h = \Sigma C_{ih} - \bar{\bar{\tau}}A_s = 0 \tag{2.8}$$

so that the intragranular shear stress, $\bar{\bar{\tau}}$, is

$$\bar{\bar{\tau}} = \frac{\Sigma C_{ih}}{A_s} \tag{2.9}$$

The effective shear stress is obtained by normalizing the sum of tangential components of intergranular forces with respect to A_t, rather than with respect to A_s, so that

$$\bar{\tau} = \frac{\Sigma C_{ih}}{A_t} \tag{2.10}$$

and therefore

$$\bar{\bar{\tau}} = \frac{\bar{\tau}}{1 - n} \tag{2.11}$$

2.2 Grain Compression Due to Pore Pressure

If the bulk modulus of solid grains is K_s, then because the pore pressure, p, acts throughout each grain it is apparent that each grain undergoes a compressive volumetric strain due to pore pressure of amount

$$-\left(\frac{\Delta V_s}{V_s}\right)_p = \frac{p}{K_s} \tag{2.12}$$

2.3 Solid Skeleton Compression Due to Pore Pressure

If each grain of the soil skeleton undergoes a compressive volumetric strain due to pore pressure of amount p/K_s, then the entire soil skeleton will undergo the same compressive volumetric strain, since the skeleton is composed of grains in contact. (This argument assumes no grain slippage.) Thus

$$-\left(\frac{\Delta V_t}{V_t}\right)_p = \frac{p}{K_s} \tag{2.13}$$

Note that the skeletal compressive volumetric strain defined by Equation 2.13 is unrelated to effective stress. It is similar in nature to displacements of a framed structure due to temperature change.

2.4 Grain Compression Due to Effective Stress

There are two components of intragranular stress: p and $\bar{\bar{\sigma}}_{ij}$. Each causes grain compression. The component of grain compressive volumetric strain due to intergranular forces (effective stress) is

$$-\left(\frac{\Delta V_s}{V_s}\right)_{\sigma} = \frac{\bar{\bar{\sigma}}_{ii}}{3K_s} = \frac{\bar{\sigma}_{ii}}{3(1 - n)K_s} \tag{2.14}$$

The intragranular shear stresses, $\bar{\bar{\sigma}}_{ij}$ $(i \neq j)$, cause grain distortion, and therefore skeletal distortion. However, this is assumed to have no effect on skeletal volume, and is therefore viewed as part of the overall skeletal shear response. The above discussion does not include dilatancy, which is caused by relative displacement between grains due to intergranular slipping, a separate mechanism.

2.5 Darcy's Law and Fluid Drag

If the volumetric flow rate of pore fluid through a soil cross section of total area A_t is Q, the discharge velocity, $\dot{w}$, is defined by the relation

$$\dot{w} = \frac{Q}{A_t} \tag{2.15}$$

Of course, the actual fluid particle velocity, $\dot{v}$, is larger than $\dot{w}$, since the actual fluid particle velocity is the ratio of volumetric flow rate to flow cross-sectional area.

$$\dot{v} = \frac{Q}{nA_t} = \frac{\dot{w}}{n} \tag{2.16}$$

Under steady flow conditions it has been found that the discharge velocity is related to the pore pressure gradient by Darcy's equation

$$\dot{w}_i = -k_{ij}p_{,j} \tag{2.17}$$

where k_{ij} is the permeability matrix. Under steady flow conditions inversion of Equations (2.17) yields

$$p_{,i} = -k_{ij}^{-1} \dot{w}_j \tag{2.18}$$

Now consider a pore fluid caused to flow under a given pore pressure gradient through a soil element of unit volume, shown schematically in Figure 2.2. The net force exerted on the bounding surface of the soil skeleton is

$$f_{si} = -(1 - n)p_{,i} \tag{2.19}$$

and is independent of the nature of the flowing fluid, and of whether the flow is steady or variable, since the pore pressure gradient is assumed fixed. The remaining portion of the pressure gradient under steady flow is the drag force exerted on the body of the soil skeleton, which is

$$f_{di} = -p_{,i} - f_{si} = -p_{,i} + (1-n)p_{,i} = -np_{,i} = nk_{ij}^{-1} \dot{w}_j \tag{2.20}$$

Under unsteady flow conditions the fluid drag force exerted on the body of the soil skeleton is assumed to still be given by the same expression

$$f_{di} = nk_{ij}^{-1} \dot{w}_j \tag{2.21}$$

2.6 General Equations

Up to this point normal stresses have been considered positive in compression. However, for reasons of notational and computational convenience, it turns out to be easier to consider normal stresses positive in tension, as well as longitudinal extensions positive in extension. Since pore pressure is compressive by nature, however, pore pressure will continue to be considered positive in compression. Thus the relation between total stress, pore pressure and effective stress is

$$\bar{\sigma}_{ij} = \sigma_{ij} + p\delta_{ij} \tag{2.22}$$

The equation of motion for the soil skeleton must consider effective stress (considered to act over the total area of a soil element), pore pressure (acting over the bounding area of solids), fluid drag force (computed per unit total volume of a soil element), gravity (acting on the solid mass) and skeletal acceleration. Referring to the soil element shown in Figure 2.3, the skeleton equation of motion is

$$\bar{\sigma}_{ij,j} - (1 - n)p_{,i} + nk_{ij}^{-1}\dot{w}_j + (1 - n)\rho_s g_i = (1 - n)\rho_s \ddot{u}_i \tag{2.23}$$

where g_i is the i^{th} component of gravity.

The equation of motion for the fluid phase must consider the pore pressure (acting over the bounding flow area), the skeletal drag force (computed per unit total volume of a soil element), gravity (acting on the fluid mass), and the fluid acceleration. Here it is important to recognize that the discharge velocity, $\dot{w}$, is measured relative to that of the soil skeleton. Again referring to the soil element shown in Figure 2.3, the fluid equation of motion is

$$-np_{,i} - nk_{ij}^{-1}\dot{w}_j + n\rho_f g_i = n\rho_f(\ddot{u}_i + \frac{\ddot{w}_i}{n}) \tag{2.24}$$

or

$$-p_{,i} - k_{ij}^{-1}\dot{w}_j + \rho_f g_i = \rho_f \ddot{u}_i + \frac{1}{n}\rho_f \ddot{w}_i \tag{2.25}$$

Addition of Equations (2.23) and (2.24), setting

$$(1 - n)\rho_s + n\rho_f = \rho \tag{2.26}$$

yields

$$\sigma_{ij,j} + \rho g_i = \rho \ddot{u}_i + \rho_f \ddot{w}_i \tag{2.27}$$

The soil skeleton stress-strain equations, in incremental form, are

$$d\bar{\sigma}_{ij} = D_{ijkl} d\varepsilon^{\sigma}_{kl} \tag{2.28}$$

where $d\varepsilon^{\sigma}_{ij}$ is the matrix of incremental skeletal strains associated with effective stress, and D_{ijkl} is the skeletal elastoplastic incremental stiffness tensor.

From Equation (2.13), the matrix of incremental skeletal strains due to pore pressure is

$$\overline{d\varepsilon}_{ij} = -\frac{dp}{3K_s} \delta_{ij} \tag{2.29}$$

Assuming there are no causes of skeletal strain other than effective stress and pore pressure, it follows that the matrix of incremental skeletal strains, $d\varepsilon_{ij}$, is given by the expression

$$d\varepsilon_{ij} = d\varepsilon^{\sigma}_{ij} + \overline{d\varepsilon}_{ij} \tag{2.30}$$

so that

$$d\varepsilon^{\sigma}_{ij} = d\varepsilon_{ij} - \overline{d\varepsilon}_{ij} \tag{2.31}$$

Substitution of Equations (2.31) and (2.29) into Equation (2.28) yields

$$d\bar{\sigma}_{ij} = D_{ijkl}(d\varepsilon_{kl} + \frac{dp}{3K_s} \delta_{kl}) \tag{2.32}$$

The pore fluid stress-strain equation is simple in concept because the pore fluid is assumed to have a constant bulk modulus, K_f, and zero shear modulus. Not quite so simple, however, is evaluation of the rate of fluid volumetric strain at a point. Note that the equations in this

section concern the displacement of a point in the soil skeleton whose initial coordinates are specified, and the pore fluid velocity at the same displaced skeletal point. The analysis is Lagrangian with respect to the soil skeleton, but neither Lagrangian nor Eulerian with respect to the pore fluid. This is because Darcy's Law applies to skeletal and pore fluid elements occupying the same point in space and time. Thus we track neither a particular fluid particle nor the fluid velocity at a fixed point; rather we track the fluid velocity at a moving skeletal point whose initial position is specified. Pore fluid velocity is thus a skeletal quantity, like skeletal displacement, because it is a vector tied to a point in the skeleton whose initial position is specified. Returning to the problem of obtaining the pore fluid stress-strain equation, we use the equation of pore fluid mass conservation to express the pore fluid volumetric strain in terms of quantities already defined. The pore fluid mass conservation equation is

$$(\rho_f \dot{w}_i)_{,i} = -\frac{\partial}{\partial t}(n\rho_f) \tag{2.33}$$

Expansion of Equation (2.33) yields

$$\rho_{f,i}\dot{w}_i + \rho_f \dot{w}_{i,i} = -\dot{n}\rho_f - n\dot{\rho}_f$$

or

$$\dot{w}_{i,i} = -\dot{n} - \frac{1}{\rho_f}(n\dot{\rho}_f + \rho_{f,i}\dot{w}_i)$$

$$= -\dot{n} - \frac{n}{\rho_f}(\dot{\rho}_f + \rho_{f,i}\frac{\dot{w}_i}{n})$$

$$= -\dot{n} - \frac{n}{\rho_f}\frac{D\rho_f}{D_t} \tag{2.34}$$

The rate of increase of porosity, $\dot{n}$, is the sum of three terms:

(+) the rate of skeletal volumetric strain, $\dot{\varepsilon}_{ii}$

(+) the rate of solid grain volume decrease due to pore pressure, per unit total volume (see Equation (2.12), $(1 - n)\dot{p}/K_s$

(-) the rate of solid grain volume increase due to effective stress, per unit total volume (see Equation (2.14),

$$-(1 - n)\left[\frac{\dot{\bar{\sigma}}_{ii}}{3(1 - n)K_s}\right] = -\frac{\dot{\bar{\sigma}}_{ii}}{3K_s}$$

and the total rate of change of pore fluid density is

$$\frac{1}{\rho_f}\frac{D\rho_f}{D_t} = \frac{\dot{p}}{K_f} \tag{2.35}$$

Thus Equation (2.34) can be written in the form

$$\dot{dw}_{i,i} = -d\varepsilon_{ii} - (1 - n)\frac{dp}{K_s} + \frac{d\bar{\sigma}_{ii}}{3K_s} - n\frac{dp}{K_f} \tag{2.36}$$

Equations (2.32) and (2.36) can be written in the form

$$d\bar{\sigma}_{ij} - \frac{D_{ijkk}}{3K_s}dp = D_{ijkl}d\varepsilon_{kl} \tag{2.37}$$

and

$$\frac{d\bar{\sigma}_{ii}}{3K_s} - \left(\frac{n}{K_f} + \frac{1 - n}{K_s}\right)dp = d\varepsilon_{ii} + \dot{dw}_{i,i} \tag{2.38}$$

Finally, the skeletal strain-displacement equations are

$$\epsilon_{ij} = \frac{1}{2}(u_{i,j} + u_{j,i}) \tag{2.39}$$

where u_i is the ith component of skeletal displacement.

Summarizing the above results, we have [cf Zienkiewicz and Bettess (1982)]:

Effective Stress Definition

$$\bar{\sigma}_{ij} = \sigma_{ij} + p\delta_{ij} \tag{2.22}$$

Soil Skeleton Equation of Motion

$$\bar{\sigma}_{ij,j} - (1 - n)p_{,i} + nk_{ij}^{-1}\dot{w}_j + (1 - n)\rho_s g_i = (1 - n)\rho_s \ddot{u}_i \tag{2.23}$$

Pore Fluid Equation of Motion

$$-p_{,i} - k_{ij}^{-1}\dot{w}_j + \rho_f g_i = \rho_f \ddot{u}_i + \frac{1}{n}\rho_f \ddot{w}_i \tag{2.25}$$

Total Density

$$(1 - n)\rho_s + n\rho_f = \rho \tag{2.26}$$

Soil Element Equation of Motion

$$\sigma_{ij,j} + \rho g_i = \rho \ddot{u}_i + \rho_f \ddot{w}_i \tag{2.27}$$

Soil Skeleton Incremental Stress-Strain Equation

$$d\bar{\sigma}_{ij} - \frac{D_{ijkk}}{3K_s} dp = D_{ijkl} d\epsilon_{kl} \tag{2.37}$$

Pore Fluid Mass Conservation Equation

$$\frac{d\bar{\sigma}_{ii}}{3K_s} - \left(\frac{n}{K_f} + \frac{1 - n}{K_s}\right)dp = d\epsilon_{ii} + d\dot{w}_{i,i} \tag{2.38}$$

Skeleton Strain-Displacement Equation

$$\varepsilon_{ij} = \frac{1}{2}(u_{i,j} + u_{j,i}) \tag{2.39}$$

Emphasis in this research effort during the last three years has been on improving current models for the skeletal elastoplastic incremental stiffness tensor, D_{ijkl}. However, it is important to keep in mind how the D tensor fits into the complete set of equations for the dynamic response of saturated soils, which are needed to solve complex dynamic problems involving wave propagation, liquefaction, and spall.

2.7 Undrained Behavior

As a particular example of the application of the above general equations to the response of a saturated soil having compressible solid grains, consider the case of undrained loading. Assume the skeletal stress-strain response to be incrementally linear, with skeletal contrained modulus M_k, coefficient of lateral stress at rest K_{ok}, and bulk modulus K_k. For undrained loading we assume no flow ($w_i = \dot{w}_i = \ddot{w}_i = 0$), and also neglect inertial effects ($\ddot{u}_i = 0$). The governing equations then reduce to:

$$\bar{\sigma}_{ij} = \sigma_{ij} + p\delta_{ij} \tag{2.22}$$

$$d\bar{\sigma}_{ij} = D_{ijkl}(d\varepsilon_{kl} + \frac{dp}{3K_s}\delta_{kl}) \tag{2.40}$$

$$d\varepsilon_{ii} = \frac{d\bar{\sigma}_{ii}}{3K_s} - (\frac{n}{K_f} + \frac{1-n}{K_s})dp \tag{2.41}$$

The skeletal incremental stiffness matrix, D_{ijkl}, is:

		kl								
		11	22	33	12	23	31	21	32	13
ij	11	M_k	$K_{ok}M_k$	$K_{ok}M_k$	0	0	0	0	0	0
	22	$K_{ok}M_k$	M_k	$K_{ok}M_k$	0	0	0	0	0	0
	33	$K_{ok}M_k$	$K_{ok}M_k$	M_k	0	0	0	0	0	0
	12	0	0	0	$2G_k$	0	0	0	0	0
	23	0	0	0	0	$2G_k$	0	0	0	0
	31	0	0	0	0	0	$2G_k$	0	0	0
	21	0	0	0	0	0	0	$2G_k$	0	0
	32	0	0	0	0	0	0	0	$2G_k$	0
	13	0	0	0	0	0	0	0	0	$2G_k$

where

$$2G_k = M_k(1 - K_{ok}) \tag{2.42}$$

and

$$\frac{1 + 2K_{ok}}{3} = \frac{K_k}{M_k} = r_k \tag{2.43}$$

Equation (2.40) yields

$$\frac{d\bar{\sigma}_{ii}}{3} = \frac{D_{iikl}}{3}(d\varepsilon_{kl} + \frac{dp}{3K_s}\delta_{kl})$$

$$= \frac{D_{iikl}d\varepsilon_{kl}}{3} + \frac{D_{iikk}}{9K_s}dp$$

$$= K_k d\varepsilon_{ii} + \frac{K_k}{K_s} dp \tag{2.44}$$

Substitution of Equation (2.44) into Equation (2.41) yields

$$d\varepsilon_{ii} = \frac{1}{K_s} (K_k d\varepsilon_{ii} + \frac{K_k}{K_s} dp) - (\frac{n}{K_f} + \frac{1 - n}{K_s}) dp$$

or

$$(1 - \frac{K_k}{K_s}) d\varepsilon_{ii} = -[\frac{1}{K_s} (1 - \frac{K_k}{K_s}) + n(\frac{1}{K_f} - \frac{1}{K_s})] dp$$

or

$$d\varepsilon_{ii} = - \left[\frac{1}{K_s} + n \left(\frac{\frac{1}{K_f} - \frac{1}{K_s}}{1 - \frac{K_k}{K_s}} \right) \right] dp = - \frac{dp}{F} \tag{2.45}$$

where

$$F = \frac{1}{\frac{1}{K_s} + n \left(\frac{\frac{1}{K_f} - \frac{1}{K_s}}{1 - \frac{K_k}{K_s}} \right)} \tag{2.46}$$

so that

$$dp = -F d\varepsilon_{ii} = -F \delta_{kl} d\varepsilon_{kl} \tag{2.47}$$

Substitution of Equation (2.22) into Equation (2.40) yields

$$d\sigma_{ij} + \delta_{ij} dp = D_{ijkl} d\varepsilon_{kl} + \frac{D_{ijkk}}{3K_s} dp$$

$$= D_{ijkl} d\varepsilon_{kl} + \frac{K_k}{K_s} \delta_{ij} dp$$

or

$$d\sigma_{ij} = D_{ijkl}d\varepsilon_{kl} - (1 - \frac{K_k}{K_s})\delta_{ij}dp \tag{2.48}$$

Substitution of Equation (2.47) into Equation (2.48) yields

$$d\sigma_{ij} = D_{ijkl}d\varepsilon_{kl} + (1 - \frac{K_k}{K_s})F\delta_{ij}\delta_{kl}d\varepsilon_{kl}$$

$$= [D_{ijkl} + (1 - \frac{K_k}{K_s})F\delta_{ij}\delta_{kl}]d\varepsilon_{kl}$$

$$= D^u_{ijkl}d\varepsilon_{kl} \tag{2.49}$$

where the undrained elastoplastic incremental stiffness tensor, D^u_{ijkl}, is defined as

$$D^u_{ijkl} = D_{ijkl} + (1 - \frac{K_k}{K_s})F\delta_{ij}\delta_{kl} \tag{2.50}$$

For the hydrostatic component of undrained loading, Equation (2.49) yields

$$\frac{d\sigma_{ii}}{3} = \frac{D_{iikl}}{3}\, d\varepsilon_{kl} + (1 - \frac{K_k}{K_s})Fd\varepsilon_{ii}$$

$$= [K_k + (1 - \frac{K_k}{K_s})F]d\varepsilon_{ii}$$

$$= \left[K_k + \frac{1 - \frac{K_k}{K_s}}{\frac{1}{K_s} + n\left(\frac{\frac{1}{K_f} - \frac{1}{K_s}}{1 - \frac{K_k}{K_s}}\right)}\right] d\varepsilon_{ii}$$

$$= \left[\frac{1 + nK_k \left(\frac{\frac{1}{K_f} - \frac{1}{K_s}}{1 - \frac{K_k}{K_s}} \right)}{\frac{1}{K_s} + n \left(\frac{\frac{1}{K_f} - \frac{1}{K_s}}{1 - \frac{K_k}{K_s}} \right)} \right] d\varepsilon_{ii} \tag{2.51}$$

which is the result obtained by [Gassmann (1951: par. 59, p. 15)].

For constrained (uniaxial) compression, Equation (2.49) yields

$$d\sigma_1 = M_k d\varepsilon_1 + (1 - \frac{K_k}{K_s}) F d\varepsilon_1$$

$$= [M_k + (1 - \frac{K_k}{K_s}) F] \, d\varepsilon_1$$

$$= \left[M_k + \frac{1 - \frac{K_k}{K_s}}{\frac{1}{K_s} + n \left(\frac{\frac{1}{K_f} - \frac{1}{K_s}}{1 - \frac{K_k}{K_s}} \right)} \right] d\varepsilon_1$$

$$= \left[\frac{1 + \left(\frac{M_k - K_k}{K_s} \right) + nM_k \left(\frac{\frac{1}{K_f} - \frac{1}{K_s}}{1 - \frac{K_k}{K_s}} \right)}{\frac{1}{K_s} + n \left(\frac{\frac{1}{K_f} - \frac{1}{K_s}}{1 - \frac{K_k}{K_s}} \right)} \right] d\varepsilon_1 \tag{2.52}$$

The relation between effective stress and total strain can be obtained by substituting Equation (2.47) into Equation (2.40), or directly from Equation (2.48):

$$d\bar{\sigma}_{ij} = \bar{D}_{ijkl} d\varepsilon_{kl} \tag{2.53}$$

where

$$\bar{D}_{ijkl} = D_{ijkl} - \frac{K_k}{K_s} F \delta_{ij} \delta_{kl} \tag{2.54}$$

Equations (2.53) and (2.54) can be used to construct effective stress paths with strain contour overlays.

Equations (2.51) and (2.52) define the undrained bulk and constrained moduli, respectively.

$$K_u = \frac{1 + nK_k \left(\frac{\frac{1}{K_f} - \frac{1}{K_s}}{1 - \frac{K_k}{K_s}} \right)}{\frac{1}{K_s} + n \left(\frac{\frac{1}{K_f} - \frac{1}{K_s}}{1 - \frac{K_k}{K_s}} \right)} \tag{2.55}$$

$$M_u = \frac{1 + \left(\frac{M_k - K_k}{K_s} \right) + nM_k \left(\frac{\frac{1}{K_f} - \frac{1}{K_s}}{1 - \frac{K_k}{K_s}} \right)}{\frac{1}{K_s} + n \left(\frac{\frac{1}{K_f} - \frac{1}{K_s}}{1 - \frac{K_k}{K_s}} \right)} \tag{2.56}$$

and from Equations (2.55) and (2.56), or directly from Equation (2.50) we can obtain the value of K_{ou}. Equations (2.55) and (2.56) yield

$$\frac{K_u}{M_u} = \frac{1 + 2K_{ou}}{3} \tag{2.57}$$

so that

$$K_{ou} = \frac{1}{2}\left(3\,\frac{K_u}{M_u} - 1\right) \tag{2.58}$$

Equation (2.50) yields

$$M_u = M_k + \left(1 - \frac{K_k}{K_s}\right) F \tag{2.59}$$

$$M_u K_{ou} = M_k K_{ok} + \left(1 - \frac{K_k}{K_s}\right) F \tag{2.60}$$

so that

$$K_{ou} = \frac{M_k K_{ok} + \left(1 - \frac{K_k}{K_s}\right) F}{M_k + \left(1 - \frac{K_k}{K_s}\right) F} \tag{2.61}$$

Combining Equations (2.47), (2.51) and (2.55) yields

$$-\frac{\Delta p}{\Delta\sigma_{ii}/3} = \frac{-\frac{\Delta p}{\Delta\varepsilon_{jj}}}{\frac{\Delta\sigma_{ii}/3}{\Delta\varepsilon_{jj}}} = \frac{F}{K_u} = B \tag{2.57}$$

The important thing to notice about Equation (2.57) is that it holds even when the principal total stress increments are unequal. Thus, for example, if

$$\Delta\sigma_2 = \Delta\sigma_3 \neq \Delta\sigma_1 \tag{2.58}$$

Equation (2.57) yields

$$\Delta p = -\frac{B}{3}(\Delta\sigma_1 + 2\Delta\sigma_3) = -B\left[\Delta\sigma_3 + \frac{1}{3}(\Delta\sigma_1 - \Delta\sigma_3)\right] \tag{2.59}$$

3.0 SOIL DYNAMIC CONSTITUTIVE MODEL REQUIREMENTS

3.1 The Nature of Soil

Soil is a particulate material. Soil particles vary in size, shape, hardness and surface texture, and although they can be bonded together by mineral deposits, this is the exception rather than the rule. There are four primary consequences of the particulate nature of soil [Lambe and Whitman (1969: Chapter 2)]:

a) Deformation of soil is partly the result of individual particle deformation, but primarily the result of interparticle sliding and rolling.

b) Soil is inherently multiphase. The soil particles constitute the solid phase, and the remaining space is pore space. The pore space is filled by pore fluid, consisting of a gaseous phase (usually air) and a liquid phase (usually water). In dry soil the liquid phase is absent, and in saturated soil the gaseous phase is absent. The pore fluid chemically influences the nature of soil particle surfaces, including contact surfaces, and hence affects the process of interparticle force transmission and resistance.

c) The pore fluid can flow through the pore space. Whether flowing or still, the pore fluid physically interacts with the soil particles, thus further influencing the process of interparticle force transmission and resistance.

d) Sudden load changes are carried jointly by the soil skeleton and the pore fluid. The resulting change in pore pressure usually

causes pore fluid flow, which alters the proportion of load carried by the soil skeleton and the pore fluid, as well as changing the configuration of the soil skeleton.

Because soil deforms primarily by interparticle slip, soil strength is basically frictional in nature; and because pore fluid pressure reduces interparticle contact normal forces, the strength of a soil element is controlled by the difference between the total normal stress acting on the element and the value of the element pore pressure, i.e., by the effective stress. Because of the nature of soil formation and deposition processes, natural soil deposits are often inhomogeneous and inherently anisotropic, and soil profiles are frequently erratically discontinuous.

3.2 Soil Stress-Strain Characteristics

Soil stress-strain characteristics are a consequence of the particulate nature of soil and the processes by which soils are formed, deposited and subsequently altered in place. The following list of soil stress-strain characteristics is prioritized for construction of soil constitutive models to predict the behavior of soil masses under complex dynamic loads, such as explosions, earthquakes, and moving vehicles:

a) Soil deformation and strength are governed by effective stress.

b) Both volumetric and deviatoric stress-strain curves are nonlinear, even at small strains, and the type of nonlinearity is stress path dependent. Figure 3.1 shows the continuous transition from concavity to convexity with respect to the vertical strain axis of a plot of vertical effective stress versus vertical strain, measured in a drained triaxial test. The parameter controlling the shape of the stress-strain curve is the

direction of the effective stress path. At mean pressures above 500 psi some volumetric stress-strain curves exhibit a convex yield region due to grain crushing at highly stressed interparticle contact points, but at even higher mean pressure the volumetric stress-strain curve again becomes concave to the strain axis. Figure 3.2 illustrates the above behavior. A similar phenomenon is observed for one-dimensional compression curves at much lower stresses, due to interparticle slip followed by subsequent skeletal stiffening.

c) Under drained conditions, shear strain and volumetric strain are coupled. This coupling is called dilatancy. Under undrained conditions the tendency of the soil skeleton to change volume is opposed by the relative incompressibility of the pore fluid, which develops an excess pore pressure sufficient to maintain the soil skeleton at constant, or near constant volume. It is vital that soil dilatancy be correctly modeled in order to obtain the correct pore pressure and effective stress under all loading conditions.

d) At large shear strain a given soil approaches a residual or ultimate shear stress and void ratio which depend on the confining pressure, but are independent of the initial void ratio prior to shearing. The residual or ultimate shear stress and void ratio define the critical state at the given confining pressure [Casagrande (1936: 262)].

e) In approaching the critical state an initially dense or over-consolidated soil will attain a peak shear stress greater than

the critical state value. The peak stress generally corresponds closely to the maximum expansion rate. At larger shear strains in a strain controlled test the shear stress decreases (strain softening) and the soil continues to expand at a decreasing rate until the critical state is attained. Both dense and loose soils show a tendency toward densification at small shear strains, due to particle rearrangement. Loose sands initially compact, then expand as they approach the critical state; normally consolidated clays compact throughout their approach to the critical state. Loose sands exhibit steadily increasing shear resistance as they approach the critical state; even normally consolidated clays can exhibit a peak shear resistance with subsequent strain softening as they approach the critical state. These basic soil stress-strain phenomena are illustrated in Figures 3.3, 3.4, 3.5 and 3.6.

f) The intermediate principal effective stress can have a significant influence on both the peak and the ultimate friction angles. Figures 3.7 through 3.26 [Merkle (1971)] show soil strength data plotted in the octahedral plane. In those plots $\overline{\phi}$ is the Mohr-Coulomb friction angle, and μ is Lode's parameter. If $\overline{\sigma}_2$ had no influence on $\overline{\phi}$, the data points would all lie on a straight line of constant $\overline{\phi}$. More will be said about these plots in Section 4.

g) Because soil particles are generally not bonded together, soil tensile strength is primarily the result of particle interlocking, and is very small. Soil tensile failure causes stress redistribution in a loaded soil mass.

h) Plastic (irrecoverable) volumetric and deviatoric strains are both generated from the onset of loading.

i) Separate yield and plastic potential functions appear to be necessary for compression and shear, for a classical plasticity model. Plastic flow is frequently nonassociative, especially in shear.

j) Soils exhibit the Baushinger effect, i.e., loading beyond the virgin yield point in one direction increases the elastic range and yield point for unloading and reloading in that direction, but decreases the elastic range and yield point for subsequent loading in the opposite direction [Timoshenko (1956 II:412); Nadai (1950:20)].

k) Soil stress-strain behavior can be strain rate dependent, both because the effective stress-strain behavior of the soil skeleton is strain rate dependent, and because of the time dependence of pore fluid flow and the associated pore pressure adjustment.

l) Cyclic loading in shear and/or compression produces a number of effects: initial densification; hysteresis; decreasing increments of permanent shear and volumetric strain with each cycle, leading eventually to stable hysteresis; stiffening; and decrease in damping.

m) Natural soil deposits exhibit both inherent (depositional) and stress- (or strain-) induced anisotropy.

n) Sample disturbance often makes the stress-strain behavior of a soil sample different in the laboratory from what it would have been in-situ.

The Soil Element Model has been and will continue to be used in this research program to test the ability of soil constitutive models to reproduce the above stress-strain characteristics. These characteristics significantly influence the response of a soil mass to complex dynamic loads associated with explosions, earthquakes and moving vehicles.

4.0 ELASTOPLASTIC MODEL DEVELOPMENT

4.1 Basic Equations

If a cylindrical soil specimen is consolidated under an isotropic stress ($\bar{\sigma}_{1c} = \bar{\sigma}_{2c} = \bar{\sigma}_{3c}$), then subjected to drained compressive loading, unloading, and reloading under constant confining stress ($\bar{\sigma}_2 = \bar{\sigma}_3 = \bar{\sigma}_{3c}$; $\bar{\sigma}_1 \geq \bar{\sigma}_{3c}$), the stress-strain curve appears as shown in Figure 4.1. Several important features are shown in Figure 4.1:

1. The stress-strain curve is nonlinear, even for small stresses and strains.
2. Upon unloading from point A, some of the total strain is recoverable (BE), but the remainder is irrecoverable (OB).
3. Reloading occurs along a path (BC) somewhat different from the unloading path (AB), until reaching the previous maximum stress. At this point additional loading approaches and proceeds along what appears to be a continuation of the virgin compression curve (OA), with little apparent influence of previous unloading or reloading.
4. Unloading and reloading occur along paths whose secant from zero to maximum stress has a slope very close to that of the initial tangent to the stress-strain curve. This means that the irrecoverable portion of any strain increment is essentially the difference between the total strain increment and the strain increment associated with a straight line stress-strain curve having a slope equal to that of the initial tangent to the actual stress-strain curve.

By convention, recoverable strains are called elastic, and irrecoverable strains are called plastic. If the unloading and reloading curves in Figure 4.1 both retraced the virgin loading curve (OA) instead of following curves (AB) and (BC) the stress-strain behavior would be called nonlinearly elastic. As it is, the linear portion of the stress-strain behavior shown in Figure 4.1 is elastic, and the nonlinear portion is plastic. Since some of the stress-strain behavior is elastic and the rest is plastic, the overall stress-strain behavior is called elastoplastic.

Multiaxial elastoplasticity theory extrapolates the above one-dimensional stress-strain observations, and assumes that plastic strains are superimposed on elastic strains calculated according to the theory of elasticity. Thus

$$\varepsilon_{ij} = \varepsilon^e_{ij} + \varepsilon^p_{ij} \tag{4.1}$$

where

$$\sigma_{ij} = D^e_{ijkl}\varepsilon^e_{kl} \tag{4.2}$$

When the elastic behavior is isotropic, Equation (4.2) reduces to the form

$$\sigma_{ij} = MK_o\varepsilon^e_{kk}\delta_{ij} + M(1 - K_o)\varepsilon^e_{ij} \tag{4.3}$$

where M = constrained elastic modulus

K_o = coefficient of elastic lateral stress at rest.

The parameters M and K_o are assumed to be constant, independent of strain.

From Equation (4.2) it follows that

$$d\sigma_{ij} = D^e_{ijkl}d\varepsilon^e_{kl} \tag{4.4}$$

so that a unique relation exists between the elastic strain increments at a point and the corresponding stress increments. However, what is known in a strain controlled formulation is not the elastic strain increments, $d\varepsilon_{ij}^{e}$, but the total strain increments, $d\varepsilon_{ij}$, which differ from the elastic strain increments according to the incremental form of Equation (4.1),

$$d\varepsilon_{ij} = d\varepsilon_{ij}^{e} + d\varepsilon_{ij}^{p} \tag{4.5}$$

Once the possibility of plastic strains is recognized, four questions arise:

1. Can plastic strains occur?
2. If they occur, what will be their relative algebraic values?
3. If they occur, what will be their actual algebraic values?
4. Will they occur?

Obviously, Question 2 is a subset of Question 3. The reasons for listing the two questions separately are the mathematical and physical conditions used to answer them, which are explained below.

The mathematical theory of elastoplasticity presented here contains four parts, each needed to answer one of the above four questions:

1. A yield criterion, assumed to be of the form

$$f(\sigma_{ij}, \varepsilon_{ij}^{p}) = 0 \tag{4.6}$$

satisfaction of which is a necessary condition for the occurrence of additional plastic strain at a point.

2. A plastic potential function, $g(\sigma_{ij})$, for which

$$d\varepsilon_{ij}^{p} = d\lambda \frac{\partial g}{\partial \sigma_{ij}} \tag{4.7}$$

which gives the relative algebraic values of the plastic strain increments, i.e. the direction of the plastic strain increment vector in stress space. Equation (4.7) is called a flow rule, and the scalar constant $d\lambda$ is determined by the next condition.

3. The requirement that Equation (4.6) be satisfied not only at the beginning of yielding, but throughout yielding as well, so that

$$df = \frac{\partial f}{\partial \sigma_{ij}} d\sigma_{ij} + \frac{\partial f}{\partial \varepsilon^p_{ij}} d\varepsilon^p_{ij} = 0 \tag{4.8}$$

Equation (4.8) is called the consistency condition, and yields the value of $d\lambda$ in Equation (4.7). It therefore permits calculation of the actual algebraic values of the plastic strain increments.

4. The requirement that the calculated plastic strain increments lead to a positive plastic work increment,

$$dW^p = \sigma_{ij} d\varepsilon^p_{ij} > 0 \tag{4.9}$$

If Equation (4.9) is not satisfied, then additional plastic strain does not occur at a point, in which case all strain increments are elastic.

Equations (4.6), (4.7), (4.8), and (4.9) have been written assuming one yield criterion (or yield surface), and one plastic potential function. There can, however, be more than one yield surface, and an equal number of corresponding plastic potential functions. If this happens, then the above four equations apply to each active yield surface, Thus, if m yield surfaces are active, there will be a set of plastic strain increments for each active yield surface, the values of

which are determined by 4m equations (counting Equation (4.7) as one tensor equation.)

The stress tensor σ_{ij} contains nine elements,

$$\sigma_{ij} = \begin{bmatrix} \sigma_{11} & \sigma_{12} & \sigma_{13} \\ \sigma_{21} & \sigma_{22} & \sigma_{23} \\ \sigma_{31} & \sigma_{32} & \sigma_{33} \end{bmatrix} \tag{4.10}$$

but only six are independent because

$$\sigma_{ji} = \sigma_{ij} \tag{4.11}$$

Each stress component, σ_{ij}, can be expresed as a function of the three principal stresses, σ_1, σ_2, σ_3, and the nine direction cosines of the three principal stress axes with respect to the arbitrary Cartesian axes used to define the σ_{ij}. However, if a unit vector pointing in the direction of the ith principal stress axis is $\bar{e}_i$, then because the three principal stress axes are orthogonal, we have

$$\bar{e}_i \cdot \bar{e}_j = \delta_{ij} \tag{4.12}$$

Equation (4.12) represents six independent scalar equations involving the nine principal stress axis direction cosines. Thus, there are only three independent principal stress axis direction cosines. Let them be α_1, α_2, and α_3. Then we can write

$$\sigma_{ij} = \sigma_{ij}(\sigma_1, \sigma_2, \sigma_3; \alpha_1, \alpha_2, \alpha_3) \tag{4.13}$$

If a material is isotropic, the dependencies of the yield function, f, in Equation (4.6) and of the plastic potential function, g, in Equation (4.7) on the principal stresses σ_1, σ_2, and σ_3 are independent of the orientation of the principal stress axes with respect

to the coordinate axes. This is a specific application of the principle of material frame indifference [Malvern (1969:389)]. This means that not only do α_1, α_2, and α_3 not appear in either equation, but also the stress functions which do appear are insensitive to subscript interchanges, i.e., they are symmetric functions of σ_1, σ_2 and σ_3. The total stress invariants I_1, I_2, and I_3 satisfy the required conditions of symmetry. They are:

$$I_1 = \sigma_{11} + \sigma_{22} + \sigma_{33} \tag{4.14}$$

$$I_2 = -\left(\begin{vmatrix} \sigma_{11} & \sigma_{12} \\ \sigma_{21} & \sigma_{22} \end{vmatrix} + \begin{vmatrix} \sigma_{22} & \sigma_{23} \\ \sigma_{32} & \sigma_{33} \end{vmatrix} + \begin{vmatrix} \sigma_{33} & \sigma_{31} \\ \sigma_{13} & \sigma_{11} \end{vmatrix} \right) \tag{4.15}$$

$$I_3 = \begin{vmatrix} \sigma_{11} & \sigma_{12} & \sigma_{13} \\ \sigma_{21} & \sigma_{22} & \sigma_{23} \\ \sigma_{31} & \sigma_{32} & \sigma_{33} \end{vmatrix} \tag{4.16}$$

Equation (4.7) gives the relative values of the plastic strain increments, from which the relative values of the principal plastic strain increments and the orientation of the principal plastic strain increment axes can be determined. Since the plastic potential function, g, is a function of the three total stress invariants, I_1, I_2, and I_3, given by Equations (4.14), (4.15), and (4.15), we have

$$g = g(I_1, I_2, I_3) \tag{4.17}$$

so that Equation (4.7) can be written in the form

$$d\varepsilon^p_{ij} = d\lambda \frac{\partial g}{\partial \sigma_{ij}} = d\lambda \left(\frac{\partial g}{\partial I_1} \frac{\partial I_1}{\partial \sigma_{ij}} + \frac{\partial g}{\partial I_2} \frac{\partial I_2}{\partial \sigma_{ij}} + \frac{\partial g}{\partial I_3} \frac{\partial I_3}{\partial \sigma_{ij}} \right) \tag{4.18}$$

Now Equations (4.14) and (4.15) yield

$$\frac{\partial I_1}{\partial \sigma_{ij}} = \begin{bmatrix} 1 & 0 & 0 \\ 0 & 1 & 0 \\ 0 & 0 & 1 \end{bmatrix} = \delta_{ij} \tag{4.19}$$

$$\frac{\partial I_2}{\partial \sigma_{ij}} = \begin{bmatrix} -(\sigma_{22} + \sigma_{33}) & \sigma_{21} & \sigma_{31} \\ \sigma_{12} & -(\sigma_{33} + \sigma_{11}) & \sigma_{32} \\ \sigma_{13} & \sigma_{23} & -(\sigma_{11} + \sigma_{22}) \end{bmatrix}$$

$$= \sigma_{ji} - I_1 \delta_{ij} = \sigma_{ij} - I_1 \delta_{ij} \tag{4.20}$$

To obtain the derivatives $\partial I_3/\partial \sigma_{ij}$ we notice that if the matrix of cofactors or signed minors of the stress matrix, $\underline{\sigma}$ is denoted $\underline{\Sigma}$, then since according to Equation (4.16) the determinant of $\underline{\sigma}$ is I_3, the inverse of $\underline{\sigma}$, denoted $\underline{\sigma}^{-1}$, is

$$\underline{\sigma}^{-1} = \frac{\underline{\Sigma}^T}{I_3} \tag{4.21}$$

Now the Laplace expansion for the determinant I_3 is

$$I_3 = \frac{1}{3} \sigma_{ij} \Sigma_{ij} \tag{4.22}$$

and direct expansion will demonstrate that

$$\frac{\partial I_3}{\partial \sigma_{ij}} = \Sigma_{ij} = I_3 \sigma_{ij}^{-1,T}$$

$$= I_3 \sigma_{ij}^{T,-1} = I_3 \sigma_{ij}^{-1} \tag{4.23}$$

Substitution of Equations (4.19), (4.20), and (4.23) into Equation (4.18) yields

$$d\varepsilon_{ij}^{p} = d\lambda\left[\frac{\partial g}{\partial I_1}\delta_{ij} + \frac{\partial g}{\partial I_2}(\sigma_{ij} - I_1\delta_{ij}) + \frac{\partial g}{\partial I_3} I_3\, \sigma_{ij}^{-1}\right] \tag{4.24}$$

Since $\underline{\sigma}^{-1}$ has the same principal axes as does $\underline{\sigma}$, it follows from Equation (4.24) that $\underline{d\varepsilon}^{p}$ also has the same principal axes as does $\underline{\sigma}$. This condition is a consequence of the assumption of material isotropy, and not an independent assumption.

A convenient assumption concerning the dependence of the yield function, f, in Equation (4.6) on plastic strain is that f is a function of stress, σ_{ij}, and plastic work, W^p, where plastic work is in turn a function of plastic strain [Malvern (1969:367)].

$$f(\sigma_{ij}, \varepsilon_{ij}^{p}) = f[\sigma_{ij}, W^{p}(\varepsilon_{ij}^{p})] \tag{4.25}$$

Now Equation (4.9) can be written in the form

$$dW^{p} = \frac{\partial W^{p}}{\partial \varepsilon_{ij}^{p}} d\varepsilon_{ij}^{p} = \sigma_{ij} d\varepsilon_{ij}^{p} \tag{4.26}$$

so that

$$\frac{\partial W^{p}}{\partial \varepsilon_{ij}^{p}} = \sigma_{ij} \tag{4.27}$$

The application of the above equations can now be outlined.

4.2 Stress Control Formulation

When stress increments are prescribed, the elastic strain increments, $d\varepsilon_{ij}^{e}$, are calculated from the equation

$$d\varepsilon_{ij}^{e} = -\frac{\nu}{E} I_1\delta_{ij} + \frac{1+\nu}{E}\sigma_{ij} \tag{4.28}$$

where E = Young's elastic modulus

ν = Poisson's ratio

Provided Equation (4.6) is satisfied, so that yielding can occur, we write Equation (4.8) in the form

$$df = \frac{\partial f}{\partial \sigma_{ij}} d\sigma_{ij} + \frac{\partial f}{\partial W^p} dW^p = 0 \tag{4.29}$$

Since the invariants I_1, I_2, and I_3 are homogeneous functions of degree 1, 2, and 3, respectively, Euler's theorem states that Equation (4.18) yields

$$dW^p = \sigma_{ij} d\varepsilon^p_{ij} = d\lambda\left(\frac{\partial g}{\partial I_1} I_1 + 2 \frac{\partial g}{\partial I_2} I_2 + 3 \frac{\partial g}{\partial I_3} I_3\right) = h d\lambda \tag{4.30}$$

where

$$h = \frac{\partial g}{\partial I_1} I_1 + 2 \frac{\partial g}{\partial I_2} I_2 + 3 \frac{\partial g}{\partial I_3} I_3 \tag{4.31}$$

Equation (4.30) can be verified by direct expansion of Equation (4.24). Thus Equation (4.29) can be written in the form

$$df = \frac{\partial f}{\partial \sigma_{ij}} d\sigma_{ij} + d\lambda\left(h \frac{\partial f}{\partial W^p}\right) = 0 \tag{4.32}$$

and therefore the flow rule proportionality constant is

$$d\lambda = - \frac{\frac{\partial f}{\partial \sigma_{ij}} d\sigma_{ij}}{h \frac{\partial f}{\partial W^p}} \tag{4.33}$$

The plastic strain increments are calculated from Equation (4.7),

$$d\varepsilon^p_{ij} = d\lambda \frac{\partial g}{\partial \sigma_{ij}} \tag{4.7}$$

and the plastic work increment is calculated from Equation (4.30)

$$dW^p = h d\lambda = - \frac{\frac{\partial f}{\partial \sigma_{ij}} d\sigma_{ij}}{\frac{\partial f}{\partial W^p}} \tag{4.34}$$

Therefore when $h d\lambda > 0$, Equation (4.9) will be satisfied. In that case yielding will occur when Equation (4.6) is also satisfied, and the total strain increments are given by Equation (4.5)

$$d\varepsilon_{ij} = d\varepsilon^e_{ij} + d\varepsilon^p_{ij} \tag{4.5}$$

The elastoplastic incremental compliance tensor is obtained by writing Equation (4.5) in the form

$$\begin{aligned} d\varepsilon_{ij} &= d\varepsilon^e_{ij} + d\varepsilon^p_{ij} \\ &= F^e_{ijkl} d\sigma_{kl} + d\lambda \frac{\partial g}{\partial \sigma_{ij}} \end{aligned} \tag{4.35}$$

where, from Equation (4.28)

$$F^e_{ijkl} = - \frac{\nu}{E} \delta_{ij}\delta_{kl} + \frac{1 + \nu}{E} \delta_{ik}\delta_{jl} \tag{4.36}$$

Substitution of Equation (4.33) into Equation (4.35) yields

$$d\varepsilon_{ij} = \left(F^e_{ijkl} - \frac{\frac{\partial g}{\partial \sigma_{ij}} \frac{\partial f}{\partial \sigma_{kl}}}{h \frac{\partial f}{\partial W^p}} \right) d\sigma_{kl} = F^{ep}_{ijkl} d\sigma_{kl} \tag{4.37}$$

where

$$F^{ep}_{ijkl} = F^e_{ijkl} - \frac{\frac{\partial g}{\partial \sigma_{ij}} \frac{\partial f}{\partial \sigma_{kl}}}{h \frac{\partial f}{\partial W^p}} \tag{4.38}$$

4.3 Strain Control Formulation

When strain increments are prescribed, the elastic strain increments are not immediately known. Combining Equations (4.4), (4.5), and (4.7) yields

$$d\sigma_{ij} = D^e_{ijkl} d\varepsilon^e_{kl} = D^e_{ijkl}(d\varepsilon_{kl} - d\varepsilon^p_{kl})$$

$$= D^e_{ijkl}(d\varepsilon_{kl} - d\lambda \frac{\partial g}{\partial \sigma_{kl}}) \tag{4.39}$$

and substitution of Equation (4.39) into Equation (4.32) yields

$$df = \frac{\partial f}{\partial \sigma_{ij}} D^e_{ijkl}(d\varepsilon_{kl} - d\lambda \frac{\partial g}{\partial \sigma_{kl}}) + d\lambda(h \frac{\partial f}{\partial W^p}) = 0 \tag{4.40}$$

and therefore the flow rule proportionality constant is

$$d\lambda = \frac{\frac{\partial f}{\partial \sigma_{ij}} D^e_{ijkl} d\varepsilon_{kl}}{\frac{\partial f}{\partial \sigma_{ij}} D^e_{ijkl} \frac{\partial g}{\partial \sigma_{kl}} - h \frac{\partial f}{\partial W^p}} \tag{4.41}$$

Provided $hd\lambda$ is positive, the plastic strain increments are calculated from Equation (4.7),

$$d\varepsilon^p_{ij} = d\lambda \frac{\partial g}{\partial \sigma_{ij}} \tag{4.7}$$

and the elastic strain increments are calculated from Equation (4.5),

$$d\varepsilon^e_{ij} = d\varepsilon_{ij} - d\varepsilon^p_{ij} \tag{4.42}$$

The stress increments are then calculated from Equation (4.4),

$$d\sigma_{ij} = D^e_{ijkl} d\varepsilon^e_{kl} \tag{4.4}$$

The elastoplastic incremental stiffness tensor is obtained by writing Equation (4.4) in the form

$$d\sigma_{ij} = D^e_{ijkl}(d\varepsilon_{kl} - d\varepsilon^p_{kl}) = D^e_{ijkl}(d\varepsilon_{kl} - d\lambda \frac{\partial g}{\partial \sigma_{kl}}) \tag{4.43}$$

where, from Equation (4.3),

$$D^e_{ijkl} = MK_o \delta_{ij}\delta_{kl} + M(1 - K_o)\delta_{ik}\delta_{jl} \tag{4.44}$$

Substitution of Equation (4.41) into Equation (4.43) yields

$$d\sigma_{ij} = \left[D^e_{ijkl} - \frac{(D^e_{ijpq} \frac{\partial g}{\partial \sigma_{pq}})(\frac{\partial f}{\partial \sigma_{rs}} D^e_{rskl})}{\frac{\partial f}{\partial \sigma_{pq}} D^e_{pqrs} \frac{\partial g}{\partial \sigma_{rs}} - h \frac{\partial f}{\partial W^p}} \right] d\varepsilon_{kl}$$

$$= D^{ep}_{ijkl} d\varepsilon_{kl} \tag{4.45}$$

where

$$D^{ep}_{ijkl} = D^e_{ijkl} - \frac{(D^e_{ijpq} \frac{\partial g}{\partial \sigma_{pq}})(\frac{\partial f}{\partial \sigma_{rs}} D^e_{rskl})}{\frac{\partial f}{\partial \sigma_{pq}} D^e_{pqrs} \frac{\partial g}{\partial \sigma_{rs}} - h \frac{\partial f}{\partial W^p}} \tag{4.46}$$

4.4 Mixed Boundary Value Formulation

When a complementary combination of stress and strain increments is prescribed (e.g. as in constrained compression), Equation (4.32) can be written in a form which is a combination of Equations (4.32) and (4.40).

$$df = [\frac{\partial f}{\partial \sigma_{ij}} d\sigma_{ij}]_{d\sigma} + [\frac{\partial f}{\partial \sigma_{ij}} D^e_{ijkl}(d\varepsilon_{kl} - d\lambda \frac{\partial g}{\partial \sigma_{kl}})]_{d\varepsilon}$$

$$+ d\lambda \, (h \frac{\partial f}{\partial W^p}) = 0 \tag{4.47}$$

where the symbols $[\ ]_{d\sigma}$ and $[\ ]_{d\varepsilon}$ mean summation only over indices of prescribed stress or strain increments. The flow rule proportionality constant is therefore

$$d\lambda = \frac{\left[\frac{\partial f}{\partial \sigma_{ij}} d\sigma_{ij}\right]_{d\sigma} + \left[\frac{\partial f}{\partial \sigma_{ij}} D^e_{ijkl} d\varepsilon_{kl}\right]_{d\varepsilon}}{\left[\frac{\partial f}{\partial \sigma_{ij}} D^e_{ijkl} \frac{\partial f}{\partial \sigma_{kl}}\right]_{d\varepsilon} - h \frac{\partial f}{\partial W^p}} \tag{4.48}$$

Equation (4.48) reduces to Equations (4.33) or (4.41) in the cases of prescribed stress or strain increments, respectively. Provided $hd\lambda$ is positive, the plastic strain increments are calculated from Equation (4.7)

$$d\varepsilon_{ij}^{p} = d\lambda \frac{\partial g}{\partial \sigma_{ij}} \tag{4.7}$$

and the elastic strain increments corresponding to the prescribed total strain increments are calculated from Equation (4.5)

$$[d\varepsilon_{ij}^{e} = d\varepsilon_{ij} - d\varepsilon_{ij}^{p}]_{d\varepsilon} \tag{4.49}$$

At this point we know some stress increments but not the corresponding elastic strain increments, and the complementary elastic strain increments but not the corresponding stress increments. To calculate the unknown stress and elastic strain increments we write Equation (4.42) in matrix form as

$$\begin{Bmatrix} \{d\sigma\}_1 \\ \hline \{\bar{d}\sigma\}_2 \end{Bmatrix} = \left[\begin{array}{c|c} \underline{D}_{11}^{e} & \underline{D}_{12}^{e} \\ \hline \underline{D}_{21}^{e} & \underline{D}_{22}^{e} \end{array}\right] \begin{Bmatrix} \{\bar{d}\varepsilon^{e}\}_1 \\ \hline \{d\varepsilon^{e}\}_2 \end{Bmatrix} \tag{4.50}$$

where an overbar indicates a matrix of prescribed quantities, and the partitioned matrices $\underline{D}_{11}^{e}$ and $\underline{D}_{22}^{e}$ are square and symmetric.
Expansion of Equation (4.5) yields

$$\{d\sigma\}_1 = \underline{D}_{11}^{e} \{\bar{d}\varepsilon^{e}\}_1 + \underline{D}_{12}^{e} \{d\varepsilon^{e}\}_2 \tag{4.51}$$

$$\{\bar{d}\sigma\}_2 = \underline{D}_{21}^{e} \{\bar{d}\varepsilon^{e}\}_1 + \underline{D}_{22}^{e} \{d\varepsilon^{e}\}_2 \tag{4.52}$$

Equation (4.52) yields

$$\{d\varepsilon^e\}_2 = \underline{D}^{e,-1}_{22} \left\{ \{\overline{d}\sigma\}_2 - \underline{D}^e_{21} \{\overline{d}\varepsilon^e\}_1 \right\} \tag{4.53}$$

and substitution of Equation (4.53) into Equation (4.51) yields

$$\{d\sigma\}_1 = \underline{D}^e_{11} \{\overline{d}\varepsilon^e\}_1 + \underline{D}^e_{12}\underline{D}^{e,-1}_{22} \left\{ \{\overline{d}\sigma\}_2 - \underline{D}^e_{21} \{\overline{d}\varepsilon^e\}_1 \right\}$$

$$= (\underline{D}^e_{11} - \underline{D}^e_{12}\underline{D}^{e,-1}_{22}\underline{D}^e_{21}) \{\overline{d}\varepsilon^e\}_1 + \underline{D}^e_{12}\underline{D}^{e,-1}_{22} \{\overline{d}\sigma\}_2 \tag{4.54}$$

The remaining unspecified total strain increments are calculated from Equation (4.5),

$$[d\varepsilon_{ij} = d\varepsilon^e_{ij} + d\varepsilon^p_{ij}]_{d\sigma} \tag{4.5}$$

The elastoplastic incremental compliance tensor, F^{ep}_{ijkl}, given by Equation (4.38), and the elastoplastic incremental stiffness tensor, D^{ep}_{ijkl}, given by Equation (4.46), are both functions of stress and plastic work only, and are therefore independent of which stress and strain increments are prescribed. Note that since

$$d\sigma_{ij} = D^{ep}_{ijkl} d\varepsilon_{kl} = D^{ep}_{ijkl} F^{ep}_{klpq} d\sigma_{pq} \tag{4.55}$$

it must be that

$$D^{ep}_{ijkl} F^{ep}_{klpq} = \delta_{ip}\sigma_{jq} \tag{4.56}$$

so that $\underline{D}^{ep}$ and $\underline{F}^{ep}$ are the inverse of one another.

4.5 Computational Format

For computing purposes, it is convenient to write many of the above equations in matrix form, as was done with Equations (4.50) through (4.54). First we set

$$\{\sigma^*\} = \begin{Bmatrix} \sigma_{11} \\ \sigma_{22} \\ \sigma_{33} \\ \sigma_{12} \\ \sigma_{23} \\ \sigma_{31} \\ \sigma_{21} \\ \sigma_{32} \\ \sigma_{13} \end{Bmatrix} \tag{4.57}$$

and

$$\{\varepsilon^*\} = \begin{Bmatrix} \varepsilon_{11} \\ \varepsilon_{22} \\ \varepsilon_{33} \\ \varepsilon_{12} \\ \varepsilon_{23} \\ \varepsilon_{31} \\ \varepsilon_{21} \\ \varepsilon_{32} \\ \varepsilon_{13} \end{Bmatrix} \tag{4.58}$$

Equations (4.57) and (4.58) indicate that the stress and strain spaces are nine-dimensional. However, since

$$\sigma_{ij} = \sigma_{ji} \tag{4.11}$$

and

$$\varepsilon_{ij} = \varepsilon_{ji} \tag{4.59}$$

all stress and strain points are restricted to six-dimensional coincident subspaces. We therefore set

$$\{\sigma\} = \begin{Bmatrix} \sigma_1 \\ \sigma_2 \\ \sigma_3 \\ \sigma_4 \\ \sigma_5 \\ \sigma_6 \end{Bmatrix} = \begin{Bmatrix} \sigma_{11} \\ \sigma_{22} \\ \sigma_{33} \\ \sqrt{2}\,\sigma_{12} \\ \sqrt{2}\,\sigma_{23} \\ \sqrt{2}\,\sigma_{31} \end{Bmatrix} \tag{4.60}$$

and

$$\{e\} = \begin{Bmatrix} \varepsilon_1 \\ \varepsilon_2 \\ \varepsilon_3 \\ \varepsilon_4 \\ \varepsilon_5 \\ \varepsilon_6 \end{Bmatrix} = \begin{Bmatrix} \varepsilon_{11} \\ \varepsilon_{22} \\ \varepsilon_{33} \\ \sqrt{2}\,\varepsilon_{12} \\ \sqrt{2}\,\varepsilon_{23} \\ \sqrt{2}\,\varepsilon_{31} \end{Bmatrix} \tag{4.61}$$

Equations (4.60) and (4.61) give the correct expressions for work and for the derivatives of the stress invariants.

$$dW = \{\sigma\}^T \{d\varepsilon\} = \{\sigma^*\}^T \{d\varepsilon^*\} \tag{4.62}$$

$$I_1 = \sigma_1 + \sigma_2 + \sigma_3 \tag{4.63}$$

$$I_2 = -(\sigma_1\sigma_2 + \sigma_2\sigma_3 + \sigma_3\sigma_1) + \frac{1}{2}(\sigma_4^2 + \sigma_5^2 + \sigma_6^2) \tag{4.64}$$

$$I_3 = \sigma_1\sigma_2\sigma_3 + \frac{1}{\sqrt{2}}\sigma_4\sigma_5\sigma_6 - \frac{1}{2}(\sigma_1\sigma_5^2 + \sigma_2\sigma_6^2 + \sigma_3\sigma_4^2) \tag{4.65}$$

$$\left\{\frac{\partial I_1}{\partial \sigma}\right\} = \begin{Bmatrix} 1 \\ 1 \\ 1 \\ 0 \\ 0 \\ 0 \end{Bmatrix} \tag{4.66}$$

$$\left\{\frac{\partial I_2}{\partial \sigma}\right\} = \begin{Bmatrix} -\sigma_2 - \sigma_3 \\ -\sigma_1 - \sigma_3 \\ -\sigma_2 - \sigma_1 \\ \sigma_4 \\ \sigma_5 \\ \sigma_6 \end{Bmatrix} = \begin{Bmatrix} \sigma_1 - I_1 \\ \sigma_2 - I_1 \\ \sigma_3 - I_1 \\ \sigma_4 \\ \sigma_5 \\ \sigma_6 \end{Bmatrix} = \begin{Bmatrix} \sigma_{11} - I_1 \\ \sigma_{22} - I_1 \\ \sigma_{33} - I_1 \\ \sqrt{2}\ \sigma_{12} \\ \sqrt{2}\ \sigma_{23} \\ \sqrt{2}\ \sigma_{31} \end{Bmatrix} \tag{4.67}$$

$$\left\{\frac{\partial I_3}{\partial \sigma}\right\} = \begin{Bmatrix} \sigma_2\sigma_3 - \frac{1}{2}\sigma_5^2 \\ \sigma_3\sigma_1 - \frac{1}{2}\sigma_6^2 \\ \sigma_1\sigma_2 - \frac{1}{2}\sigma_4^2 \\ \frac{1}{\sqrt{2}}\sigma_5\sigma_6 - \sigma_3\sigma_4 \\ \frac{1}{\sqrt{2}}\sigma_6\sigma_4 - \sigma_1\sigma_5 \\ \frac{1}{\sqrt{2}}\sigma_4\sigma_5 - \sigma_2\sigma_6 \end{Bmatrix} = \begin{Bmatrix} \Sigma_{11} \\ \Sigma_{22} \\ \Sigma_{33} \\ \sqrt{2}\ \Sigma_{12} \\ \sqrt{2}\ \Sigma_{23} \\ \sqrt{2}\ \Sigma_{31} \end{Bmatrix} \tag{4.68}$$

There are other six-element stress and strain vectors which give the correct expressions for work and for the derivatives of the stress invariants; for example:

$$\begin{Bmatrix} \sigma_{11} \\ \sigma_{22} \\ \sigma_{33} \\ \sigma_{12} \\ \sigma_{23} \\ \sigma_{31} \end{Bmatrix} \text{ and } \begin{Bmatrix} \varepsilon_{11} \\ \varepsilon_{22} \\ \varepsilon_{33} \\ 2\varepsilon_{12} \\ 2\varepsilon_{23} \\ 2\varepsilon_{31} \end{Bmatrix}$$

The reason for defining the six-dimensional stress and strain vectors by Equations (4.60) and (4.61) is that if the 9 x 9 elastoplastic incremental stiffness matrix, $\underline{D}^{ep}$, in the equation

$$\{d\sigma^*\} = \underline{D}^{ep} \{d\varepsilon^*\} \tag{4.69}$$

is symmetric, then the stress and strain vectors, $\{\sigma\}$ and $\{\varepsilon\}$ defined by Equations (4.60) and (4.61) are the only stress and strain vectors for which the 6 x 6 elastoplastic incremental stiffness matrix, $\underline{C}^{ep}$, in the equation

$$\{d\sigma\} = \underline{C}^{ep} \{d\varepsilon\} \tag{4.70}$$

will also always be symmetric.

In matrix form, the equations for a complementary combination of prescribed stress and strain increments are as follows. Let

$\{d\alpha\}$ = column matrix of unknown stress increments

$\{d\beta\}$ = column matrix of prescribed stress increments

$\{d\gamma\}$ = column matrix of prescribed strain increments

$\{d\delta\}$ = column matrix of unknown strain increments

Then Equation (4.47) can be written in the form

$$df = \left\{\frac{\partial f}{\partial \beta}\right\}^T \{d\beta\} + \left[\left\{\frac{\partial f}{\partial \alpha}\right\}^T \underline{C}^e_{11} \left\{\{d\gamma\} - d\lambda \left\{\frac{\partial g}{\partial \alpha}\right\}\right\}\right] + d\lambda \left(h \frac{\partial f}{\partial W^p}\right) = 0 \tag{4.71}$$

so that the flow rule proportionality constant is therefore

$$d\lambda = \frac{\left\{\frac{\partial f}{\partial \beta}\right\}^T \{d\beta\} + \left\{\frac{\partial f}{\partial \alpha}\right\}^T \underline{C}^e_{11} \{d\gamma\}}{\left\{\frac{\partial f}{\partial \alpha}\right\}^T \underline{C}^e_{11} \left\{\frac{\partial g}{\partial \alpha}\right\} - h \frac{\partial f}{\partial W^p}} \tag{4.72}$$

The reduced elastic stiffness matrix, $\underline{C}^e_{11}$, appearing in Equations (4.71) and (4.72) contains only those elements associated with the prescribed strain increments, $\{d\gamma\}$, and the corresponding (unknown) stress increments, $\{d\alpha\}$. Provided $hd\lambda$ is positive, the plastic strain increments are calculated from the matrix form of Equation (4.7),

$$\{de^p\} = d\lambda \{\frac{\partial g}{\partial \sigma}\} \tag{4.73}$$

and the elastic strain increments corresponding to the prescribed total strain increments are calculated from Equation (4.5)

$$\{d\gamma^e\} = \{d\gamma\} - \{d\gamma^p\} \tag{4.74}$$

Equations (4.50) through (4.54) take the form

$$\left\{\begin{array}{c}\{d\alpha\} \\ \hline \{d\beta\}\end{array}\right\} = \left[\begin{array}{c|c}\underline{C}^e_{11} & \underline{C}^e_{12} \\ \hline \underline{C}^e_{21} & \underline{C}^e_{22}\end{array}\right]\left\{\begin{array}{c}\{d\gamma^e\} \\ \hline \{d\delta^e\}\end{array}\right\} \tag{4.75}$$

or

$$\{d\alpha\} = \underline{C}^e_{11} \{d\gamma^e\} + \underline{C}^e_{12} \{d\delta^e\} \tag{4.76}$$

$$\{d\beta\} = \underline{C}^e_{21} \{d\gamma^e\} + \underline{C}^e_{22} \{d\delta^e\} \tag{4.77}$$

so that

$$\{d\delta^e\} = \underline{C}^{e,-1}_{22}\left\{\{d\beta\} - \underline{C}^e_{21} \{d\gamma^e\}\right\} \tag{4.78}$$

and therefore

$$\{d\alpha\} = (\underline{C}^e_{11} - \underline{C}^e_{12}\underline{C}^{e,-1}_{22}\underline{C}^e_{21}) \{d\gamma^e\} + \underline{C}^e_{12}\underline{C}^{e,-1}_{22} \{d\beta\} \tag{4.79}$$

and

$$\{d\delta\} = \{d\delta^e\} + \{d\delta^p\} \tag{4.80}$$

The elastoplastic incremental stiffness matrix is, from Equation (4.46),

$$\underline{C}^{ep} = \underline{C}^{e} - \frac{\underline{C}^{e} \left\{\frac{\partial g}{\partial \sigma}\right\} \left\{\frac{\partial f}{\partial \sigma}\right\}^{T} \underline{C}^{e}}{\left\{\frac{\partial f}{\partial \sigma}\right\}^{T} \underline{C}^{e} \left\{\frac{\partial g}{\partial \sigma}\right\} - h \frac{\partial f}{\partial W^{p}}} \tag{4.81}$$

4.6 Material Behavior

So far the discussion of the theory of elastoplasticity has been mathematical. Material behavior comes into play in selecting the yield function, f, and plastic potential function, g, on the basis of test data. Frequently the mathematical form of the yield function is based on strength or failure data, and a hardening function is added to convert the failure criterion to a yield function. [Newmark (1960:24)] pointed out that the definition of failure should be as precise as is the resulting failure criterion. From a mathematical viewpoint, once the yield function and plastic potential function are defined, failure occurs when the elastoplastic incremental stiffness matrix, $\underline{C}^{ep}$, defined by Equation (4.81), becomes singular, i.e. when

$$|\underline{C}^{ep}| = 0 \tag{4.82}$$

The theory of plasticity was first developed for metals, for which the yield function is often independent of the hydrostatic stress component. (However, ductility of metals often increases with increasing hydrostatic stress.) What this means mathematically is that in three-dimensional principal stress space metallic yield functions which are independent of the hydrostatic stress component are right cylinders, with their axis along the line $\sigma_1 = \sigma_2 = \sigma_3$, called the hydrostatic axis. In such cases interest naturally centers on the shape of the intersection of the yield surface with a plane normal to the hydrostatic axis, called a deviator or octahedral plane, and having the equation

$$\sigma_1 + \sigma_2 + \sigma_3 = I_1 = \text{constant} \tag{4.83}$$

Figure 4.2 shows the hydrostatic axis and an octahedral plane in principal stress space.

For soils the hydrostatic stress component definitely influences the failure surface, but often in such a way that octahedral cross-sections of the failure surface at different values of I_1 are geometrically similar, increasing in size as a function of I_1. When this happens all strength data can be plotted on a single octahedral plot by normalizing the data with respect to the I_1 size function. This is how Figures 3.7 through 3.26 were obtained. For example, The Drucker-Prager failure surface assumes that octahedral cross-sections are circular, with the radius a linear function of I_1 [Drucker and Prager (1952:158)].

The geometrical justification for plotting shear strength data in the octahedral plane using coordinates

$$\sin \bar{\phi} = \frac{\bar{\sigma}_1 - \bar{\sigma}_3}{\bar{\sigma}_1 + \bar{\sigma}_3} \tag{4.84}$$

and

$$\mu = \frac{2\bar{\sigma}_2 - \bar{\sigma}_1 - \bar{\sigma}_3}{\bar{\sigma}_1 - \bar{\sigma}_3} \tag{4.85}$$

as shown in Figure 4.3 can be found in [Merkle (1971:346)]. Using the form shown in Figure 4.4, strength data from many different investigations can be compared on a common basis.

Although the Mohr-Coulomb friction angle, $\bar{\phi}$, and Lode's parameter, μ, are useful for plotting strength data in the octahedral plane, the invariant quantities

$$\sigma_{oct} = \frac{I_1}{3} \tag{4.86}$$

$$\tau_{oct} = \sqrt{\frac{2J_2}{3}} = \frac{1}{3}\sqrt{(\sigma_1 - \sigma_2)^2 + (\sigma_2 - \sigma_3)^2 + (\sigma_3 - \sigma_1)^2} \tag{4.87}$$

$$\cos 3\omega = \frac{\frac{J_3}{2}}{(\frac{J_2}{3})^{3/2}} \tag{4.88}$$

$$J_3 = (\sigma_1 - \sigma_{oct})(\sigma_2 - \sigma_{oct})(\sigma_3 - \sigma_{oct}) \tag{4.89}$$

are more useful in constructing curves to fit the data. The variables σ_{oct}, τ_{oct} and ω are shown in Figure 4.3, where σ_1, σ_2, and σ_3 represent principal stresses.

4.7 Drucker's Equivalent Stress Function

Although his principal concern was developing an invariant shearing stress-strain relation, rather than defining the shape of the octahedral cross-secion of a failure surface, [Drucker (1949:352)] proposed what amounts to a formula for variation of τ_{oct} with ω. He proposed the following expression for an equivalent shearing stress, $\bar{\tau}_{eq}$:

$$\bar{\tau}_{eq} = \tau_{oct}(1 - 2.25J_3^2/J_2^3)^{1/6} \tag{4.90}$$

where from Equation (4.88) we have

$$\frac{J_3^2}{J_2^3} = \frac{\cos^2 3\omega}{6.75} = \frac{1 + \cos 6\omega}{13.5} \tag{4.91}$$

Substitution of Equation (4.91) into Equation (4.90) yields

$$\tau_{oct} = \frac{\bar{\tau}_{eq}}{(1 - \frac{1 + \cos 6\omega}{6})^{1/6}} \tag{4.92}$$

Equation (4.90) defines a smooth curve in the octahedral plane for which lines of symmetry occur at 30 degree intervals [cf Hill (1950:18)]. It causes the value of τ_{oct} to be the same in triaxial extension ($\omega = 60^\circ$) as in triaxial compression ($\omega = 120^\circ$), and as Hill explains, such an octahedral cross-section corresponds to an isotropic material which does not exhibit a Baushinger effect. Equation (4.92) can be written in terms of Lode's parameter, μ, instead of the octahedral polar angle, ω, by using the relation [Merkle (1971:733)]

$$\cos^2 3\omega = 6.75 \frac{J_3^2}{J_2^3} = \frac{\mu^2(9 - \mu^2)^2}{(3 + \mu^2)^3} \tag{4.93}$$

so that Equation (4.92) takes the form

$$\tau_{oct} = \frac{\bar{\tau}_{eq}}{\left[1 - \frac{\mu^2(9 - \mu^2)^2}{3(3 + \mu^2)^3}\right]^{1/6}} \tag{4.94}$$

When $\mu = \pm 1$, Equation (4.49) yields

$$\tau_{oct} = \frac{\bar{\tau}_{eq}}{(\frac{2}{3})^{1/6}} = 1.07\ \bar{\tau}_{eq} \tag{4.95}$$

and when $\mu = 0$, Equation (4.494) yields

$$\tau_{oct} = \bar{\tau}_{eq} \tag{4.96}$$

4.8 Topping's Failure Criterion

[Topping (1955:186)] proposed a Mohr circle type relation in the octahedral plane, to account for the possibility that the octahedral shear stress values at failure in triaxial compression and triaxial extension may be different at the same octahedral normal stress. His equation is

$$\tau_{oct} = \tau_c \cos^2 \frac{3\omega}{2} + \tau_e \sin^2 \frac{3\omega}{2}$$

$$= \left(\frac{\tau_c + \tau_e}{2} \right) + \left(\frac{\tau_c - \tau_e}{2} \right) \cos 3\omega \qquad (4.97)$$

Equation (4.97) can also be written in the form

$$\tau_{oct} = A + B \left(\frac{J_3}{J_2^{3/2}} \right) \qquad (4.98)$$

where

$$A = 0.5(\tau_c + \tau_e) \qquad (4.99)$$

$$B = 1.3(\tau_c - \tau_e) \qquad (4.100)$$

or

$$\tau_{oct} = A - C \left[\frac{\mu(9 - \frac{2}{\mu})}{(3 + \mu^2)^{3/2}} \right] \qquad (4.101)$$

where

$$C = 0.5(\tau_c - \tau_e) \qquad (4.102)$$

Note that Equation (4.101) permits evaluation of the constants A and C by a straight line plot.

4.9 Kirkpatrick's Failure Criterion

[Kirkpatrick (1957)] performed both conventional triaxial and thick-walled cylinder tests on Loch Aline sand, for the purpose of determining the shape of the failure surface octahedral cross-section. His results are shown in Figure 3.10, and he concluded that the Mohr-Coulomb failure criterion was a good fit to the data. In fact, Kirkpatrick felt the Mohr-Coulomb criterion fit his data so well that he decided not to modify the axial load capability of his thick cylinder device to obtain μ values other than those shown in Figure 3.10.

Both Topping's and Kirkpatricks's results were cited by [Newmark (1960:28)] as examples of failure criteria having roughly triangular octahedral cross-sections, and unequal [octahedral shear] strengths in triaxial compression and extension.

4.10 Coleman's Failure Criterion

[Coleman (1960:182)] proposed a failure criterion based on an invariant formulation of the Mohr-Coulomb failure criterion for a cohesionless material. From Figure 4.3 we have (for d = o),

$$\sqrt{3}\left(\frac{\tau_{oct}}{\sigma_{oct}}\right)\sin\omega_2 = \left[\sqrt{6} - \sqrt{3}\left(\frac{\tau_{oct}}{\sigma_{oct}}\right)\cos\omega_2\right]\frac{\sin\bar{\phi}}{\sqrt{3}} \tag{4.103}$$

so that

$$\sin\bar{\phi} = \frac{\sqrt{3}\left(\frac{\tau_{oct}}{\sigma_{oct}}\right)\sin\omega_2}{\sqrt{2} - \left(\frac{\tau_{oct}}{\sigma_{oct}}\right)\cos\omega_2} \tag{4.104}$$

When $\mu = +1$

$$\omega_2 = 60^\circ$$

$$\sin\omega_2 = \frac{\sqrt{3}}{2}$$

$$\cos\omega_2 = \frac{1}{2} = -\frac{1}{2}(\cos 3\omega_2)^{1/3}$$

and when $\mu = -1$

$$\omega_2 = 120^\circ$$

$$\sin\omega_2 = \frac{\sqrt{3}}{2}$$

$$\cos\omega_2 = -\frac{1}{2} = -\frac{1}{2}(\cos 3\omega_2)^{1/3}$$

Therefore, if we replace sin ω_2 by $\sqrt{3}/2$, and cos ω_2 by $-1/2(\cos 3\omega_2)^{1/3}$, the resulting expression will match Equation (4.103) for $\mu = \pm 1$. The resulting expression is

$$\sin \bar{\phi} = \frac{\sqrt{3}\left(\frac{\tau_{oct}}{\sigma_{oct}}\right)\frac{\sqrt{3}}{2}}{\sqrt{2} + \left(\frac{\tau_{oct}}{\sigma_{oct}}\right)\frac{1}{2}(\cos 3\omega_2)^{1/3}}$$

$$= \frac{\sqrt{3}J_2}{\frac{2I_1}{3} + \left(\frac{J_3}{2}\right)^{1/3}} \tag{4.105}$$

Clearing of fractions and squaring yields

$$3J_2 = \left[\frac{2I_1}{3} + \left(\frac{J_3}{2}\right)^{1/3}\right]^2 \sin^2\bar{\phi} \tag{4.106}$$

which is Coleman's expression. The mathematically convenient feature of Equation (4.105) is that the invariants appear separately, and in a numerator.

Equation (4.103) can also be written in the form

$$\frac{\tau_{oct}}{\sigma_{oct}} = \frac{\sqrt{2(3 + \mu^2)}\sin\bar{\phi}}{3 + \mu \sin\bar{\phi}} \tag{4.107}$$

When $\mu = -1$ (triaxial compression) Equation (4.107) yields

$$\left(\frac{\tau_{oct}}{\sigma_{oct}}\right)_c = \frac{2\sqrt{2}\sin\bar{\phi}_c}{3 - \sin\bar{\phi}_c} \tag{4.108}$$

and when $\mu = 1$ (triaxial extension) Equation (4.107) yields

$$\left(\frac{\tau_{oct}}{\sigma_{oct}}\right)_e = \frac{2\sqrt{2}\sin\bar{\phi}_e}{3 + \sin\bar{\phi}_e} \tag{4.109}$$

4.11 Lomize and Kryzhanovsky's Failure Criterion

[Lomize and Kryzhanovsky (1967)] performed stress-controlled true triaxial tests on a quartz sand from the Volga region, using μ = -1, 0 and 1. They defined strength as the peak value of τ_{oct} on a plot of τ_{oct} versus γ_{oct}, at constant σ_{oct} and μ, and used the following invariant expression as their empirical failure criterion:

$$\left(\frac{I_1^3}{I_3}\right)^{\alpha} D_k = \pi^* \tag{4.110}$$

where

$$D_k = \frac{1}{\sqrt{6}} \frac{\tau_{oct}}{\sigma_{oct}} \tag{4.111}$$

$$\alpha = 1.73 \tag{4.112}$$

$$\pi^* = 260 \tag{4.113}$$

Now

$$I_3 = \sigma_{oct}^3 \left(6\sqrt{3} \cos 3\omega \; D_k^3 - 9D_k^2 + 1\right) \tag{4.114}$$

where

$$\cos 3\omega = - \frac{\mu(9 - \mu^2)}{(3 + \mu^2)^{3/2}} \tag{4.115}$$

so that

$$\frac{I_1^3}{I_3} = \frac{27}{6\sqrt{3} \cos 3\omega D_k^3 - 9D_k^2 + 1} \tag{4.116}$$

Equation (4.110) can therefore be written in the form

$$\left(6\sqrt{3} \cos 3\omega D_k^3 - 9D_k^2 + 1\right)^{1.73} = \frac{(27)^{1.73}}{260} D_k$$

or

$$D_k = \frac{(6\sqrt{3}\cos 3\omega D_k^3 - 9D_k^2 + 1)^{1.73}}{1.1516} \tag{4.117}$$

Equations (4.115) and (4.117) can be used to find the value of D_k for a given value of μ, by iteration. Figure 3.24 is a plot of the results.

For a more thorough review of investigations of the effect of the intermediate principal stress on soil shear strength, see [Merkle (1971:Chapter 6)].

4.12 Modified Lade Model

[Lade (1972:137, 138)] simplified the failure criterion of Lomize and Kryzhanovsky by deleting the factor D_k in Equation (4.110). The failure criterion which Lade fit to true triaxial test data on Monterey No. 0 Sand was written in the form

$$I_1^3 - k_1 I_3 = 0 \tag{4.118}$$

Using this failure criterion as a basis, Lade developed an elastoplastic constitutive model having one associative and one nonassociative yield surface. His equations are given below, from [Lade and Nelson (1981)]. The associative compressive yield surface and plastic potential function are

$$f_c = f_c'(\sigma) - f_c''(W_c) = 0 \tag{4.119}$$

where

$$f_c' = I_1^2 + 2I_2 = \sigma_1^2 + \sigma_2^2 + \sigma_3^2 \tag{4.120}$$

$$f_c'' = p_a^2 \left(\frac{W_c}{Cp_a}\right)^{1/p} \tag{4.121}$$

and

$$g_c = f_c' \tag{4.122}$$

p_a = atmospheric pressure

The nonassociative expansive yield surface and plastic potential function are

$$f_p = f_p'(\sigma) - f_p''(W_p) = 0 \tag{4.123}$$

where

$$f_p' = \left(\frac{I_1^3}{I_3} - 27\right)\left(\frac{I_1}{p_a}\right)^m \tag{4.124}$$

$$f_p' = \eta_1 \text{ at failure} \tag{4.125}$$

$$f_p'' = ae^{-bWp}\left(\frac{W_p}{p_a}\right)^{1/q}, \quad (q > 0) \tag{4.126}$$

and

$$g_p = I_1^3 - [27 + \eta_2\left(\frac{p_a}{I_1}\right)^m]I_3 \tag{4.127}$$

The octahedral cross-section of Lade's failure surface can be computed as follows

$\bar{\phi}_c$ = friction angle for triaxial compression

$$N_\phi = \frac{1 + \sin \bar{\phi}_c}{1 - \sin \phi_c} \tag{4.128}$$

$$k_1 = \frac{(N_\phi + 2)^3}{N_\phi} \tag{4.129}$$

$$B = 1 - \frac{27}{k_1} \tag{4.130}$$

$$A = \frac{\cos 3\omega}{\sqrt{2}} \tag{4.131}$$

$$z = D_k = \frac{\tau_{oct}}{\sigma_{oct}} = \frac{B}{1.5 - Az} \text{ (iterate)} \tag{4.132}$$

Octahedral cross-section values are tabulated for $\bar{\phi}_c = 30^\circ$ in Table 4.1, and plotted in Figure 4.5. This plot happens to be an excellent fit to Von Karman's data in Figure 3.7.

Lade and Nelson state (p.504) that their "yield function defines the stress levels at which plastic strain increments will occur" [emphasis added]. The paper is silent about testing a given total strain increment to see whether it will cause additional plastic strain, and in this respect the model appears to be deficient. However, the deficiency is easy to correct, and the correction is discussed below.

It is convenient to let the index 1 refer to quantities related to the collapse yield surface, and the index 2 refer to quantities related to the expansive yield surface. In addition, define the {s} matrix by Equation (4.60), the {e} matrix by Equation (4.61), and the 6 x 6 elastic stiffness matrix, $\underline{C}^e$ based on Equation (4.44), i.e.,

$$\underline{C}^e = M \begin{bmatrix} 1 & K_o & K_o & 0 & 0 & 0 \\ K_o & 1 & K_o & 0 & 0 & 0 \\ K_o & K_o & 1 & 0 & 0 & 0 \\ 0 & 0 & 0 & 1-K_o & 0 & 0 \\ 0 & 0 & 0 & 0 & 1-K_o & 0 \\ 0 & 0 & 0 & 0 & 0 & 1-K_o \end{bmatrix} \tag{4.133}$$

Then

$$\{d\varepsilon\} = \{d\varepsilon^e\} + \{d\varepsilon^p\} \tag{4.134}$$

where

$$\{d\varepsilon^p\} = \{d\varepsilon^{p1}\} + \{d\varepsilon^{p2}\} \tag{4.135}$$

$$\{d\sigma\} = \underline{C}^e \{d\varepsilon^e\} \tag{4.136}$$

Assuming both yield surfaces are active (which may not be the case), each of the two consistency conditions takes the form

$$df_j = \{\frac{\partial f_j}{\partial \sigma}\}^T \{d\sigma\} + \frac{\partial f_j}{\partial W^{pj}} \{\frac{\partial W^{pj}}{\partial \varepsilon^{pj}}\}^T \{d\varepsilon^{pj}\}$$

$$= \{\frac{\partial f_j}{\partial \sigma}\}^T \{d\sigma\} + h_j \frac{\partial f_j}{\partial W^{pj}} = 0, \quad (j = 1, 2; \text{ no sum}) \tag{4.137}$$

Now let

$$F_{ij} = \frac{\partial f_j}{\partial \sigma_i} \tag{4.138}$$

$$G_{ij} = \frac{\partial g_j}{\partial \sigma_i} \tag{4.139}$$

Then

$$\{d\varepsilon^p\} = \underline{G} \{d\lambda\} \tag{4.140}$$

In addition, let

$$D_{ij} = h_i \frac{\partial f_j}{\partial W^{pj}} \delta_{ij} \qquad \text{(no sum)} \tag{4.141}$$

Equation (4.137) can now be written for a strain controlled condition in the form

$$\{df\} = \underline{F}^T \{d\sigma\} + \lceil D \rfloor \{d\lambda\}$$

$$= \underline{F}^T \underline{C}^e \{\{d\varepsilon\} - \underline{G} \{d\lambda\}\} + \lceil D \rfloor \{d\lambda\} = \{0\} \quad (4.142)$$

and Equation (4.142) can be solved for $\{d\lambda\}$.

$$\{d\lambda\} = (\underline{F}^T \underline{C}^e \underline{G} - \lceil D \rfloor)^{-1} \underline{F}^T \underline{C}^e \{d\varepsilon\} \quad (4.143)$$

To determine whether both yield surfaces are active, we examine the plastic work increments,

$$dW^{pj} = h_j d\lambda_j \qquad (j=1, 2; \text{ no sum}) \quad (4.144)$$

Now let

$$h_{ij} = h_i \delta_{ij} \qquad (\text{no sum}) \quad (4.145)$$

Then Equation (4.144) can be written in the form

$$\{dW^p\} = \lceil h \rfloor \{d\lambda\} = \{\lceil h \rfloor (\underline{F}^T \underline{C}^e \underline{G} - \lceil D \rfloor)^{-1} \underline{F}^T \underline{C}^e\} \{d\varepsilon\} = \underline{Q} \{de\} \quad (4.146)$$

where

$$\underline{Q} = \lceil h \rfloor (\underline{F}^T \underline{C}^e \underline{G} - \lceil D \rfloor)^{-1} \underline{F}^T \underline{C}^e \quad (4.147)$$

The Q matrix is 2 x 6, which means that Equation (4.146) requires the total strain increment vector $\{d\varepsilon\}$ to have positive dot products with both the vectors $\lfloor Q \rfloor_1$ and $\lfloor Q \rfloor_2$ in order for both yield surfaces to be active. This requirement is shown graphically in Figure 4.6. The $\underline{Q}$ matrix depends only on the current stress and both the collapse and expansive plastic work. Thus it is possible to tell beforehand whether a given total strain increment will cause both yield surfaces to be active, when the current stress point lies on the intersection of the two current yield surfaces.

If $\vec{d\varepsilon} \cdot \vec{Q}_1$ and $\vec{d\varepsilon} \cdot \vec{Q}_2$ are not both positive, then each yield surface must be examined separately to see whether it is active alone.

Thus there are four possibilities, as shown below. However, it is not

		Surface 2(P)	
		Active	Inactive
Surface 1 (C)	Active	CP	C
	Inactive	P	E

clear from a comparison of Equations (4.72) and (4.143) that the outcome of the above tests will be unique, unless the matrix $\underline{F}^T\underline{C}^e\underline{G}$ is diagonal.

Provided both yield surfaces are active, substitution of Equations (4.134), (4.140) and (4.143) into Equation (4.136) yields

$$\{d\sigma\} = \underline{C}^e \{d\varepsilon^e\} = \underline{C}^e \{\{d\varepsilon\} - \{d\varepsilon^p\}\} = \underline{C}^e \{\{d\varepsilon\} - \underline{G}\{d\lambda\}\}$$

$$= \underline{C}^e [\underline{I} - \underline{G}(\underline{F}^T\underline{C}^e\underline{G} - \Gamma_D)^{-1} \underline{F}^T\underline{C}^e] \{d\varepsilon\} = \underline{C}^{ep} \{d\varepsilon\} \qquad (4.148)$$

where the elastoplastic incremental stiffness matrix, $\underline{C}^{ep}$, is

$$\underline{C}^{ep} = \underline{C}^e - \underline{C}^e\underline{G}(\underline{F}^T\underline{C}^e\underline{G} - \Gamma_D)^{-1} \underline{F}^T\underline{C}^e \qquad (4.149)$$

Figures 4.7 through 4.11 show stress-strain curves for Antelope Valley Sand using the Lade model, computed by the ARA Soil Element Model (SEM) program using model parameters given by [Lade (1981)]. Figure 4.7 shows hydrostatic compression with unloading and reloading. Since Lade's model unloads and reloads elastically, it does not show hysteresis. The elastic moduli are independent of strain, so the two unloading lines in Figure 4.7 are parallel. Figure 4.8 shows uniaxial compression with unloading. Figures 4.9, 4.10 and 4.11 show curves for three isotropically consolidated drained triaxial compression tests, at constant cell pressure equal to the consolidation stress. Figure 4.9 shows plots of principal stress difference versus axial strain. Since the three samples were at

the same void ratio prior to consolidation, the sample subjected to the lowest consolidation stress (14 psi) behaved as a dense sand, increasing in volume for axial strains larger than about 5.5 percent. The sample subjected to the highest consolidation stress (71 psi) behaved as a loose sand, decreasing in volume throughout shear. Figure 4.10 shows volumetric strain plotted against axial strain, and Figure 4.11 shows the hydrostatic component of stress plotted against volumetric strain. Figures 4.7 and 4.11 would be identical if the soil were linearly elastic. Obviously it is not. Comparison of these two figures emphasizes the stress path dependence of the stress-strain behavior of Antelope Valley Sand.

4.13 Model Development

The modified Lade model discussed above is a partly nonassociative, isotropic hardening elastoplastic model, with both yield functions and both plastic potential functions related to stress through the total stress invariants, I_1, I_2, and I_3. Using the total stress invariants has the mathematical advantage that differentiation with respect to total stress is straightforward. However, Lade's model has the disadvantages that it cannot, in general, achieve an exact fit to different friction angles in triaxial compression and extension, and the total stress invariants, I_2 and I_3, lack a simple physical interpretation.

In contrast to the above situation, octahedral strength plots of the type shown in Figures 3.7 through 3.26 and Figures 4.3 through 4.5 do have a simple physical interpetation. They relate $\bar{\phi}$ and μ; or τ_{oct} and ω; or J_2 and J_3, where J_2 and J_3 are the second and third deviator stress invariants, arising in the solution of the principal stress characteristic equation. Thus the question naturally arises whether it

might be more convenient, especially from the standpoint of physical interpretation, to make the yield and potential functions explicitly depend on I_1, J_2, and J_3, rather than on I_1, I_2, and I_3.

First of all, it is well known that the plastic work increment, dW^p, can be expressed as the sum of a volumetric term and a deviatoric or distortional term. This is done by defining the stress deviator components, s_{ij}, and plastic strain deviator components, e^p_{ij}, by the equations

$$s_{ij} = \sigma_{ij} - \frac{\sigma_{kk}}{3}\delta_{ij} \tag{4.150}$$

$$e^p_{ij} = \varepsilon^p_{ij} - \frac{\varepsilon^p_{kk}}{3}\delta_{ij} \tag{4.151}$$

The expression for the plastic work increment can now be written in the form

$$dW^p = \sigma_{ij}d\varepsilon^p_{ij} = (s_{ij} + \frac{\sigma_{kk}}{3}\delta_{ij})(de^e_{ij} + \frac{d\varepsilon^p_{mm}}{3}\delta_{ij})$$

$$= \frac{\sigma_{kk}}{3}d\varepsilon^p_{mm} + s_{ij}de^p_{ij} \tag{4.152}$$

The first term in Equation (4.152) is the volumetric plastic work increment; the second term is the deviatoric or distortional plastic work increment. So far, so good; Equation (4.152) suggests that relating f and g to volumetric and distortional invariants has a physical basis.

The main question, then, is whether the flow rule will have a convenient mathematical form if we write

$$g = g(I_1, J_2, J_3) \tag{4.153}$$

In place of Equation (4.18), we can write

$$d\varepsilon_{ij}^{p} = d\lambda\left(\frac{\partial g}{\partial I_1}\frac{\partial I_1}{\partial \sigma_{ij}} + \frac{\partial g}{\partial J_2}\frac{\partial J_2}{\partial s_{kl}}\frac{\partial s_{kl}}{\partial \sigma_{ij}} + \frac{\partial g}{\partial J_3}\frac{\partial J_3}{\partial s_{kl}}\frac{\partial s_{kl}}{\partial \sigma_{ij}}\right) \tag{4.154}$$

where

$$\frac{\partial I_1}{\partial \sigma_{ij}} = \delta_{ij} \tag{4.19}$$

and by analogy with Equations (4.20) and (4.23).

$$\frac{\partial J_2}{\partial s_{kl}} = s_{lk} = s_{kl} \tag{4.155}$$

$$\frac{\partial J_3}{\partial s_{kl}} = S_{kl} \tag{4.156}$$

and from Equation (4.150)

$$\frac{\partial s_{kl}}{\partial \sigma_{ij}} = \delta_{ik}\delta_{jl} - \frac{1}{3}\delta_{kl}\delta_{ij} \tag{4.157}$$

Equation (4.54) can now be written in the form

$$\begin{aligned} d\varepsilon_{ij}^{p} &= d\lambda\left[\frac{\partial g}{\partial I_1}\delta_{ij} + \left(\frac{\partial g}{\partial J_2}\right)(s_{lk})\left(\delta_{ik}\delta_{jl} - \frac{1}{3}\delta_{kl}\delta_{ij}\right)\right. \\ &\quad \left. + \left(\frac{\partial g}{\partial J_3}\right)(S_{kl})\left(\delta_{ik}\delta_{jl} - \frac{1}{3}\delta_{kl}\delta_{ij}\right)\right] \\ &= d\lambda\left[\frac{\partial g}{\partial I_1}\delta_{ij} + \frac{\partial g}{\partial J_2}s_{ij} + \frac{\partial g}{\partial J_3}\left(S_{ij} - \frac{J_2}{3}\delta_{ij}\right)\right] \end{aligned} \tag{4.158}$$

Equation (4.158) yields the volumetric plastic strain increment,

$$d\varepsilon_{ii}^{p} = d\lambda\left(3\frac{\partial g}{\partial I_1}\right) = d\lambda\left(\frac{\partial g}{\partial \sigma_{oct}}\right) \tag{4.159}$$

so that the deviatoric plastic strain increments are

$$de_{ij}^{p} = d\varepsilon_{ij}^{p} - \frac{d\varepsilon_{kk}^{p}}{3}\delta_{ij}$$

$$= d\lambda\left[\frac{\partial g}{\partial J_2} s_{ij} + \frac{\partial g}{\partial J_3}\left(S_{ij} - \frac{J_2}{3}\delta_{ij}\right)\right] \tag{4.160}$$

Equation (4.160) seems workable enough, so we proceed to investigate the form of the expression for the plastic work increment, dW^p.

Equation (4.152) yields

$$dW^p = d\lambda\left[\frac{\partial g}{\partial I_1} I_1 + \left(2\frac{\partial g}{\partial J_2} J_2 + 3\frac{\partial g}{\partial J_3} J_3\right)\right] \tag{4.161}$$

The first term in brackets on the RHS of Equation (4.161) is the volumetric term; the last two terms comprise the distortional term. Equation (4.31) thus has two alternate forms:

$$h = \frac{\partial g}{\partial I_1} I_1 + 2\frac{\partial g}{\partial I_2} I_2 + 3\frac{\partial g}{\partial I_3} I_3$$

$$= \frac{\partial g}{\partial I_1} I_1 + 2\frac{\partial g}{\partial J_2} J_2 + 3\frac{\partial g}{\partial J_3} J_3 \tag{4.162}$$

which means that

$$2\frac{\partial g}{\partial I_2} I_2 + 3\frac{\partial g}{\partial I_3} I_3 = 2\frac{\partial g}{\partial J_2} J_2 + 3\frac{\partial g}{\partial J_3} J_3 \tag{4.163}$$

Thus, there appears to be no reason for not using J_2 and J_3 instead of I_2 and I_3 in the formulation of the yield and potential functions, and good physical justification for doing so.

The proposed expansive yield criterion is of the form of Equation (4.123), i.e.

$$f_p = f_p'(\sigma_{oct}, J_2, J_3) - f_p''(W_p) = 0 \tag{4.164}$$

where

$$f_p' = \left(\frac{\tau_{oct}}{p_a}\right)(1 - e \cos 3\omega)\left(\frac{p_a}{\sigma_{oct}} + b\right) \tag{4.165}$$

$$f_p'' = a \qquad \text{at failure} \tag{4.166}$$

p_a = atmospheric pressure

At failure, substitution of Equations (4.165) and (4.166) into Equation (4.164) yields

$$\left(\frac{\tau_{oct}}{p_a}\right)(1 - e \cos 3\omega) = \frac{a}{\frac{p_a}{\sigma_{oct}} + b} = \frac{a\left(\frac{\sigma_{oct}}{p_a}\right)}{1 + b\left(\frac{\sigma_{oct}}{p_a}\right)} \tag{4.167}$$

The parameters a, b, and e can be determined from a series of triaxial compression and extension tests. For triaxial compression ($\omega = 120^\circ$), Equation (4.167) reduces to

$$\frac{\tau_{oct}}{p_a} = \frac{\left(\frac{a}{1 - e}\right)\left(\frac{\sigma_{oct}}{p_a}\right)}{1 + b\left(\frac{\sigma_{oct}}{p_a}\right)}$$

or

$$\frac{\sigma_{oct}}{\tau_{oct}} = \frac{1 - e}{a}\left[1 + b\left(\frac{\sigma_{oct}}{p_a}\right)\right] = k_{ic} + k_{2c}\left(\frac{\sigma_{oct}}{p_a}\right) \tag{4.168}$$

where

$$k_{ic} = \frac{1 - e}{a} \tag{4.169}$$

$$k_{2c} = b\left(\frac{1 - e}{a}\right) \tag{4.170}$$

For triaxial extension ($\omega = 60^\circ$), Equation (4.167) reduces to

$$\frac{\tau_{oct}}{p_a} = \frac{\left(\frac{a}{1+e}\right)\left(\frac{\sigma_{oct}}{p_a}\right)}{1 + b\left(\frac{\sigma_{oct}}{p_a}\right)}$$

or

$$\frac{\sigma_{oct}}{\tau_{oct}} = \frac{1+e}{a}\left[1 + b\left(\frac{\sigma_{oct}}{p_a}\right)\right] = k_{1e} + k_{2e}\left(\frac{\sigma_{oct}}{p_a}\right) \tag{4.171}$$

where

$$k_{1e} = \frac{1+e}{a} \tag{4.172}$$

$$k_{2e} = b\left(\frac{1+e}{a}\right) \tag{4.173}$$

Plots of Equations (4.168) and (4.171) are shown in Figure 4.12. Such plots are often referred to as Southwell plots [Timoshenko and Gere (1961:191)]. Having determined the parameters k_{1c}, k_{2c}, k_{1e}, and k_{2e}, the parameter b can be calculated from the expressions

$$b = \frac{k_{2c}}{k_{1c}} = \frac{k_{2e}}{k_{1e}} \tag{4.174}$$

which provides a consistency check. The parameters a and e can be calculated from Equations (4.169) and (4.172), written in the form

$$k_{1c}a + e = 1$$

$$k_{1e}a - e = 1$$

so that

$$a = \frac{2}{k_{1e} + k_{1c}} \tag{4.175}$$

$$e = 1 - k_{1c}a = 1 - \frac{2k_{1c}}{k_{1c} + k_{1e}} = \frac{k_{1e} - k_{1c}}{k_{1e} + k_{1c}} \tag{4.176}$$

Having calculated the parameters a and b (and e) from triaxial compression and extension tests, the accuracy of the assumed octahedral cross-sect[illegible]orm can be investigated by a series of true triaxial tests. If, in Equation (4.167) we set

$$\frac{a}{1 + b\left(\frac{\sigma_{oct}}{p_a}\right)} = p \tag{4.177}$$

then Equation (4.167) can be written in the form

$$\frac{\tau_{oct}}{\sigma_{oct}} = \frac{p}{1 - e\cos 3\omega} \tag{4.178}$$

which is the equation for an ellipse in polar coordinates.
Equation (4.178) can be written in a linear form to obtain the octahedral eccentricity, e, as a consistency check on the previously determined value from Equation (4.176)

$$\frac{p\sigma_{oct}}{\tau_{oct}} = 1 - e\cos 3\omega \tag{4.179}$$

A plot of Equation (4.179) is shown in Figure 4.13

Octahedral cross-section data for the case ($b = o$; $\bar{\phi}_c = 32^\circ$; $\bar{\phi}_e = 35^\circ$) are tabulated in Table 4.2 and plotted in Figure 4.13. The calculation sequence used to obtain the values shown in Table 4.2 and Figure 4.13 is as follows

$$\tan \omega_2 = \frac{\sqrt{3}}{\mu} \tag{4.180}$$

$$z_c = \frac{2\sqrt{2}\sin\bar{\phi}_c}{3 - \sin\bar{\phi}_c} \tag{4.181}$$

$$z_e = \frac{2\sqrt{2}\sin\bar{\phi}_e}{3 + \sin\bar{\phi}_e} \tag{4.182}$$

$$a = \frac{2z_c z_e}{z_c + z_e} \tag{4.183}$$

$$e = \frac{z_c - z_e}{z_c + z_e} \tag{4.184}$$

$$z = \frac{a}{1 - e\cos 3\omega_2} \tag{4.185}$$

$$\sin \bar{\phi} = \frac{\sqrt{3}\, z \sin\omega_2}{2 - z\cos\omega_2} \tag{4.186}$$

The forms of the compressive yield criterion (cap), and the plastic potential functions for the proposed model are yet to be determined, and will be the object of major effort during FY84.

5.0 SUMMARY

Recognizing the load-deformation response of a soil mass is governed by effective stress, this report begins by developing the general equations for dynamic response of a saturated soil element. Particular attention is paid to the physical significance of the parameters and the equations. These equations are the framework into which a soil constitutive model must fit. As an example of the application of the general equations, the problem of determining incremental total stress moduli for static undrained (no flow) conditions is examined, for both isotropic (hydrostatic) and constrained (one-dimensional) compression. The results for isotropic compression agree with those of Gassmann. The results for constrained compression should be useful for studies of soil liquefaction under explosive or earthquake loading.

Types of soil stress-strain behavior observed in tests are examined, to see what features a dynamic soil constitutive model should possess. Included are effective stress dependence, nonlinearity, stress path dependence, dilatancy, criticial state behavior at large shear strains, peak strength behavior (or lack of it), influence of the intermediate principal stress on shear stength, low tensile strength, inelasticity, nonassociated plastic behavior, the Baushinger effect, rate dependence, hysteresis, decrease of damping with the number of cycles of reversed loading, anisotropy, and sample disturbance.

The soil constitutive model proposed for complex dynamic loading is an isotropic, strain hardening elastoplastic model. The basic equations of elastoplaticity are developed in this report for the purpose of emphasizing their logical structure. A direct (non-iterative) solution is

developed for the case of mixed boundary conditions, because several of the most common laboratory soil tests are of this type (e.g. strain-controlled triaxial compression and confined or uniaxial compression), and also because mixed boundary values occur frequently in dynamic finite difference and finite element computer calculations of the type in which the proposed model will be used. Criteria for distinguishing between loading and unloading are carefully examined, because of the oscillatory nature of soil stress-strain response under explosive and earthquake loading.

The proposed model shear failure criterion has the following convenient features:

1. It is related to stress through the first total stress invariant and the second and third deviator stress invariants, each of which has a simple physical interpretation.
2. Its parameters can be determined from simple linear plots.
3. The model can match unequal friction angles in triaxial compression and extension.
4. The ratio of octahedral shear to octahedral normal stress can be calculated directly (without iteration) when the value of Lode's parameter is known.

Other features of the model are yet to be determined.

The objectives of the next year's effort are to complete the proposed model formulation, and to demonstrate its ability to reproduce important aspects of observed soil stress-strain behavior discussed in Section 3.

REFERENCES

Bell, J.M., "Stress Strain Characteristics of Cohesionless Granular Materials Subjected to Statically Applied Homogeneous Loads in an Open Stress System," Ph.D. Thesis, Cal. Tech., (1965).

Boker, R., "Die Mechanik der Bleibenden Formanderung in kristallinisch aufgebauten Korpern," MITTEILUNGEN UBER FORSCHUNGSARBEITEN AUF DEM GEBEITE DES INGENIEURWESSENS, Vol. 175/176, (1915), pp. 1-51.

Casagrande, A., "Characteristics of Cohesionless Soils Affecting the Stability of Slopes and Earth Fills," Journal of The Boston Society of Civil Engineers, Vol. 23, (January 1936), pp. 13-32; reprinted in CONTRIBUTIONS TO SOIL MECHANICS 1925-1940, BSCE, (1940), pp. 257-276.

Casbarian, A.O., "Effects of Rotation of the Principal Stress Axes and of the Intermediate Principal Stress on the Shear Strength of a Saturated Remolded Clay," Ph.D. Thesis, Cornell University, (1964).

Colemen, J.D., "Suction and the Yield and Failure Surface for Soil in the Principal Effective Stress Space," Geotechnique, Vol. 10, No. 4, (1960), pp. 181-183.

Dass, W.C., D.H. Merkle, and J.L. Bratton, "Fundamental Properties of Soils for Complex Dynamic Loadings: Dynamic Constitutive Modeling of Sandy Soils," Annual Technical Report No. 2, Applied Research Associates report to the Air Force Office of Scientific Research, (April 1983), 107 pp.

Drucker, D.C., "Relation of Experiments to Mathematical Theories of Plasticity," ASME Journal of Applied Mechanics, Vol. 16, (December 1949), pp. 349-357.

Drucker, D.C. and W. Prager, "Soil Mechanics and Plastic Analysis or Limit Design," Quarterly of Applied Mathematics, Vol. X, No. 2, (1952), pp. 157-165.

Gassmann, F., "Uber die Elastizitat Poroser Medien," VIERTELJAHRSSCHRIFT DER NATURFORSCHENDEN GESELLSCHAFT IN ZURICH, Jahrgang 96, Heft 1, (March 1951), pp. 1-23; see also E.L. Hamilton, "Elastic Properties of Marine Sediments," Journal of Geophysical Research, Vol. 76, No. 2, (January 1971), p. 583.

Green G.E. and Bishop, A.W., "A Note on the Strength of Sand Under Generalized Strain Conditions," Geotechnique, Vol. 19, No. 1, (1969), pp. 144-149.

Habib, P., "Influence of the Variation of the Intermediate Principal Stress on the Shearing Strength of Soils," Proc. 3rd ICSMFE, Vol. I, (1953), pp. 131-136, translated by Cadet K.R. King at the USAF Academy.

REFERENCES, Continued

Haythornthwaite, R.M., "Mechanics of Triaxial Test for Soils," ASCE Proc., Vol. 86, No. SM5, (1960), pp. 35-62.

Hill, R., The Mathematical Theory of Plasticity, Oxford University Press, (1950).

Kirkpatrick, W.M., "The Condition of Failure for Sands," Proc. 4th ICSMFE, Vol. I, (1957), pp. 172-178.

Kjellman, W., "Report on an Apparatus for Consumate Investigation of the Mechanical Properties of Soils," Proc. 1st ICSMFE, Vol. II, (1936), pp. 16-20.

Lade, P.V., "Model by Lade," Part 5 of Evaluation of Constitutive Parameters for Geologic Materials, Symposium on Implementation of Computer Procedures and Stress-Strain Laws in Geotechnical Engineering, Chicago, IL, (3-6 August 1981), edited by C.S. Desai, Acorn Press, (1981), pp. 5-1 through 5-24.

Lade, P.V., "The Stress-Strain and Strength Characteristics of Cohesionless Soils," Ph.D. Thesis, University of California at Berkeley, (August 1972), 765 pp.

Lade, P.V. and R.B. Nelson, "Incrementalization Procedure for Elasto-Plastic Constitutive Model with Multiple, Simultaneous Yield Surfaces," Implementation of Computer Procedures and Stress-Strain Laws in Geotechnical Engineering, edited by C.S. Desai and S.L. Saxena, Vol. II, Acorn Press, (August 1981), pp. 503-518.

Lambe, T.W. and R.V. Whitman, Soil Mechanics, Wiley, (1969).

Lenoe, E.M., "Deformation and Failure of Granular Media Under Three-Dimensional Stress," Experimental Mechanics, Vol. 6, No. 2, (1966), pp. 99-104.

Lomize, G.M. and Kryzhanovsky, A.L., "On The Strength of Sand," Proc. Oslo Geot. Conf., Vol. 1, (1967), pp. 215-219.

Malvern, L.E., Introduction to the Mechanics of a Continuous Medium, Prentice-Hall, (1969).

Merkle, D.H., "The Effective Stress Mechanics of Undrained Shear Strength," Ph.D. Thesis, MIT, (1971); published as Air Force Weapons Laboratory Report AFWL-TR-71-85, (July 1971), 802 pp.

Nadai, A., Theory of Flow and Fracture of Solids, Volume I, 2nd Edition, McGraw-Hill, (1950).

REFERENCES, Continued

Newmark, N.M., "Failure Hypotheses for Soils," opening address in Proceedings of the Research Conference on the Shear Strength of Cohesive Soils, ASCE, (1961), pp. 17-32.

Procter, D.C. and Barden, L., Correspondence on "A Note on the Drained Strength of Sand Under Generalized Strain Conditions," by G.E. Green and A.W. Bishop, Geotechnique, Vol. 19, No. 3, (1969), pp. 424-426.

Rutledge, P.C., "Theories of Failure of Materials Applied to the Shearing Resistance of Soils," presented at SPEE Civil Engineering Division Conference on Soil Mechanics at State College, PA; published in Proc. Conf. on Soil Mechanics and Its Application, Purdue University, (1940), pp. 191-204.

Saada, A.S. and Baah, A.K., "Deformation and Failure of a Cross Anisotropic Clay Under Combined Stresses," Soil Mech. Lab., Case Inst. of Techn., Cleveland, OH, (1966).

Shibata, T. and Karube, D., "Influence of the Variation of the Intermediate Principal Stress on the Mechanical Properties of Normally Consolidated Clay," Proc. 6th ISCMFE, Vol. I, (1965), pp. 359-363.

Skempton, A.W. and Sowa, V.A., "The Behavior of Saturated Clays During Sampling and Testing," Geotechnique, Vol. 13, No. 4, (1963), pp. 269-290.

Sowa, V.A., "A Comparision of the Effects of Isotropic and Anisotropic Consolidation on the Shear Behavior of a Clay," Ph.D. Thesis, Univ. of London, (1963).

Timoshenko, S.P., Strength of Materials, Part II, Advanced Theory and Problems, 3rd Edition, (1956).

Timoshenko, S.P. and J.M. Gere, Theory of Elastic Stability, 2nd Edition, McGraw-Hill, (1961).

Topping, A.D., "The Use of Experimental Constants in the Application of Theories of Strength to Rock," Proc. 2nd Midwest Conf. on Solid Mech., (1955), pp. 178-192.

von Karman, T., "Festigkeitsversuche unter allseitigem Druck," ZEITSCRIFT DES VEREINS DEUTSCHER INGENIEURE, Vol. 55, (1911), pp. 1749-1757.

Wade, N.H., "Plane Strain Failure Characteristics of a Saturated Clay," Ph.D. Thesis, Univ. of London, (1963).

Wood, C.C., "Shear Strength and Volume Change Characteristics of Compacted Soil Under Conditions of Plane Strain," Ph.D. Thesis, Univ. of London, (1958).

REFERENCES, Concluded

Wu, T.H., Loh, A.K., and Malvern, L.E., "Study of Failure Envelope of Soils," ASCE Proc., Vol. 89, No. SM1, (1963), pp. 145-181.

Yong, R.N. and Warkentin, B.P., Introduction to Soil Behavior, Macmillian, (1966).

Zienkiewicz, O.C. and P. Bettess, "Soils and Other Saturated Media Under Transient, Dynamic Conditions; General Formulation and the Validity of Various Simplifying Assumptions," Chapter 1 in Soil Mechanics-Transient and Cyclic Loads, edited by O.C. Zienkiewicz and G.N. Pande, Wiley, (1982), pp. 1-16.

TABLE 4.1

LADE FAILURE SURFACE OCTAHEDRAL CROSS-SECTION
FOR $\bar{\phi}_c$ = 30 DEGREES

$\omega 2$	μ	z	$\sin \bar{\phi}$
DEG			
120	-1.000	0.56569	0.500
115	-0.808	0.56149	0.534
110	-0.630	0.55012	0.559
105	-0.464	0.53434	0.576
100	-0.305	0.51694	0.586
95	-0.152	0.49991	0.592
90	0.000	0.48442	0.594
85	0.152	0.47071	0.591
80	0.305	0.45893	0.587
75	0.464	0.44949	0.579
70	0.630	0.44263	0.570
65	0.808	0.43847	0.560
60	1.000	0.43708	0.548

$$\mu = \frac{\sqrt{3}}{\tan \omega}$$

$$\sin \bar{\phi} = \frac{\sqrt{3}\, z \sin \omega}{\sqrt{2} - z \cos \omega}$$

TABLE 4.2

PROPOSED FAILURE SURFACE OCTAHEDRAL CROSS-SECTION
FOR (b = 0; $\bar{\phi}_c$ = 32 DEGREES; $\bar{\phi}_e$ = 35 DEGREES)

μ	ω_2	z	sin ϕ
-1.0	120.000	0.60679	0.530
-0.9	117.457	0.60589	0.550
-0.8	114.791	0.60304	0.569
-0.7	112.006	0.59810	0.586
-0.6	109.107	0.59105	0.602
-0.5	106.102	0.58198	0.614
-0.4	103.004	0.57118	0.625
-0.3	99.826	0.55901	0.632
-0.2	96.587	0.54597	0.636
-0.1	93.304	0.53259	0.637
0	90.000	0.51938	0.636
0.1	86.696	0.50681	0.633
0.2	83.413	0.49526	0.628
0.3	80.174	0.48500	0.622
0.4	76.996	0.47620	0.615
0.5	73.898	0.46894	0.608
0.6	70.893	0.46321	0.600
0.7	67.994	0.45897	0.593
0.8	65.209	0.45610	0.586
0.9	62.543	0.45449	0.580
1.0	60.000	0.45398	0.574

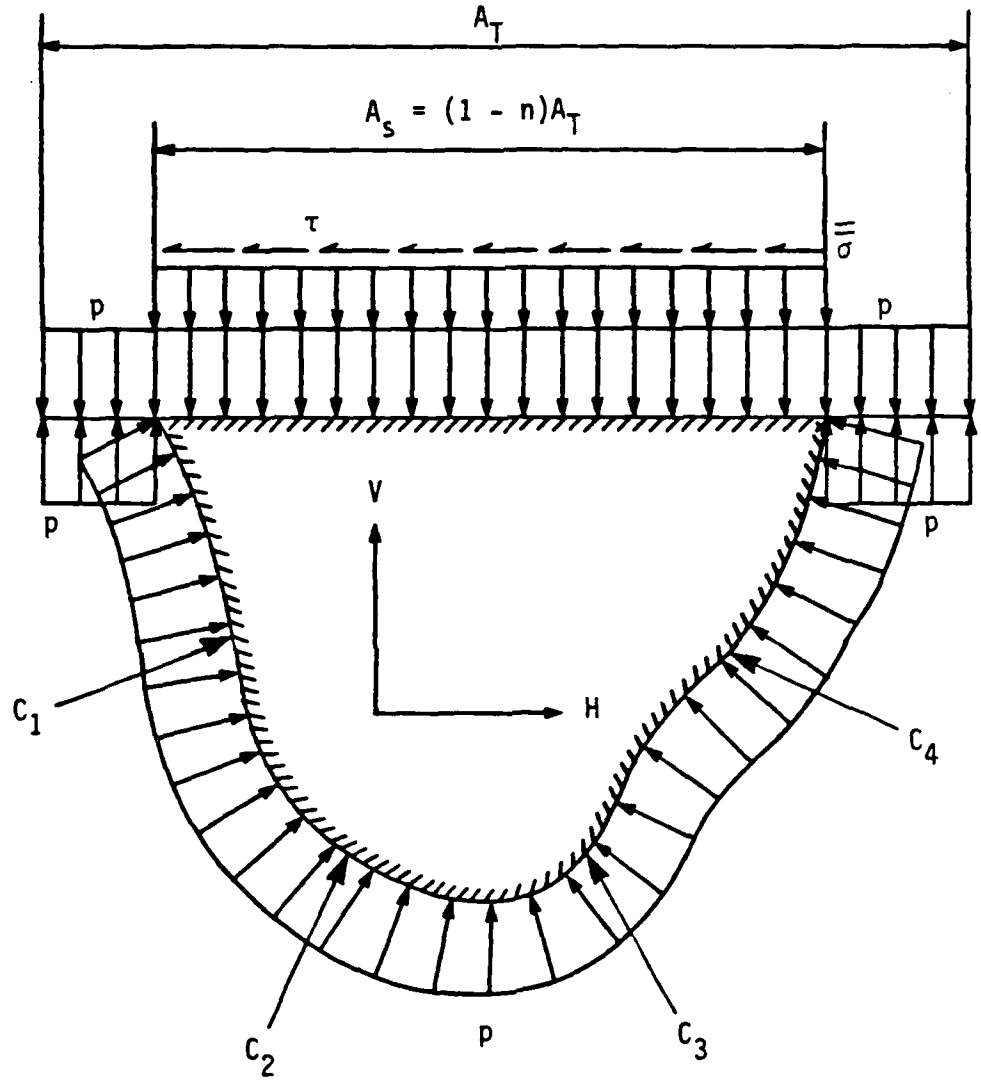

Figure 2.1 Free Body Diagram for Definition of Effective Stress in Soil.

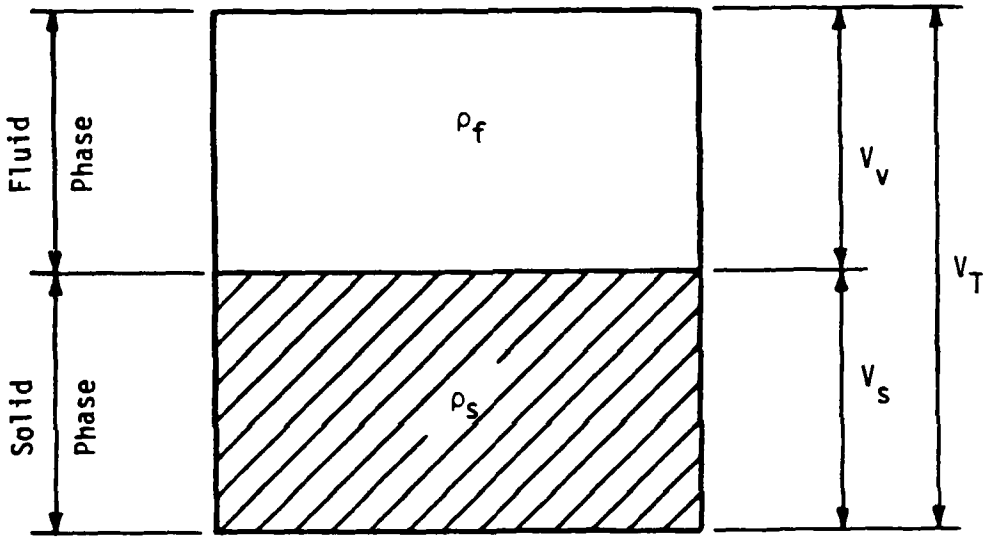

$$\frac{V_v}{V_T} = n$$

$$\frac{V_s}{V_T} = 1 - n$$

Figure 2.2. Saturated Soil Phase Diagram.

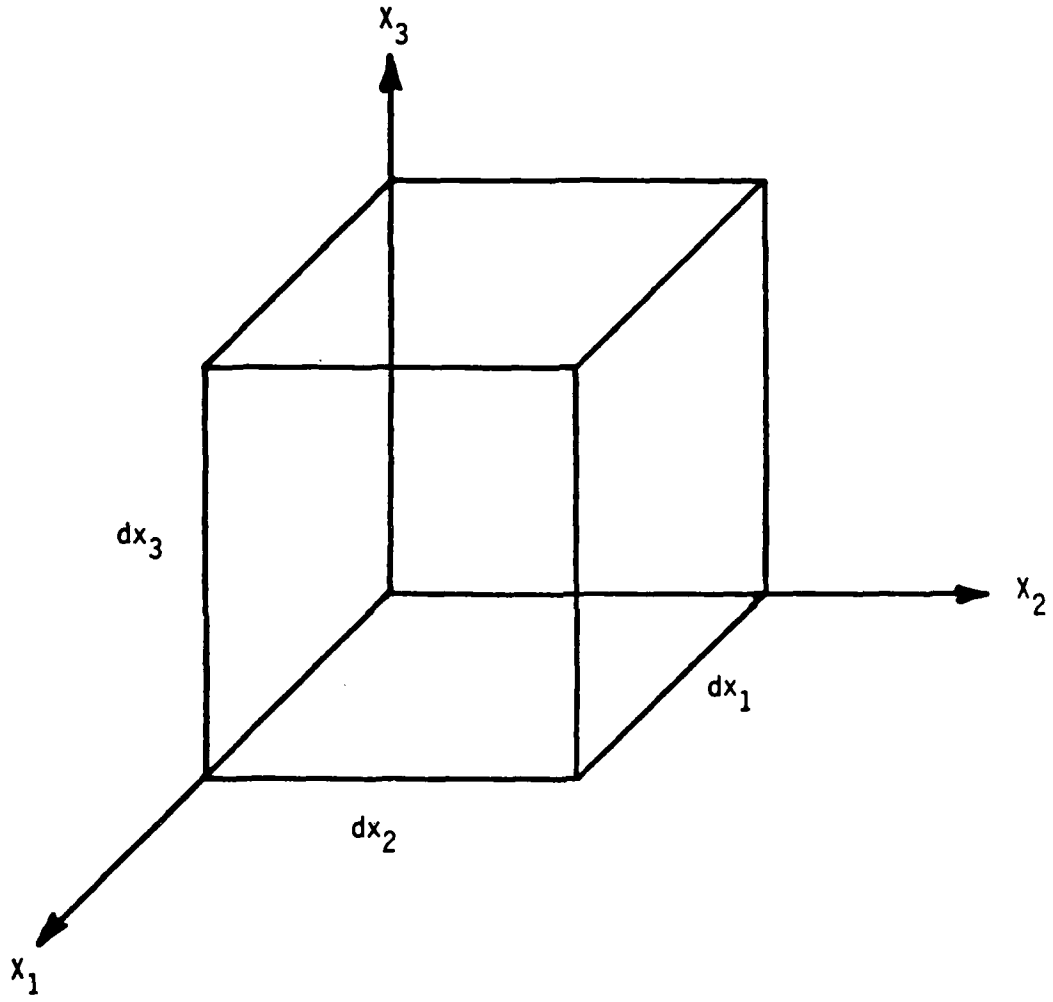

Figure 2.3. Soil Element Used in Deriving Basic Equations.

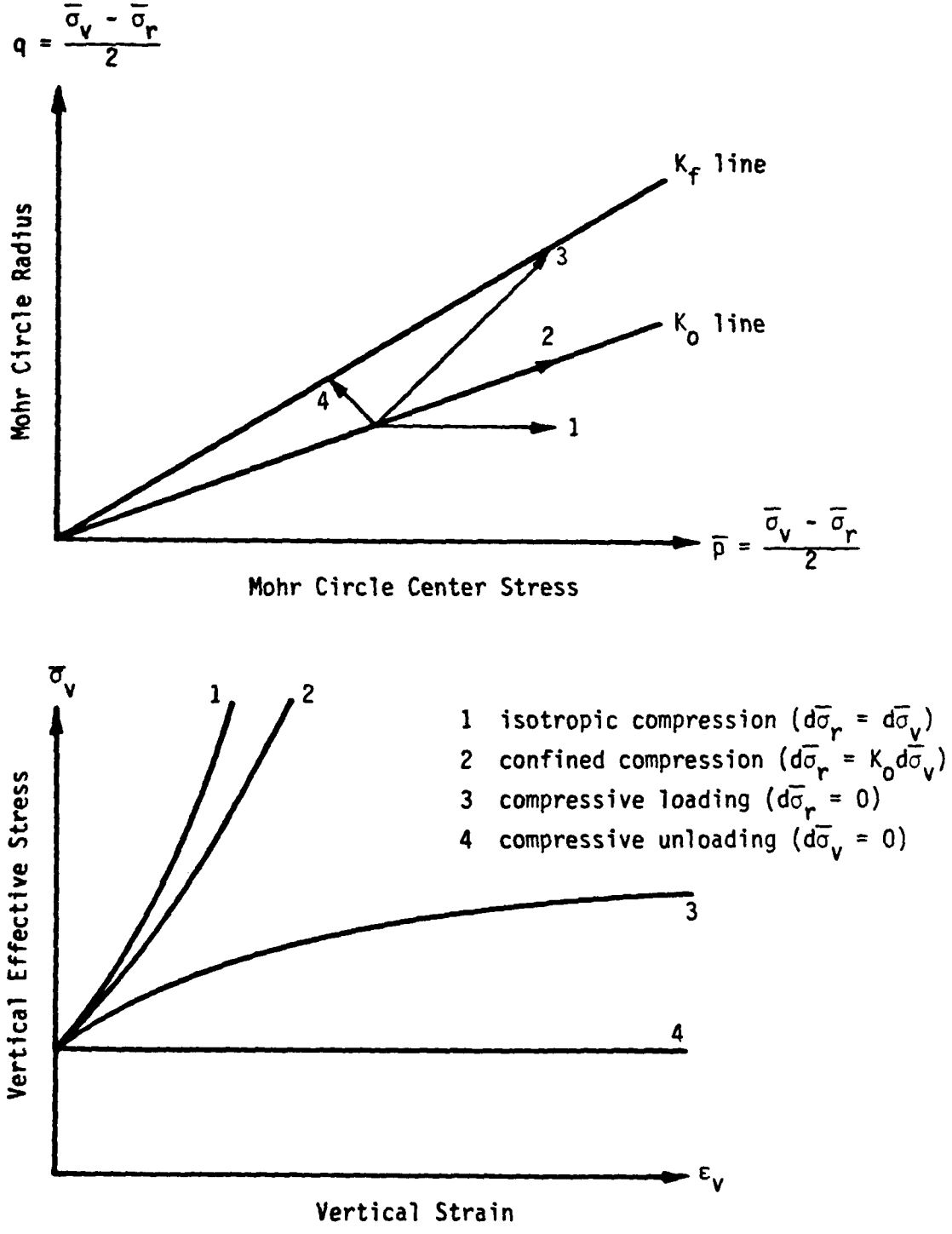

Figure 3.1. Influence of Effective Stress Path on Stress-Strain Curve Nonlinearity [after Lambe and Whitman (1969: 120, 129, 325)].

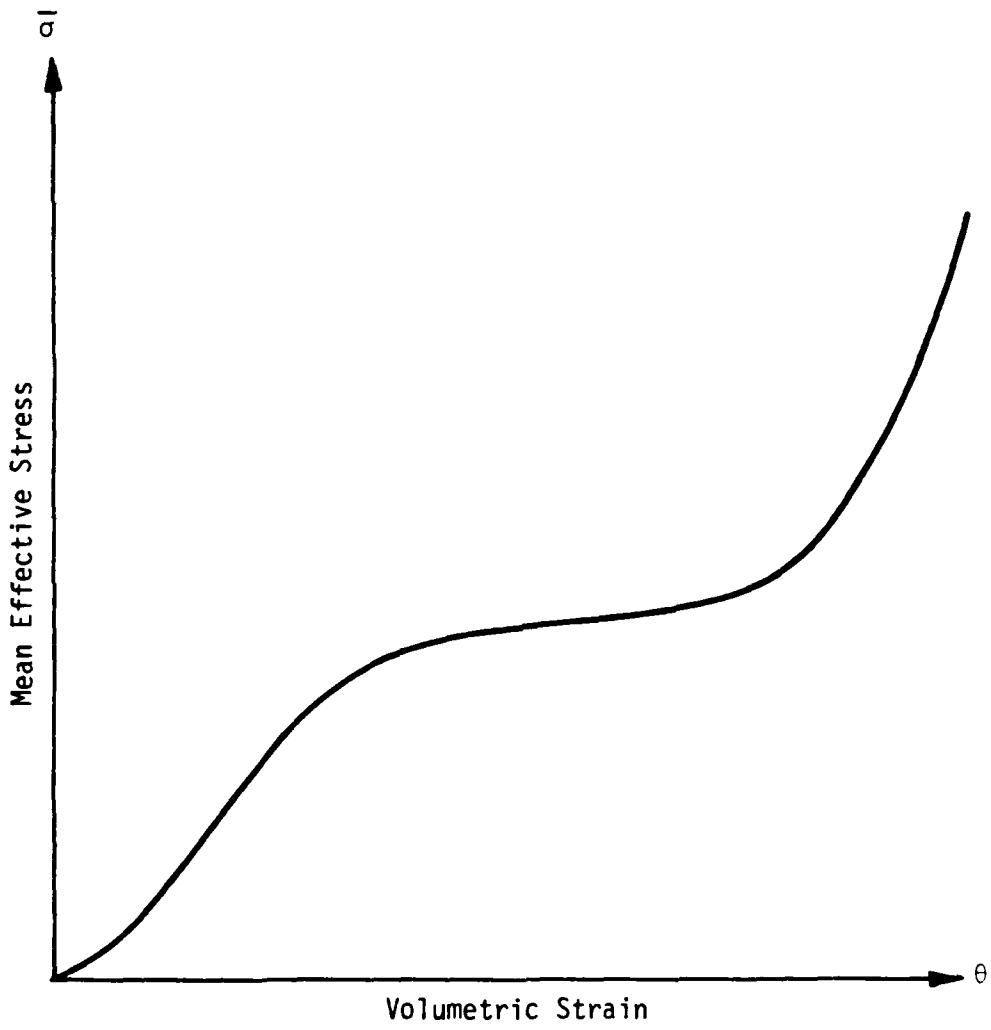

Figure 3.2 Compressive Stress-Strain Curve Exhibiting Yielding Due to Grain Crushing at Interparticle Contacts [after Lambe and Whitman (1969:298)].

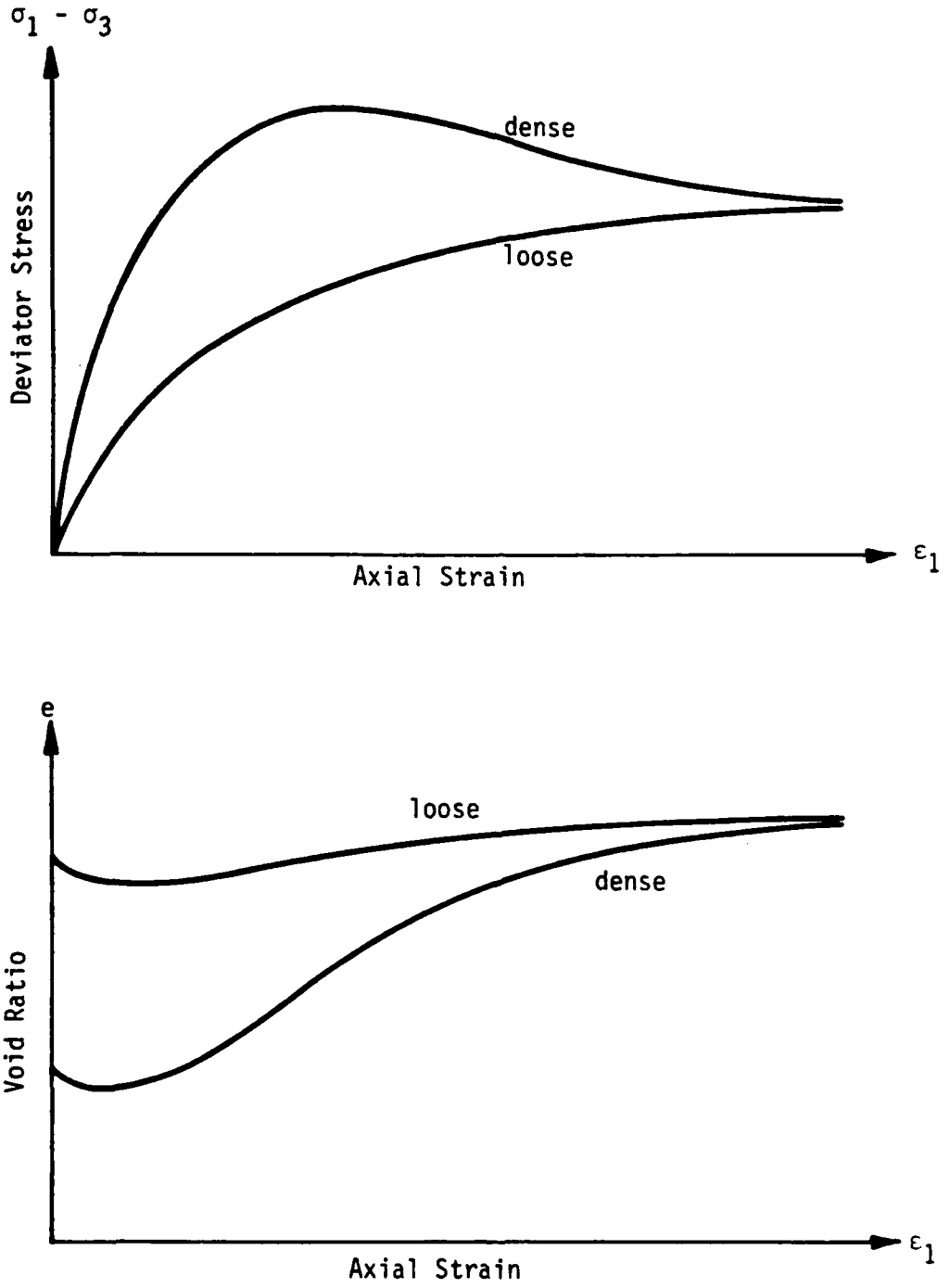

Figure 3.3 Drained Stress-Strain Curves for Loose and Dense Samples of the Same Sand, Under the Same Constant Confining Pressure [after Lambe and Whitman (1969:131)].

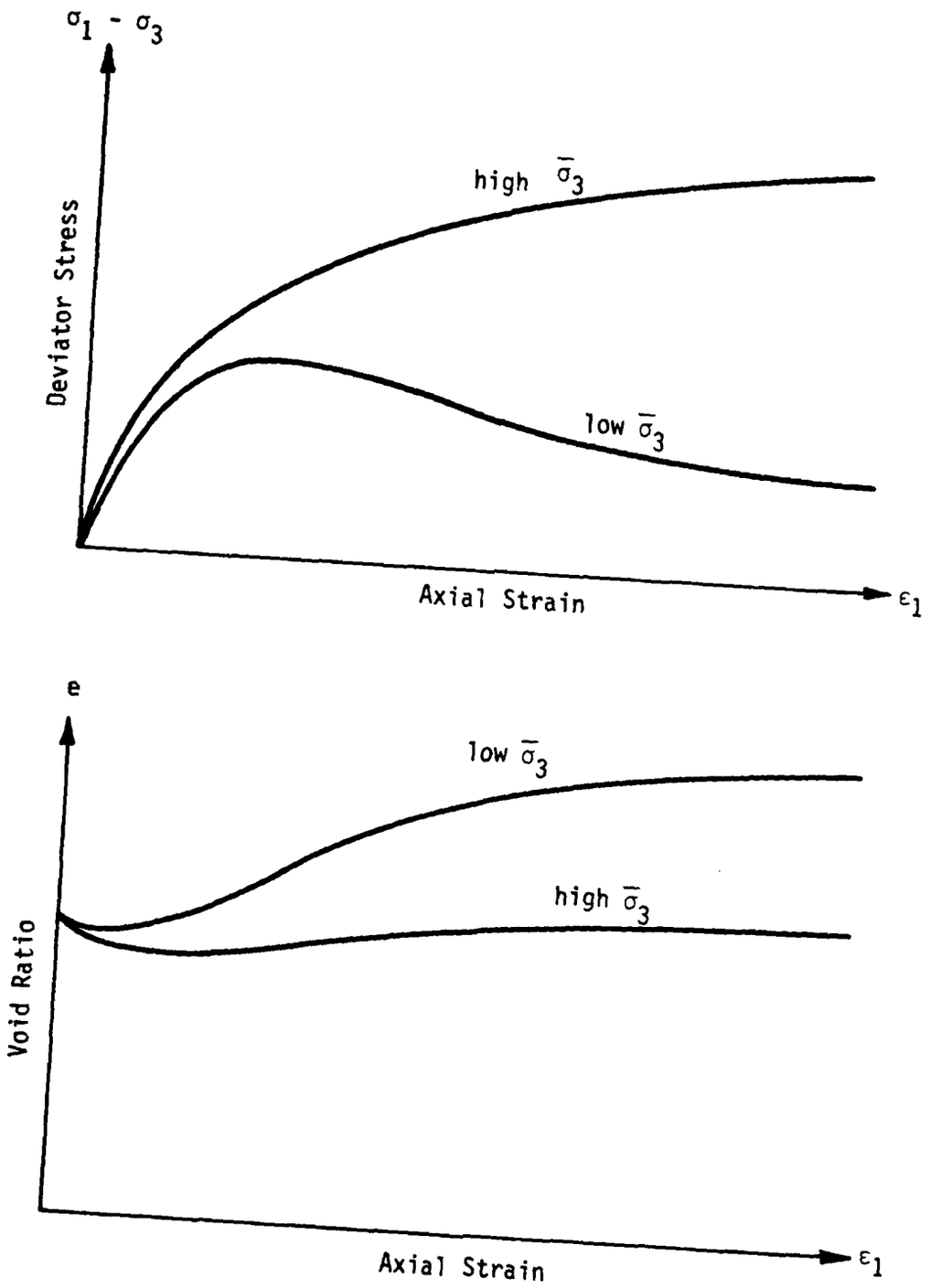

Figure 3.4. Drained Stress-Strain Curves for a Sand at the Same Initial Void Ratio, Under High and Low Constant Confining Pressures [after Lambe and Whitman (1969: 131)].

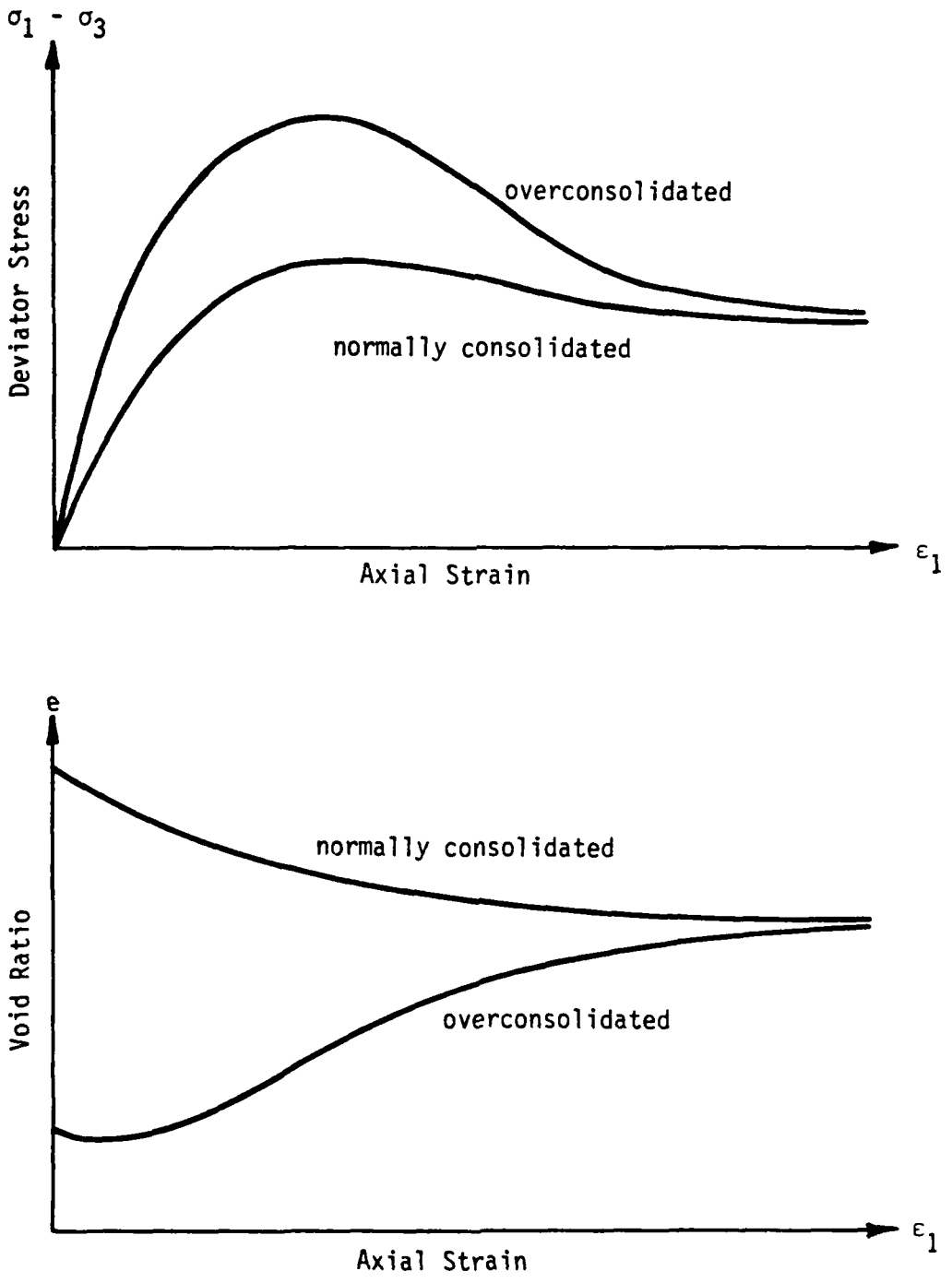

Figure 3.5. Drained Stress-Strain Curves for Normally Consolidated and Overconsolidated Samples of the Same Clay, Under the Same Constant Confining Pressure [after Lambe and Whitman (1969:302, 312)].

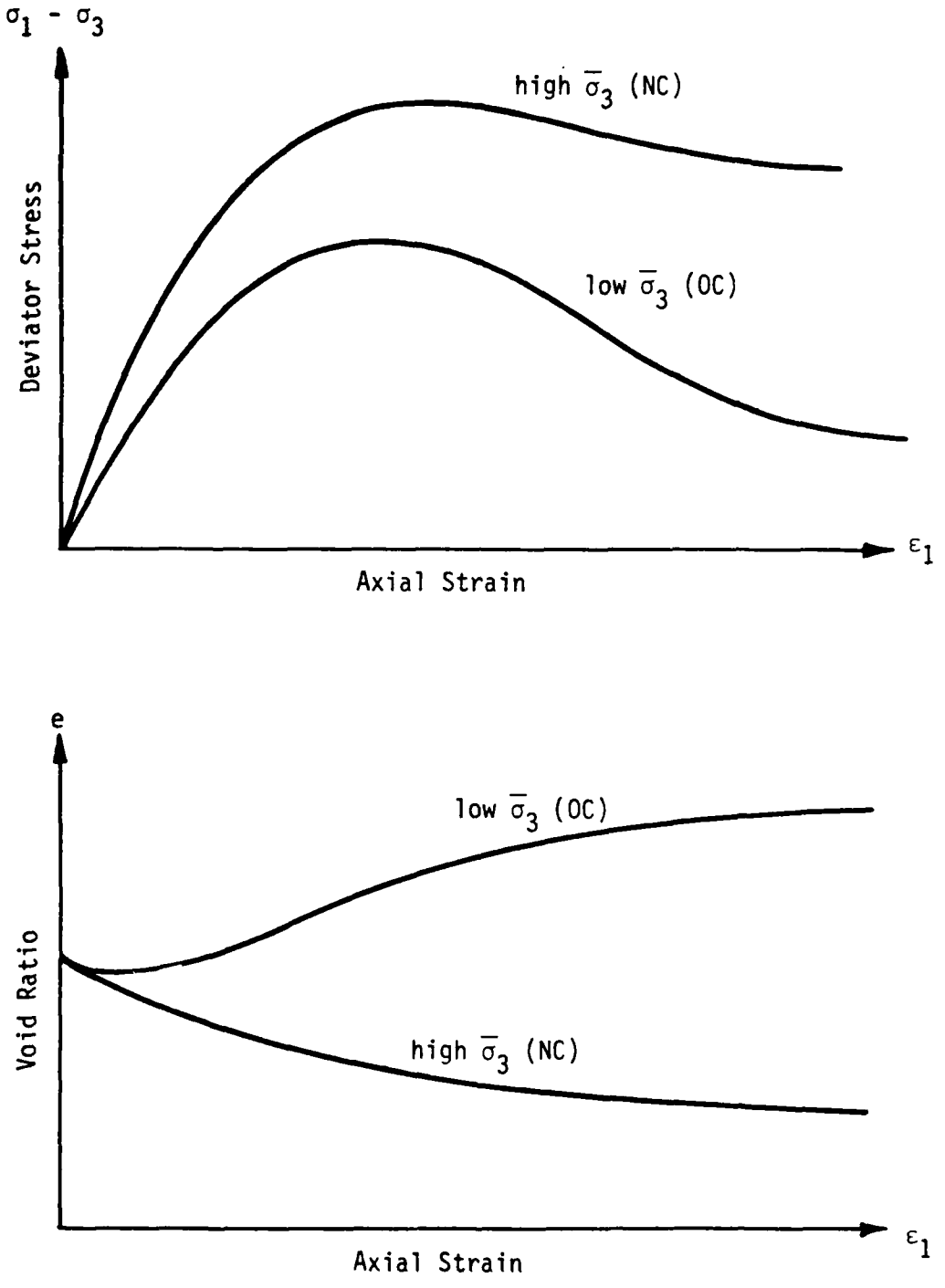

Figure 3.6. Drained Stress-Strain Curves for a Clay at the Same Initial Void Ratio, Under High and Low Constant Confining Pressures [after Lambe and Whitman (1969:302, 312)].

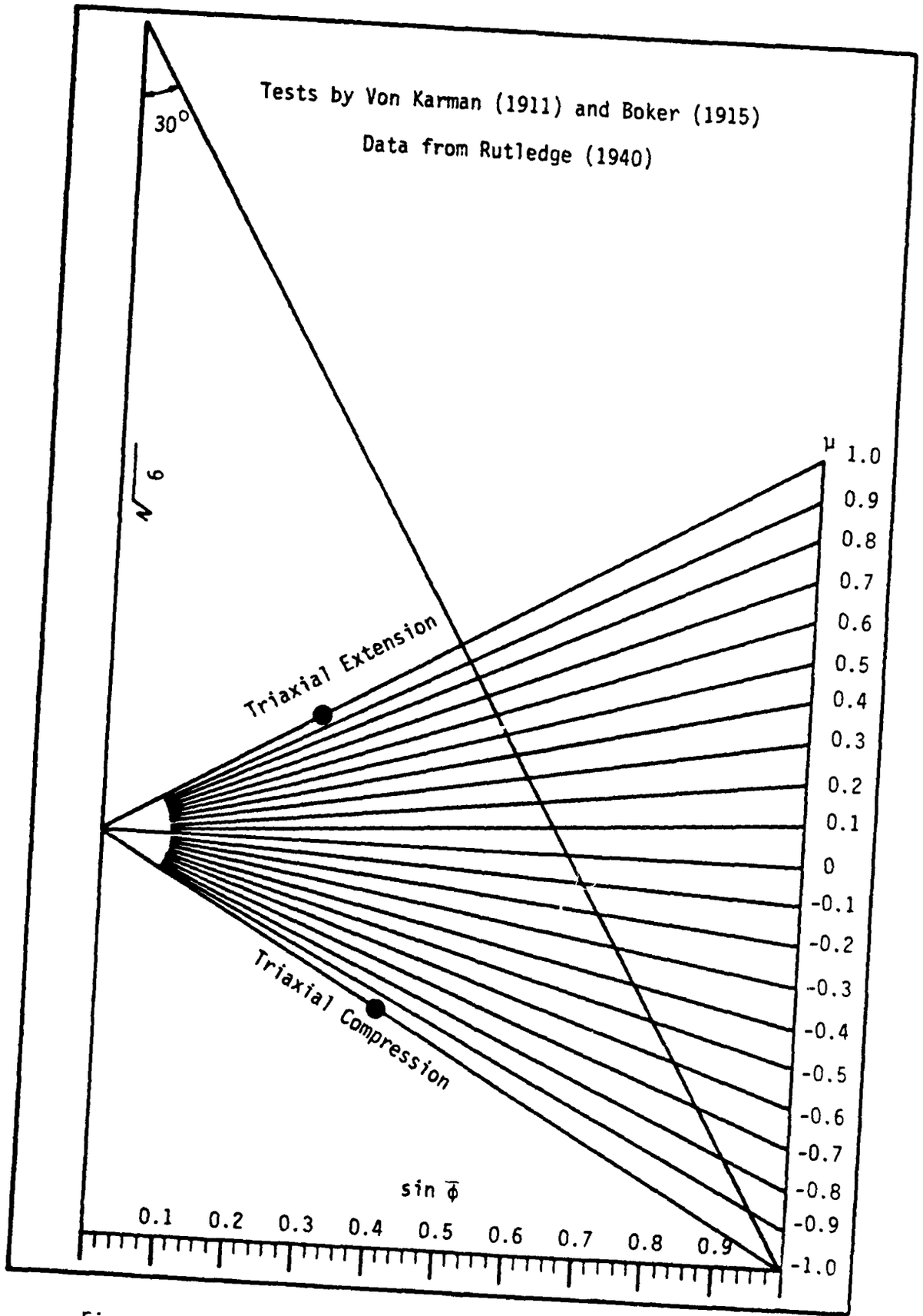

Figure 3.7. Effect of $\bar{\sigma}_2$ on the Strength of Carrara Marble, 10 Ksi < $\bar{p}$ < 40 Ksi.

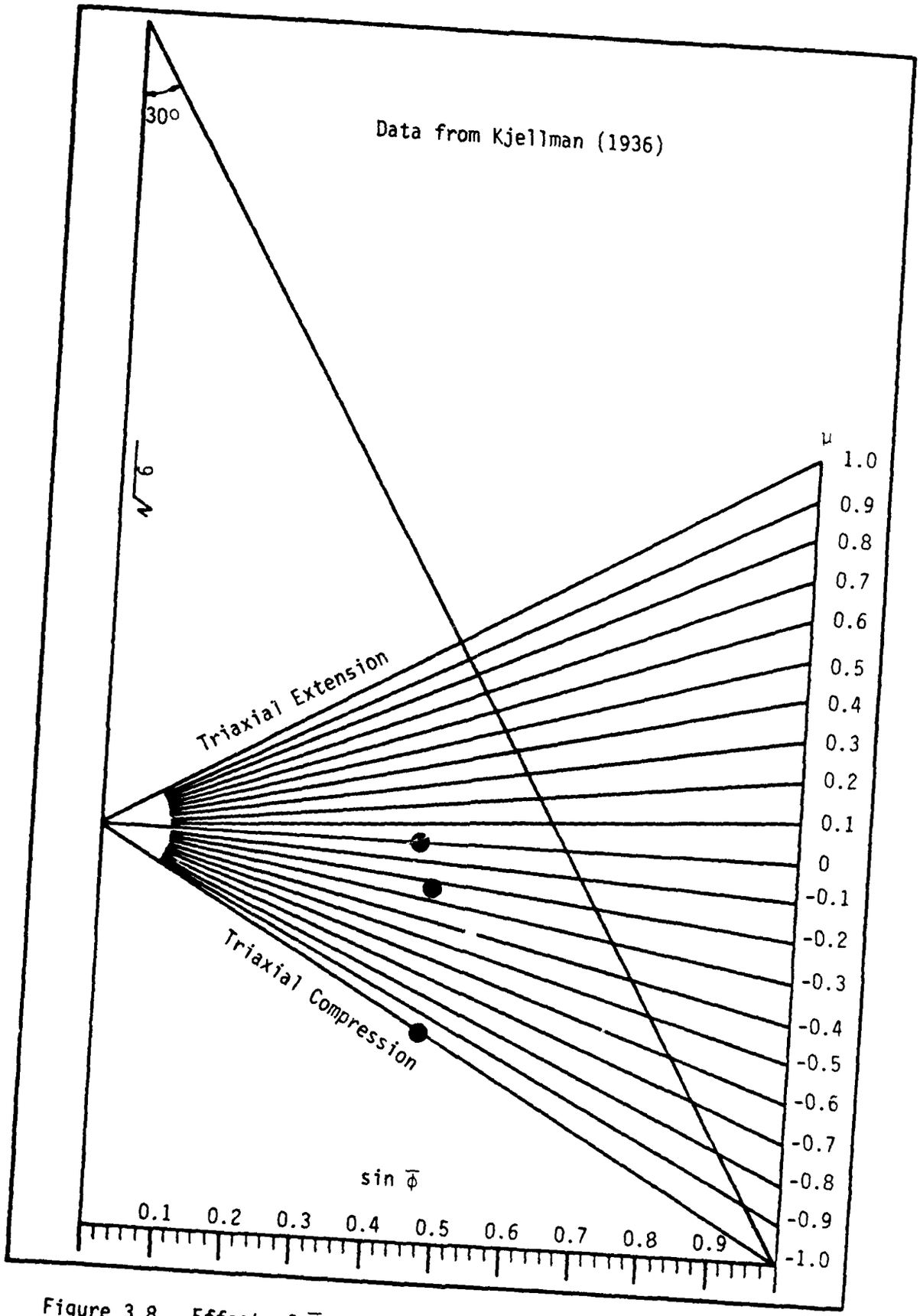

Figure 3.8. Effect of $\bar{\sigma}_2$ on the Strength of Dry German Quartz Sand.

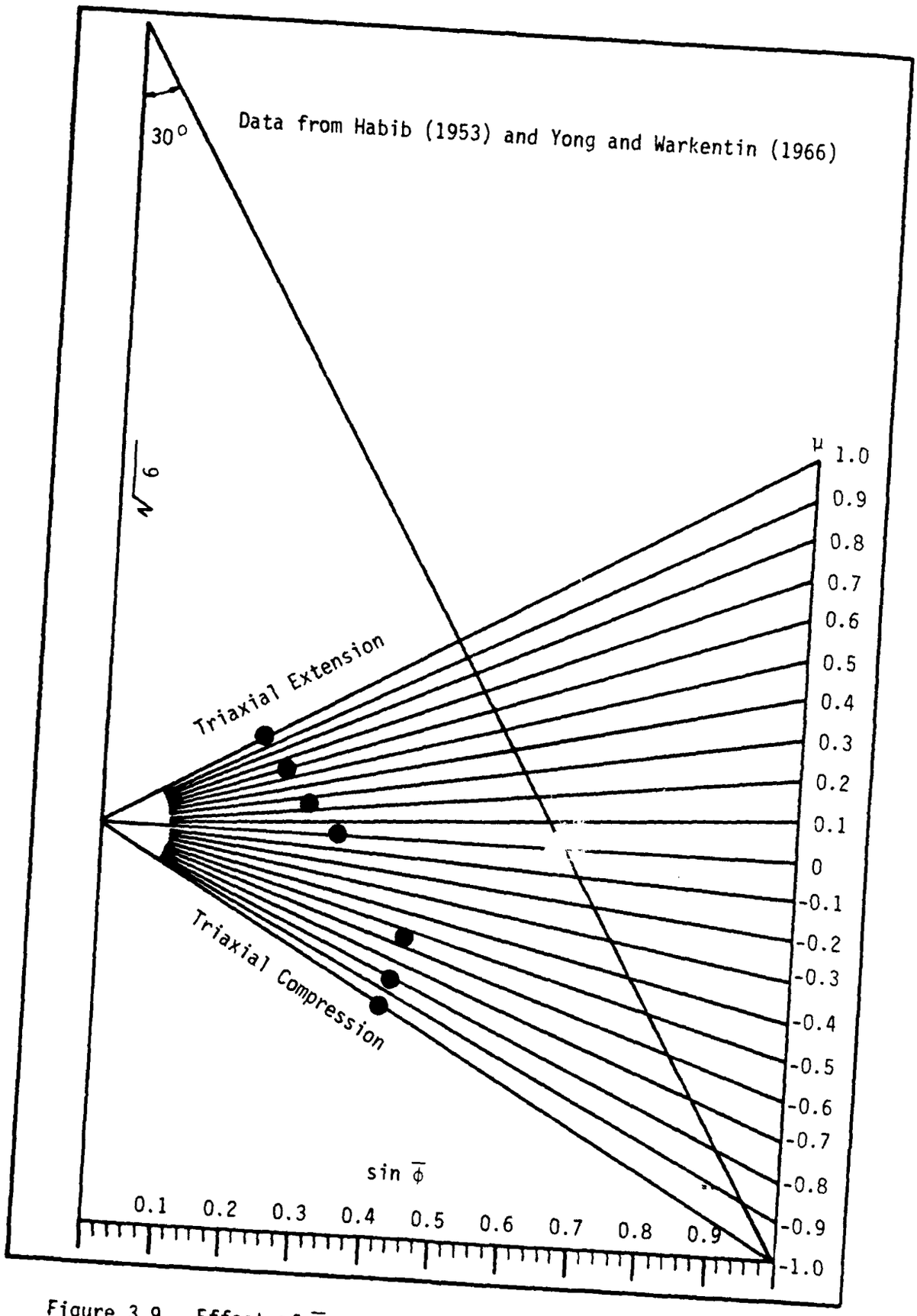

Figure 3.9. Effect of $\bar{\sigma}_2$ on the Strength of Fontainebleau Sand.

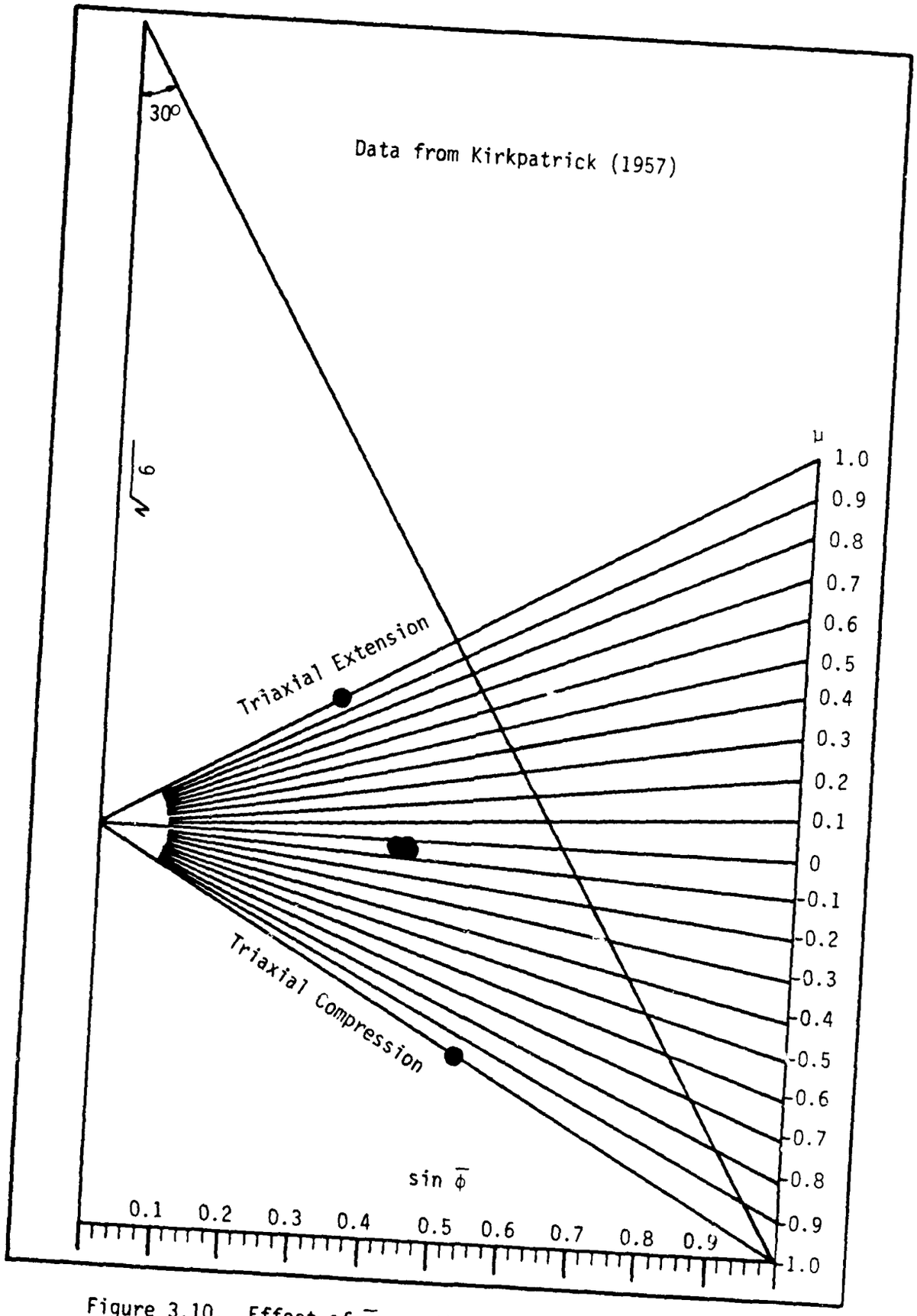

Figure 3.10. Effect of $\bar{\sigma}_2$ on the Strength of Loch Aline Sand.

AD-A139 358 FUNDAMENTAL PROPERTIES OF SOILS FOR COMPLEX DYNAMIC LOADINGS; DYNAMIC CON..(U) APPLIED RESEARCH ASSOCIATES INC ALBUQUERQUE NM D H MERKLE ET AL. 01 DEC 83 2/2

UNCLASSIFIED AFOSR-TR-84-0166 F49620-80-C-0088 F/G 8/13 NL

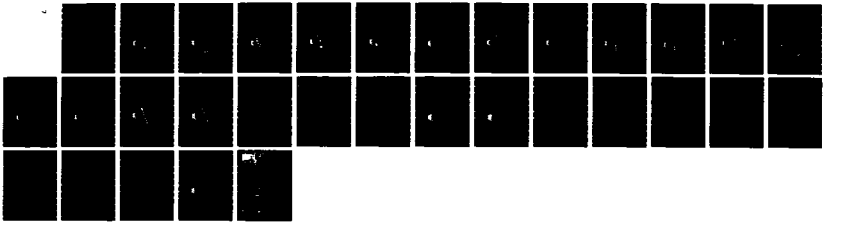

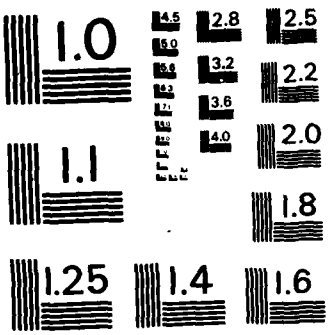

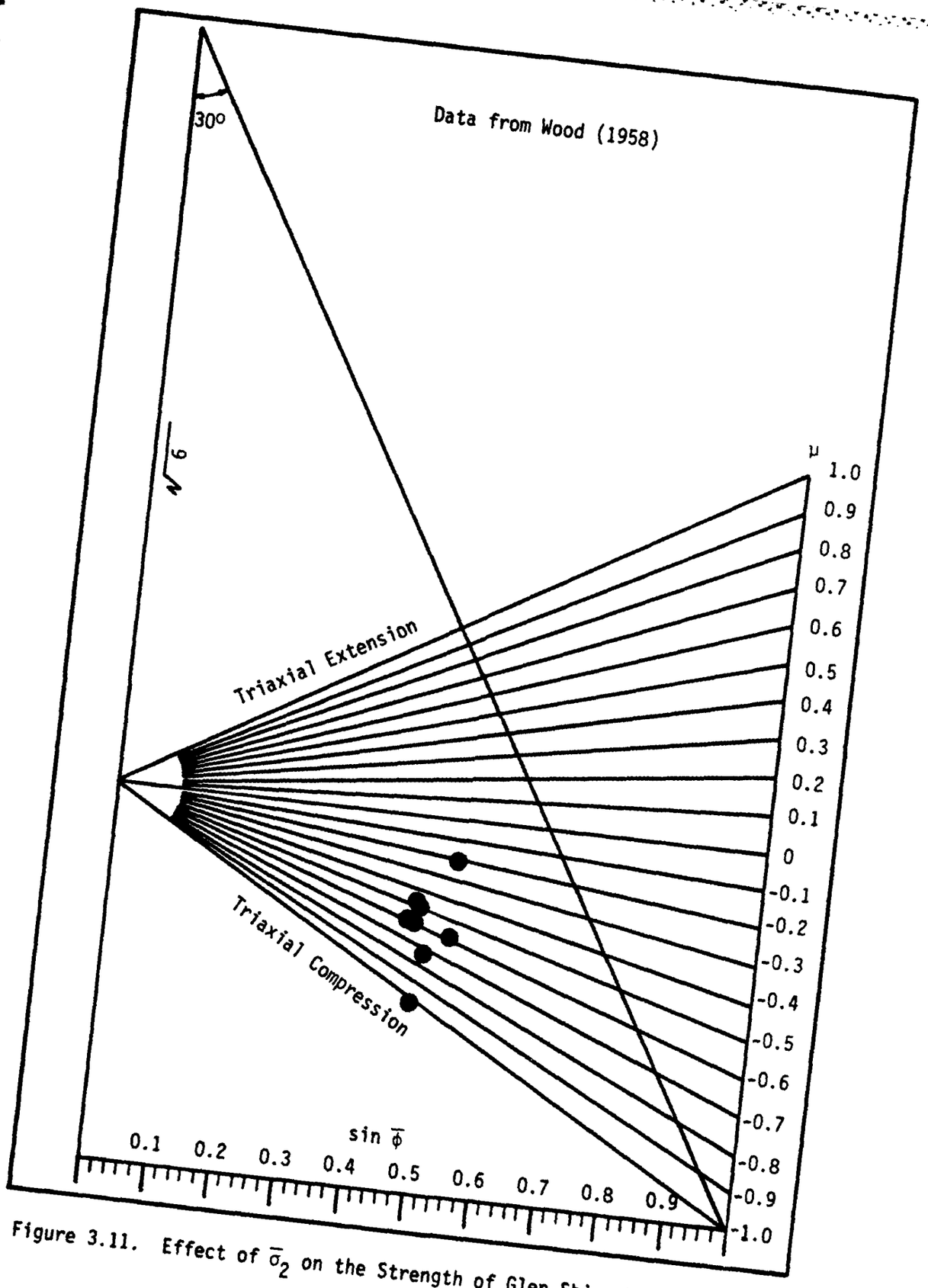

Figure 3.11. Effect of $\bar{\sigma}_2$ on the Strength of Glen Shira Dam Material.

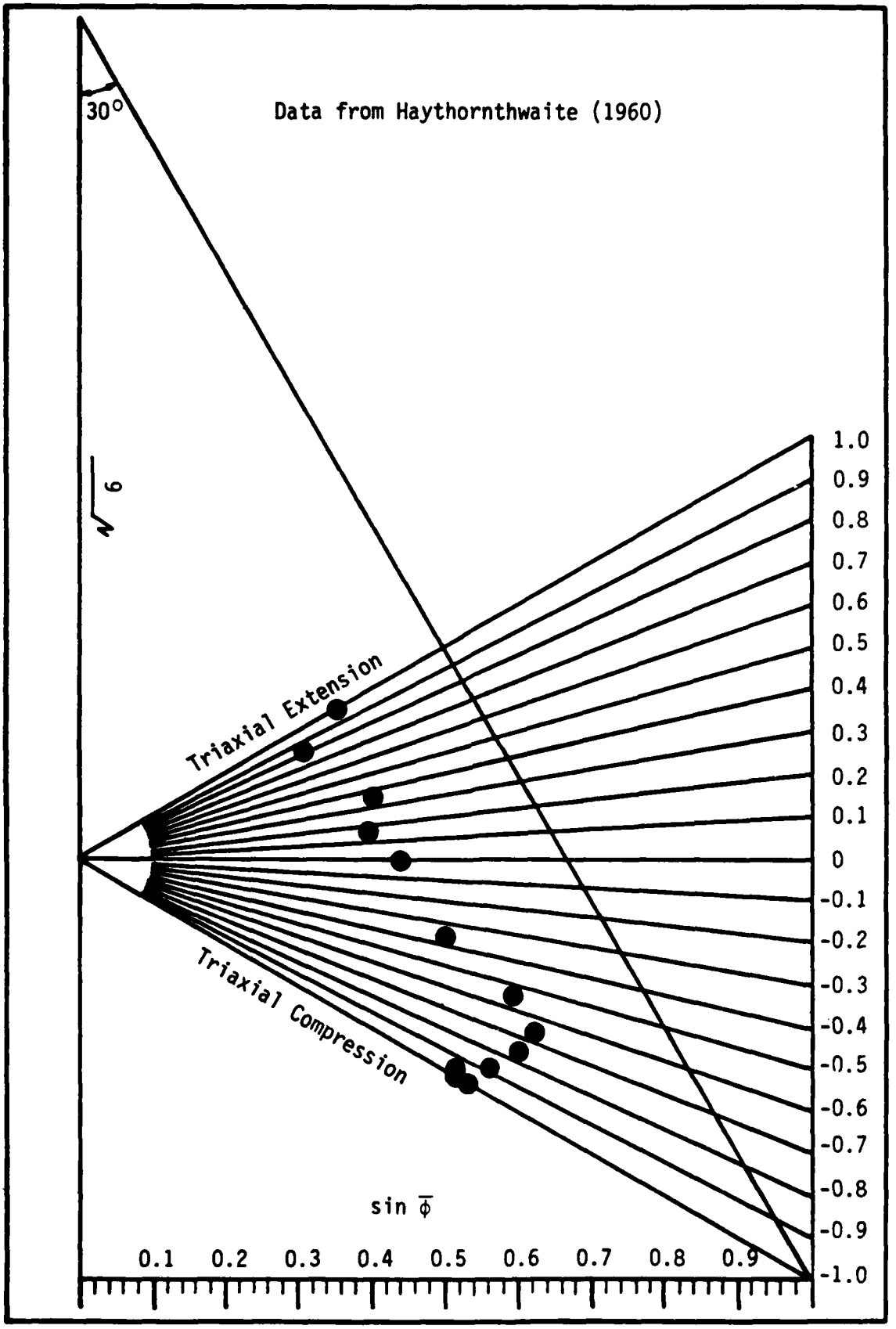

Figure 3.12. Effect of $\bar{\sigma}_2$ on the Strength of a Clayey Silt.

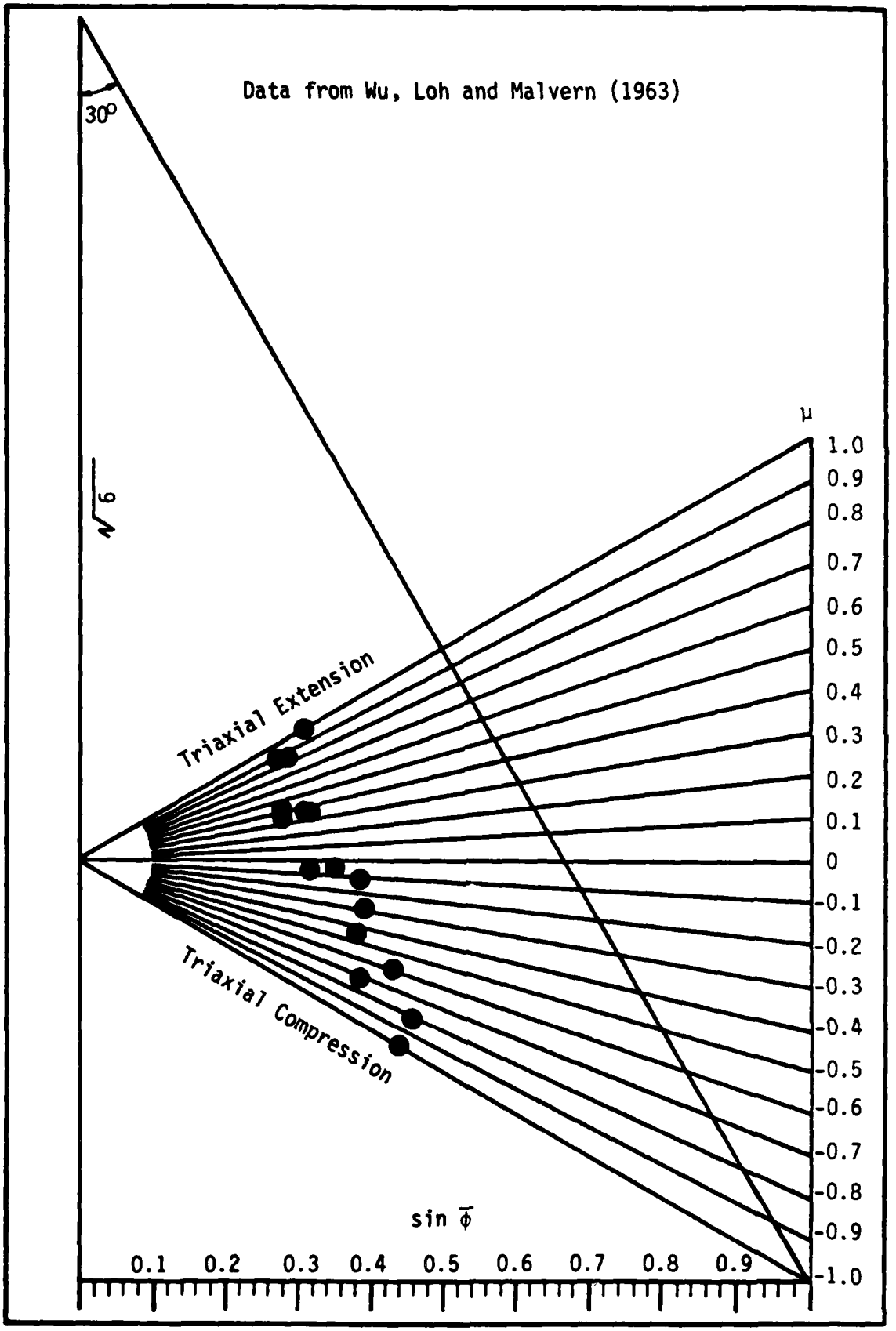

Figure 3.13. Effect of $\bar{\sigma}_2$ on the Strength of Remolded Sault Ste. Marie Clay.

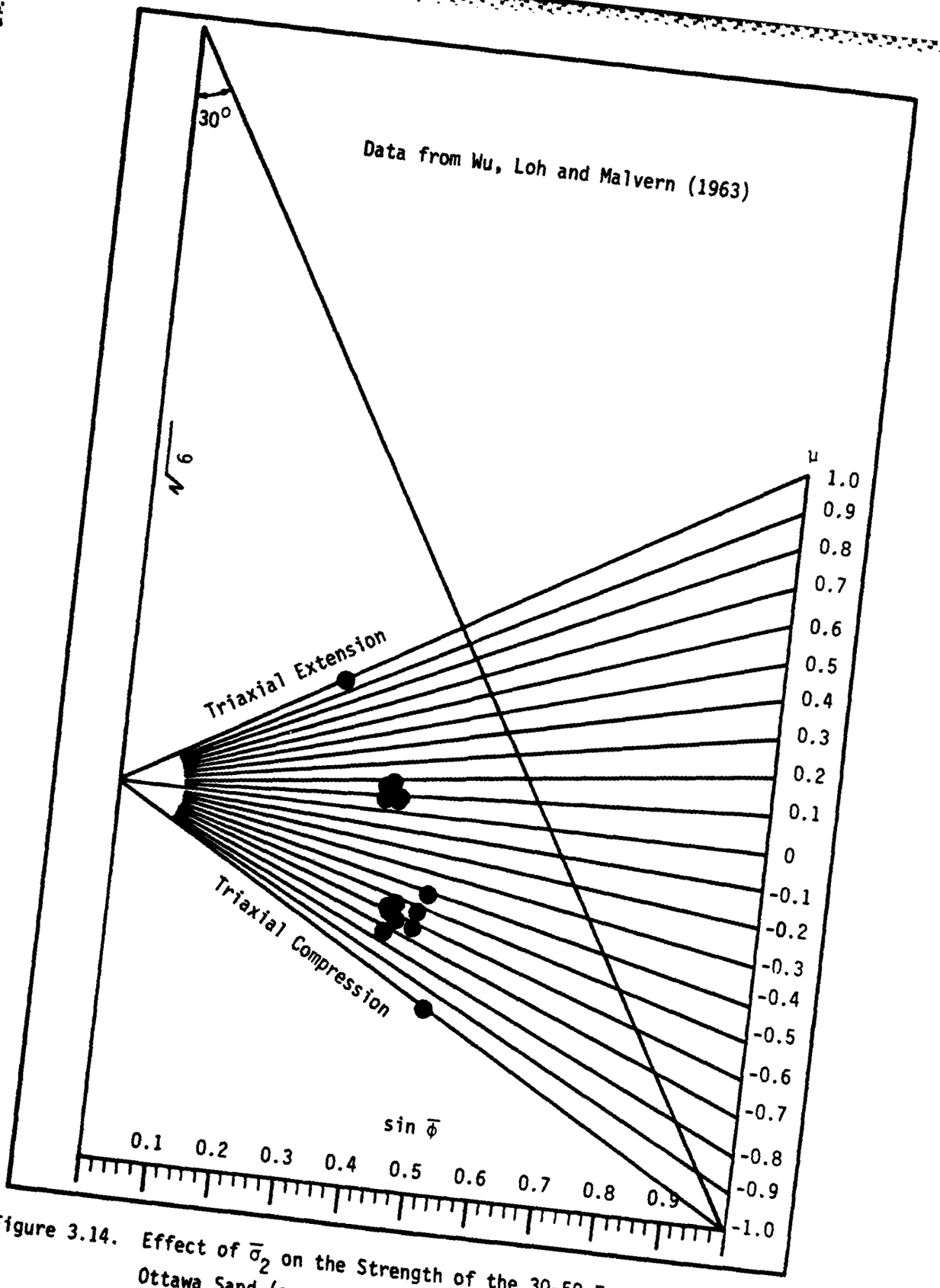

Figure 3.14. Effect of $\bar{\sigma}_2$ on the Strength of the 30-50 Fraction of Standard Ottawa Sand (e = 0.47 to 0.52).

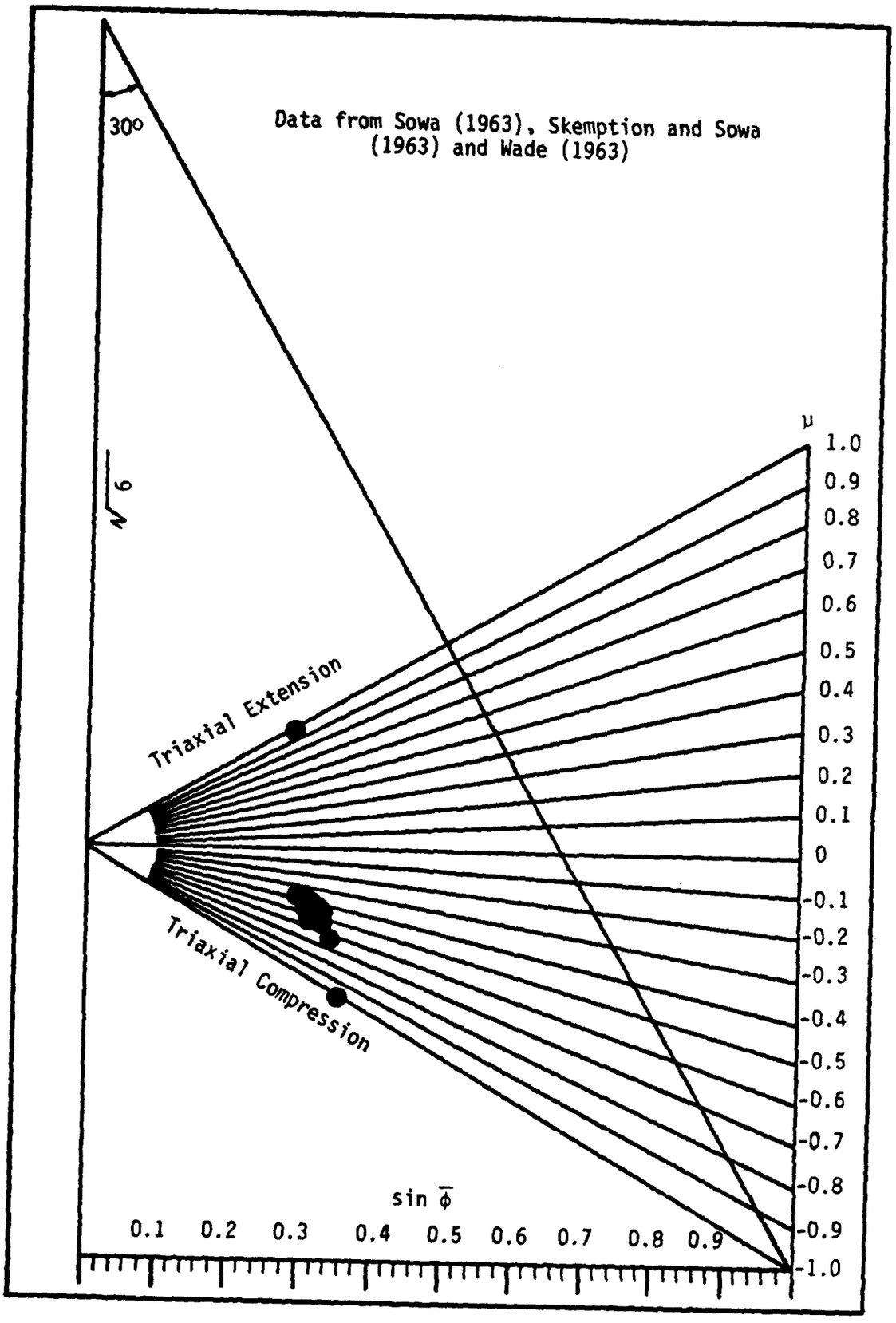

Figure 3.15. Effect of $\bar{\sigma}_2$ on the Strength of Remolded Weald Clay.

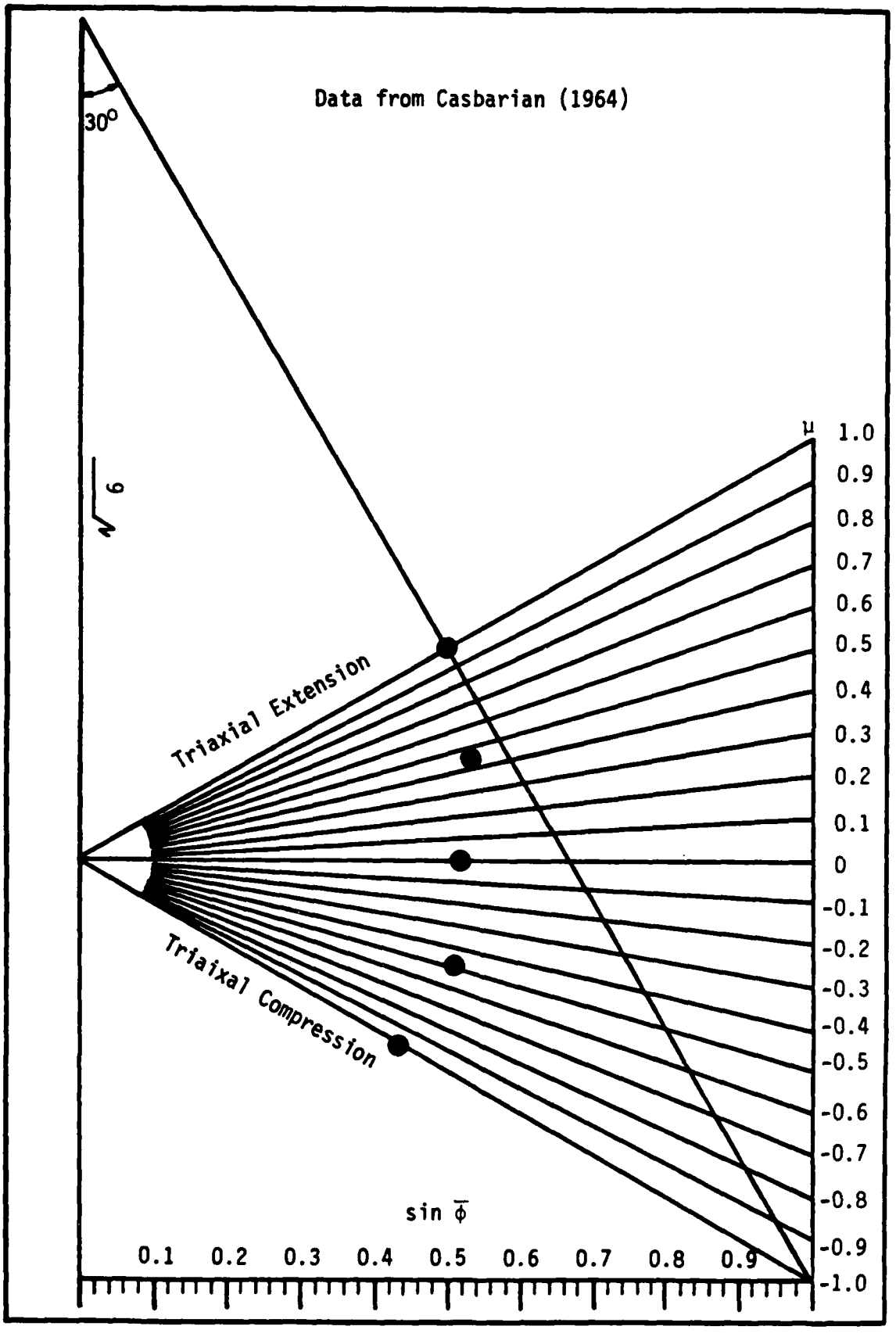

Figure 3.16. Effect of $\bar{\sigma}_2$ on the Strength of Remolded Commercial Kaolinite, σ_c = 7 Psi.

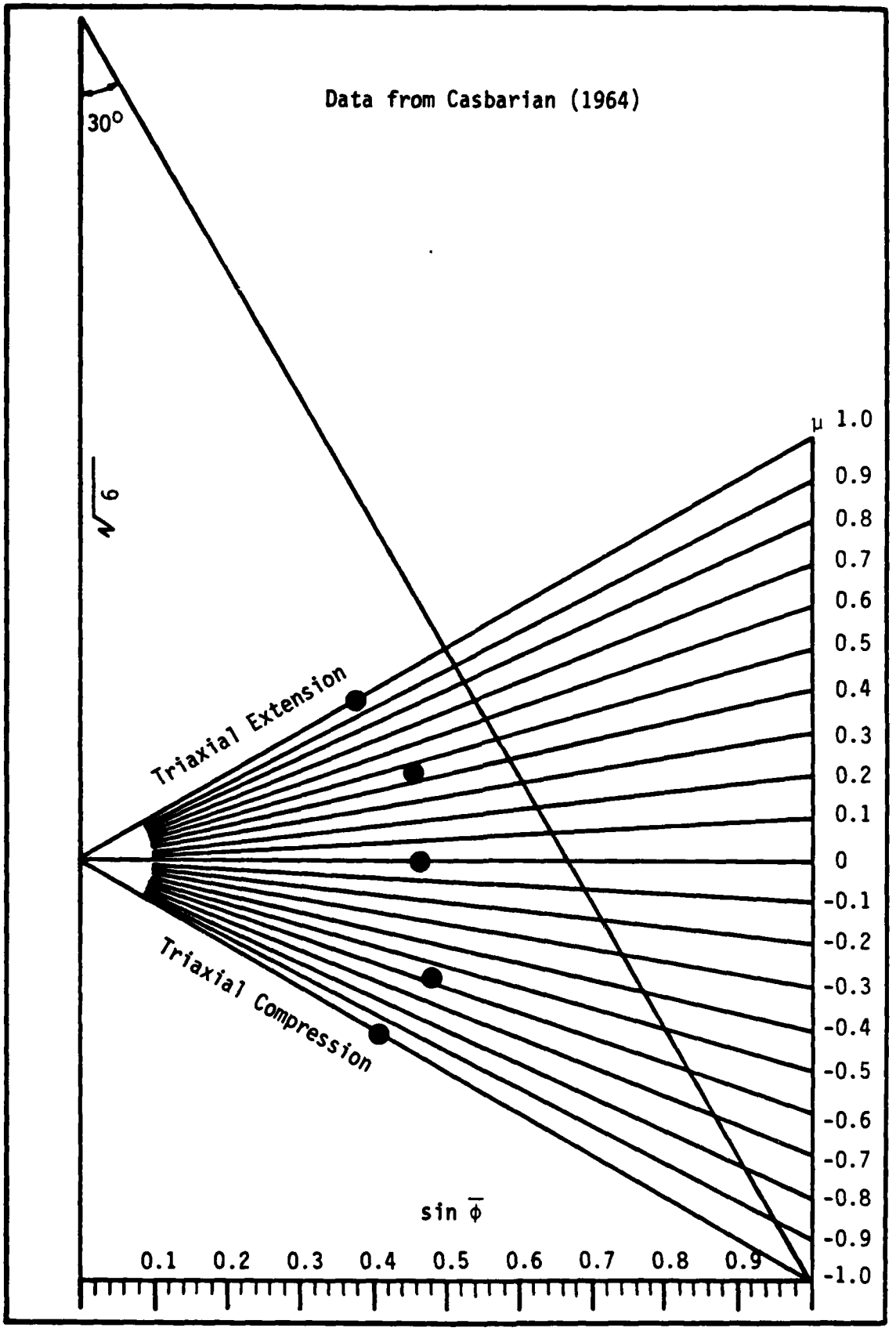

Figure 3.17. Effect of $\bar{\sigma}_2$ on the Strength of Remolded Commercial Kaolinite, σ_c = 25 Psi.

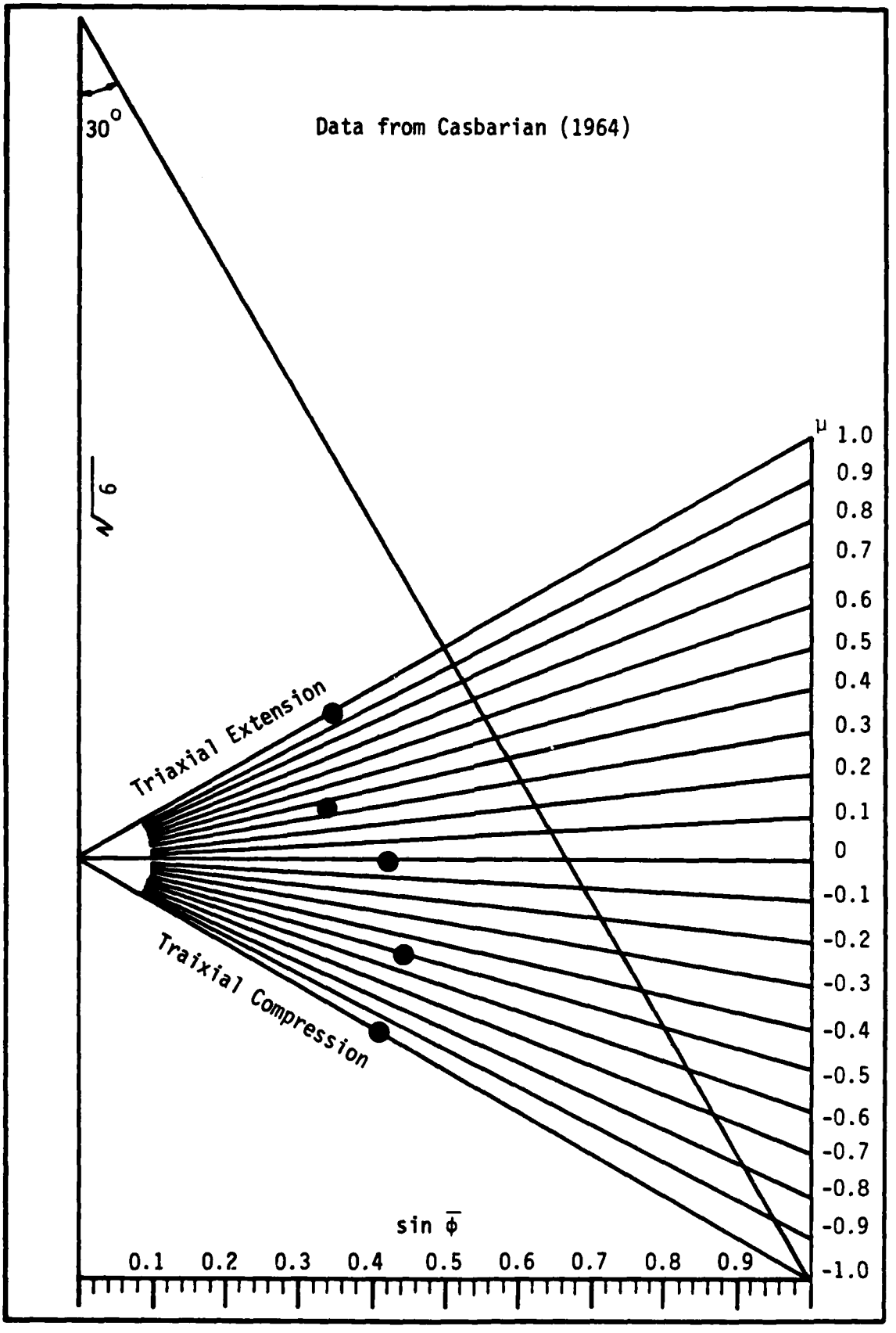

Figure 3.18. Effect of $\bar{\sigma}_2$ on the Strength of Remolded Commercial Kaolinite, σ_c = 70 Psi.

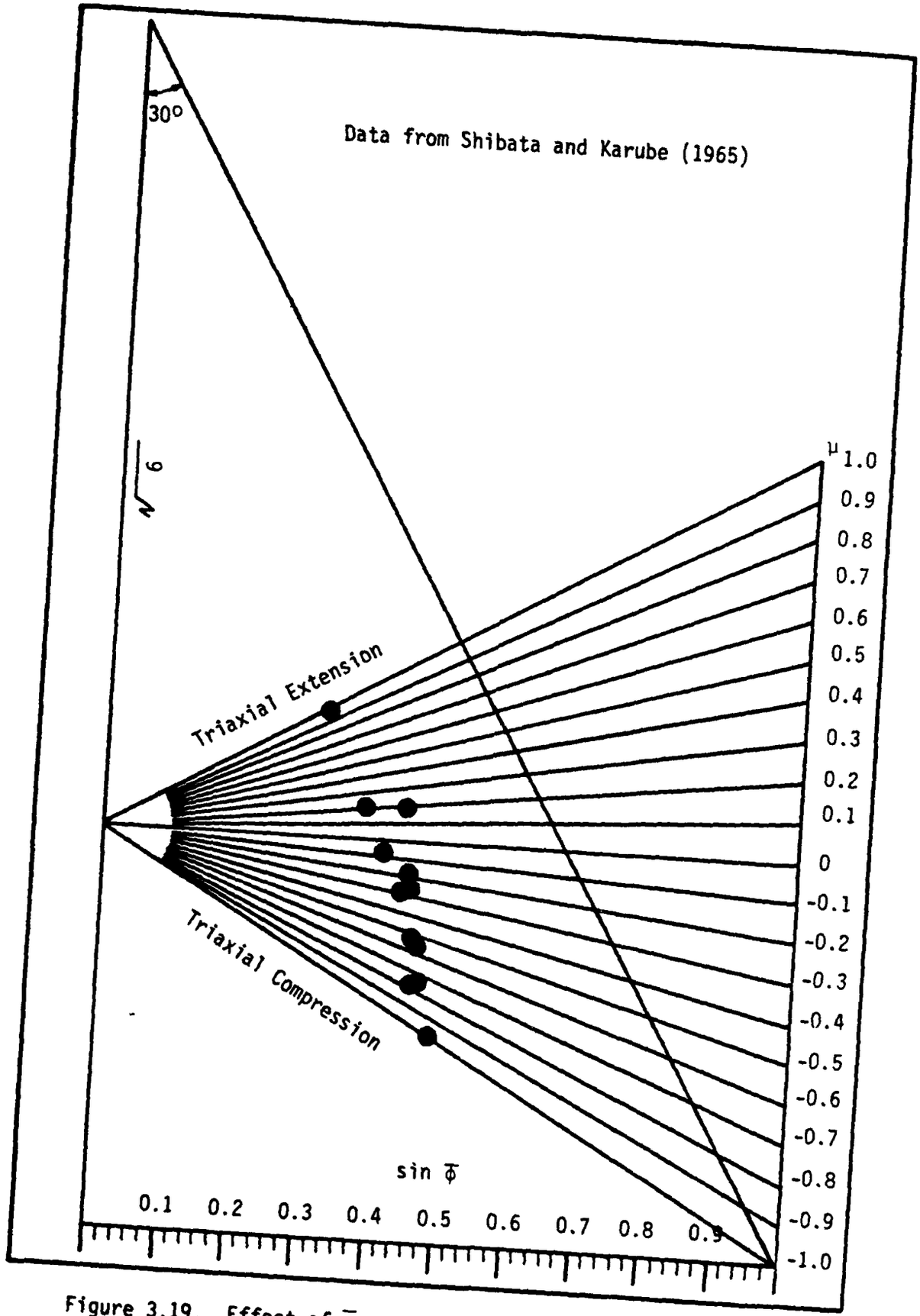

Figure 3.19. Effect of $\bar{\sigma}_2$ on the Strength of Remolded Osaka Alluvial Clay at $(\bar{\sigma}_1/\bar{\sigma}_3)_{max}$.

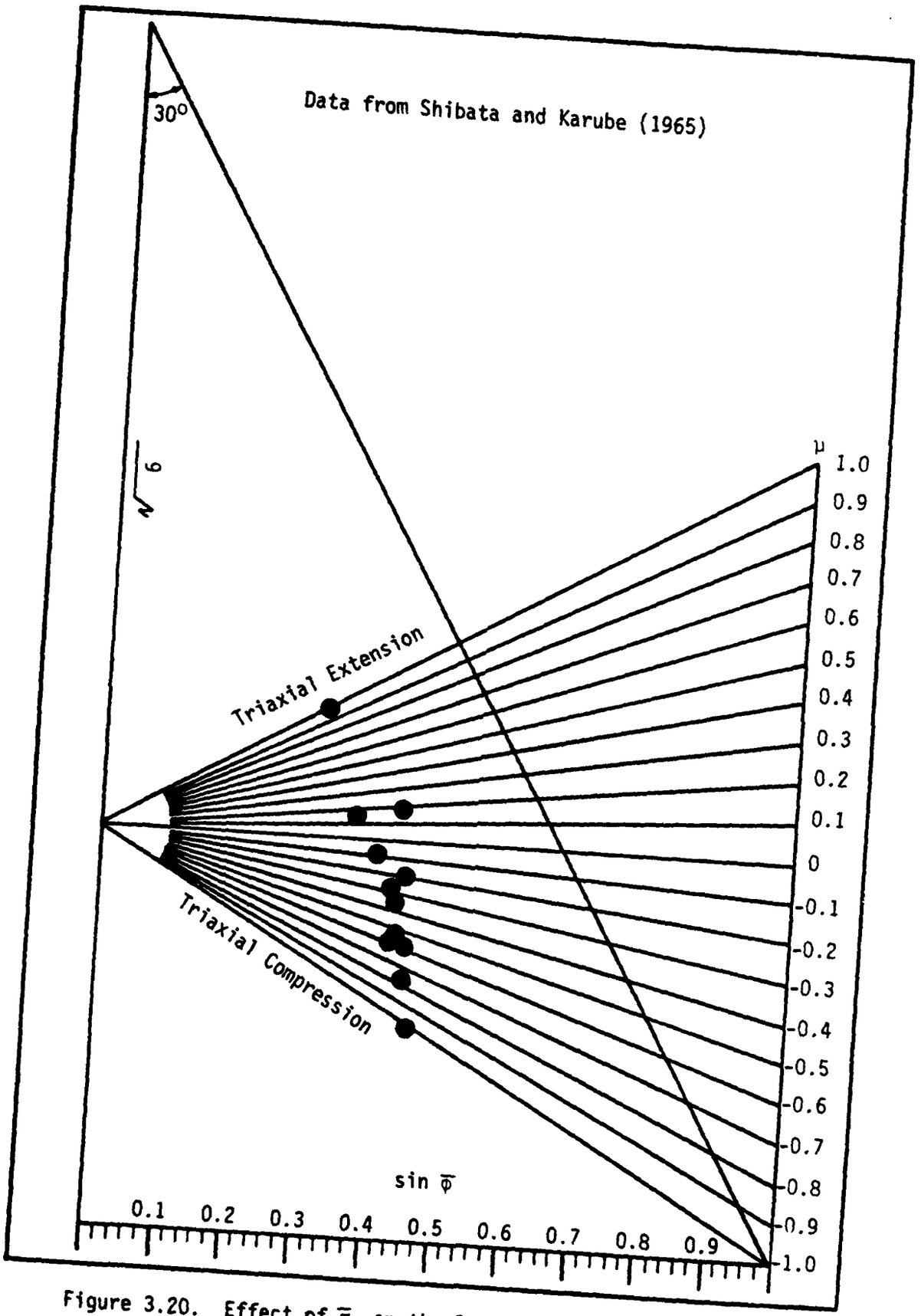

Figure 3.20. Effect of $\bar{\sigma}_2$ on the Strength of Remolded Osaka Alluvial Clay at $(\bar{\sigma}_1 - \bar{\sigma}_3)_{max}$.

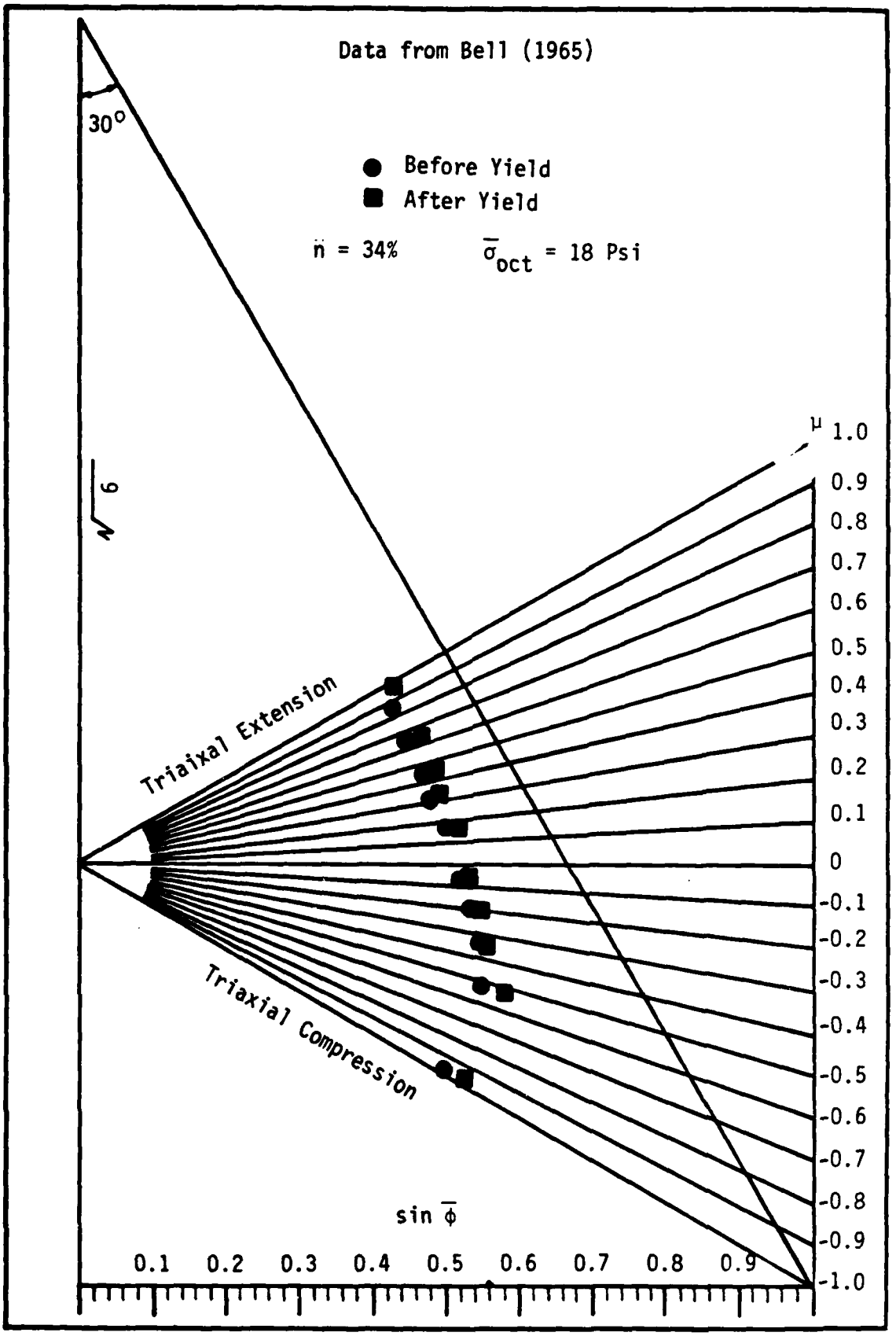

Figure 3.21. Effect of $\bar{\sigma}_2$ on the Strength of Standard Ottawa Sand.

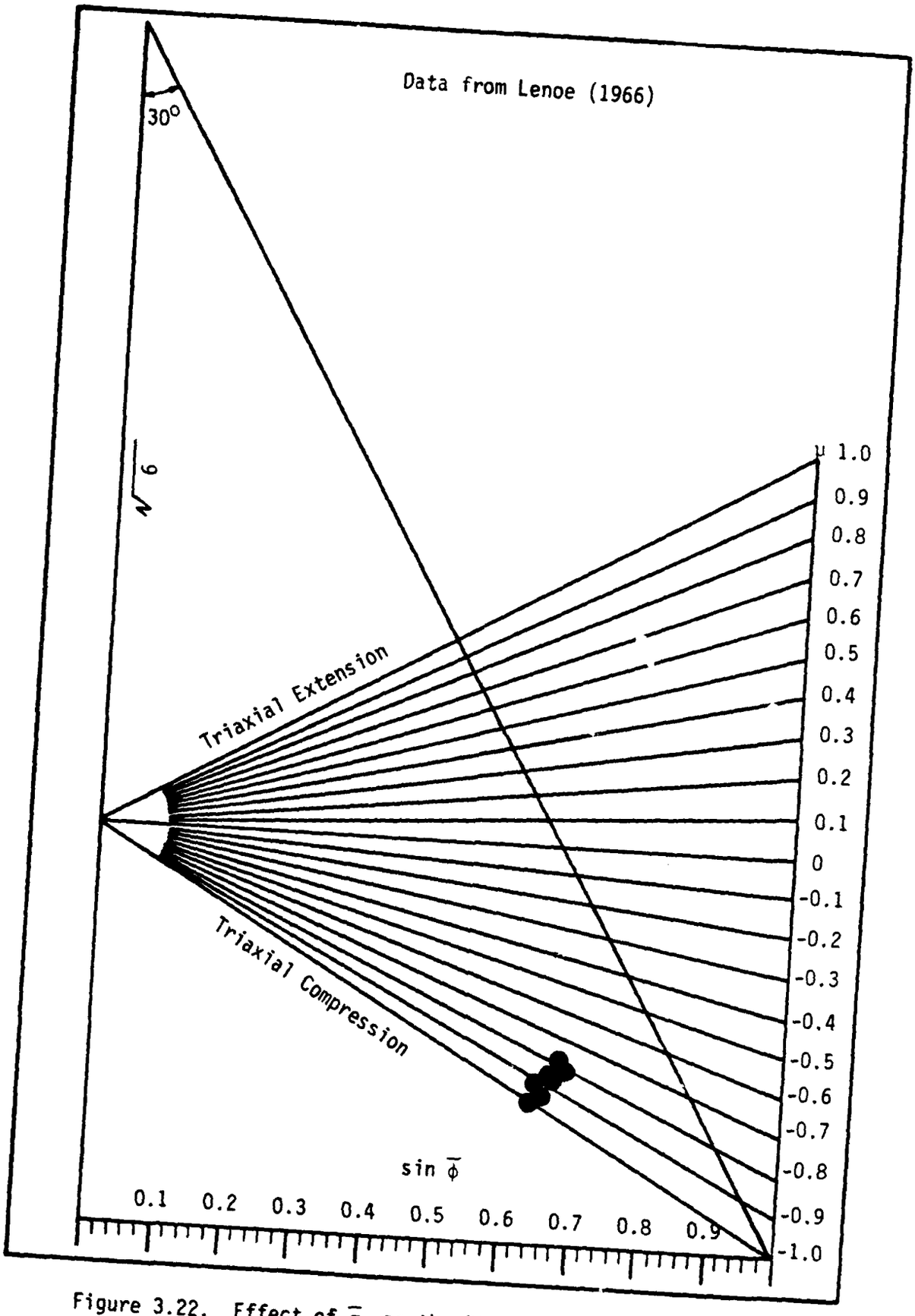

Figure 3.22. Effect of $\bar{\sigma}_2$ on the Strength of a Silty Sand.

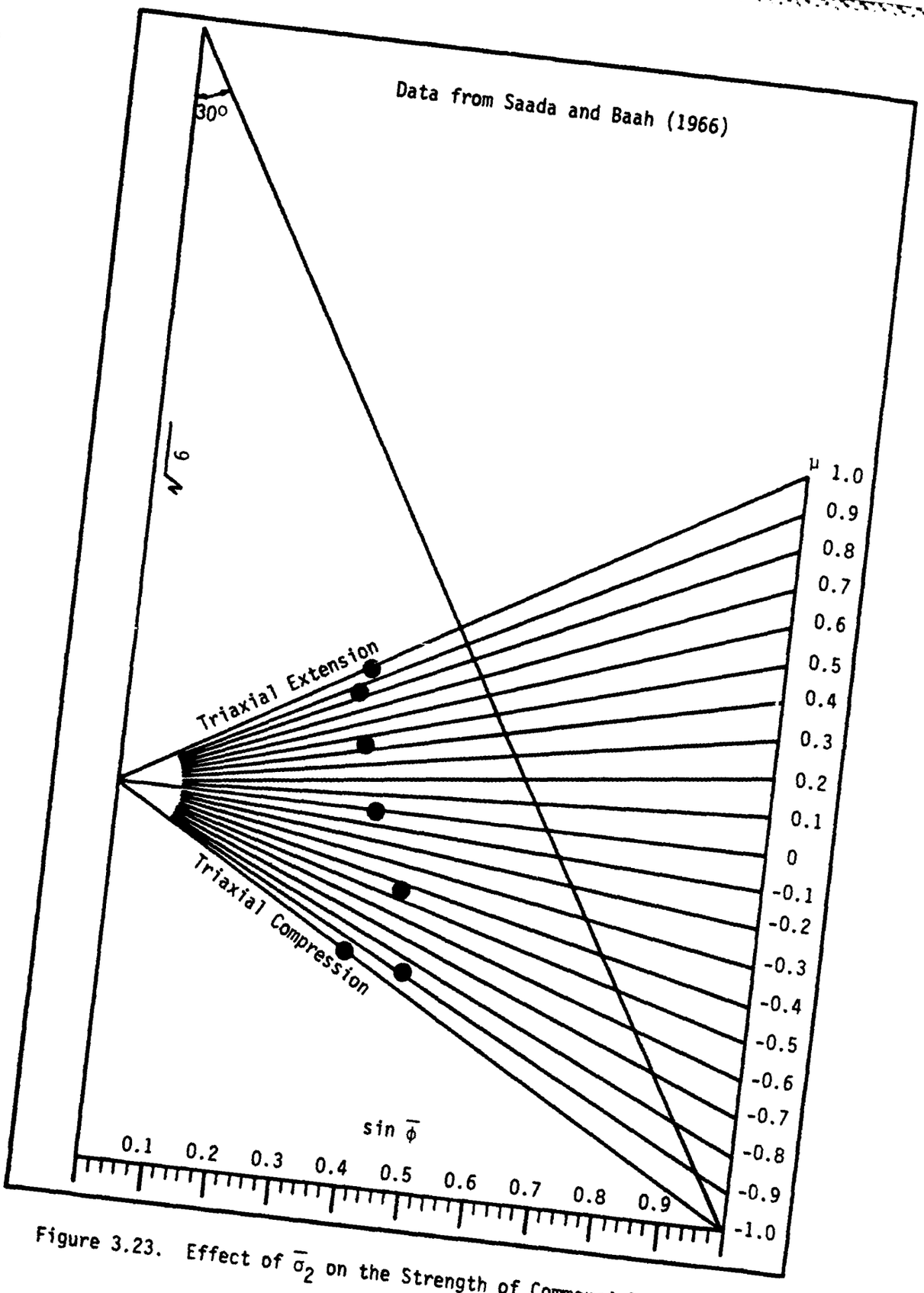

Figure 3.23. Effect of $\bar{\sigma}_2$ on the Strength of Commercial Kaolinite.

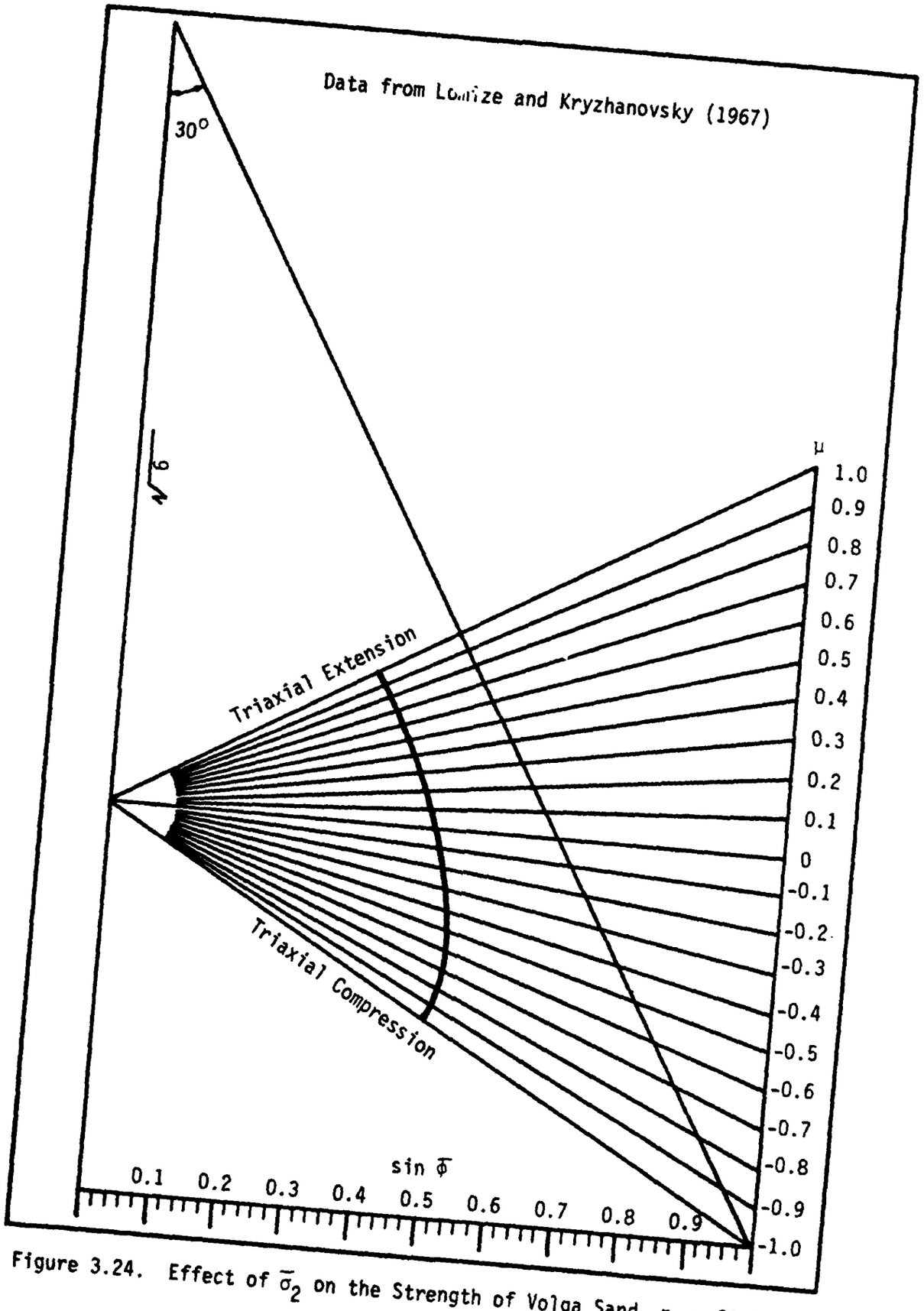

Figure 3.24. Effect of $\bar{\sigma}_2$ on the Strength of Volga Sand, n_i = 39.3%.

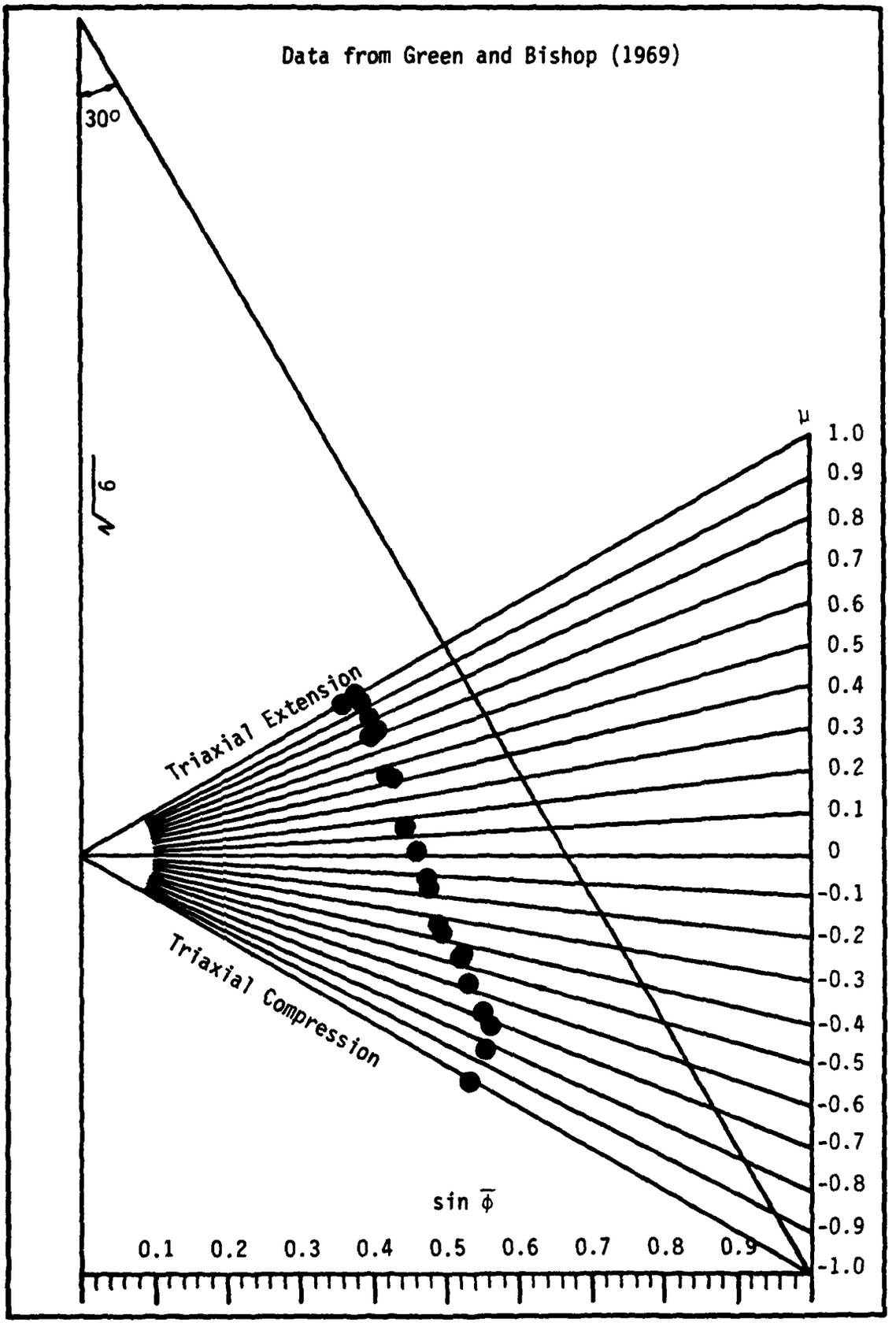

Figure 3.25. Effect of $\bar{\sigma}_2$ on the Strength of Ham River Sand, n_i = 39.0%.

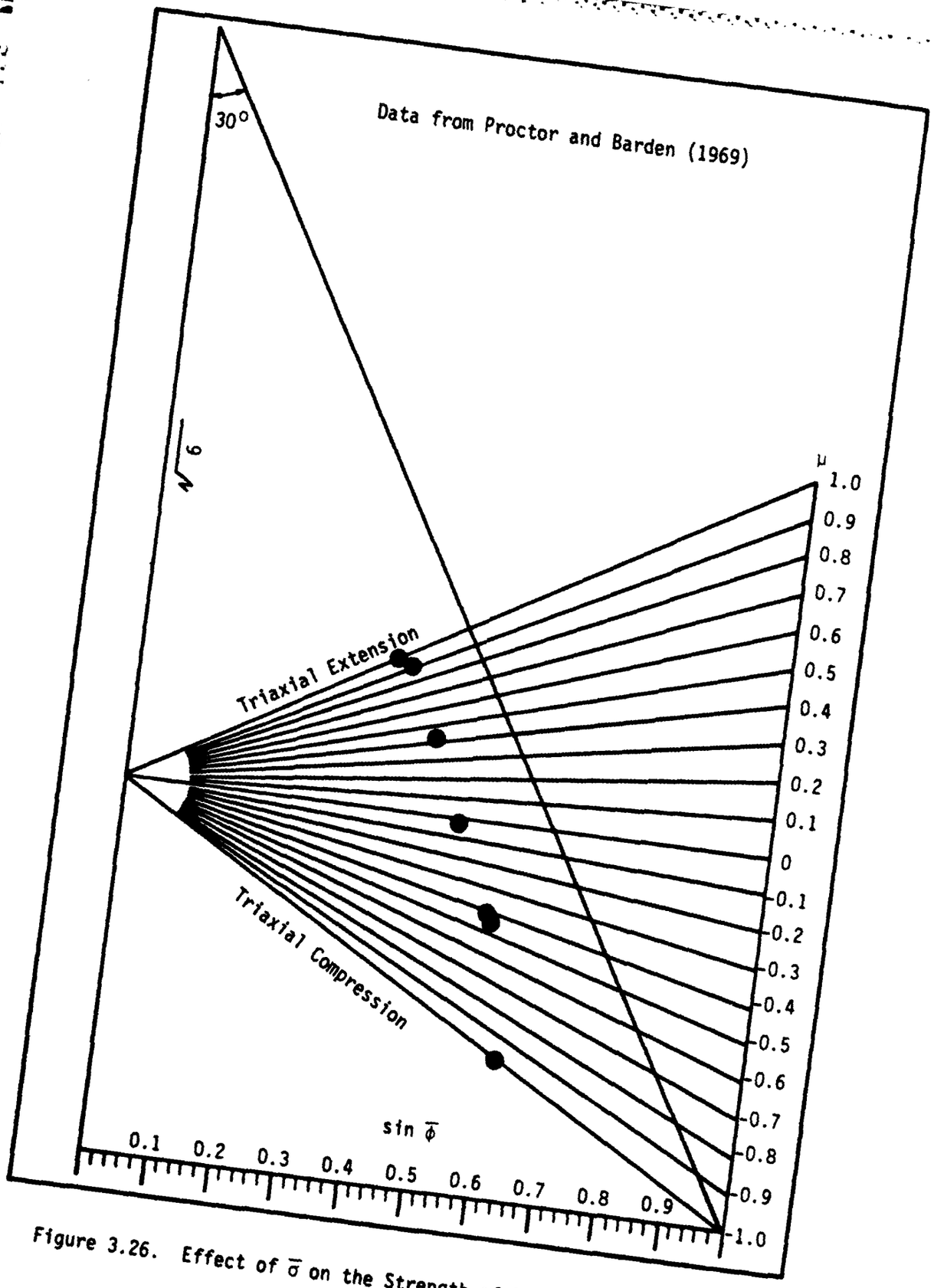

Figure 3.26. Effect of $\bar{\sigma}$ on the Strength of River Welland Sand.

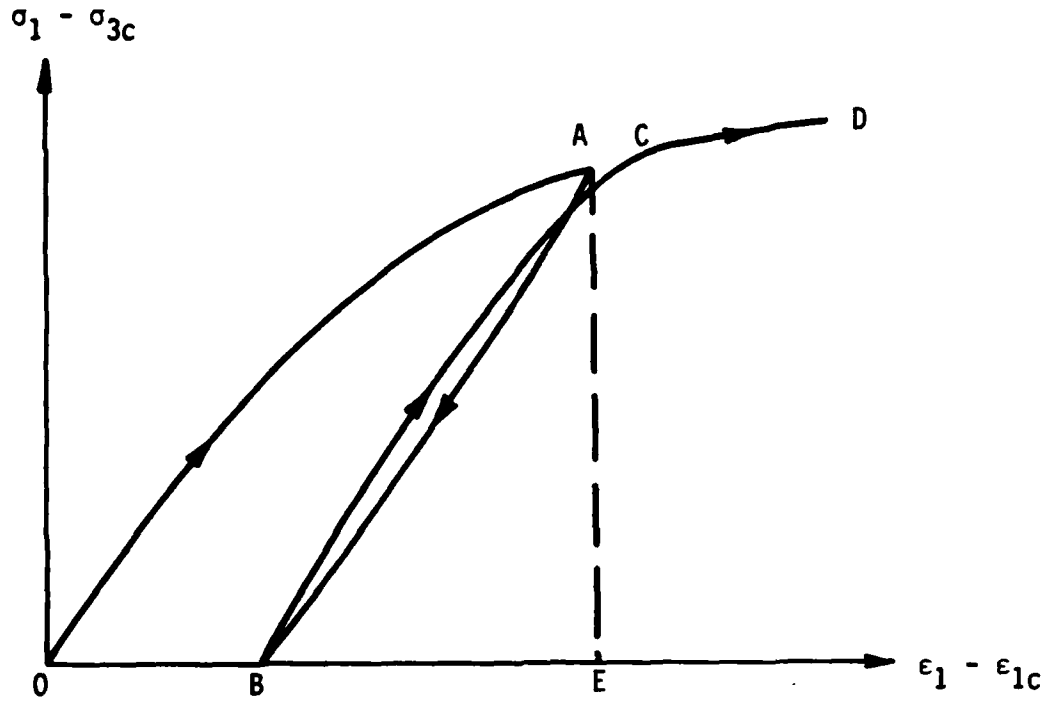

Figure 4.1. Drained Triaxial Compression Stress-Strain Curve

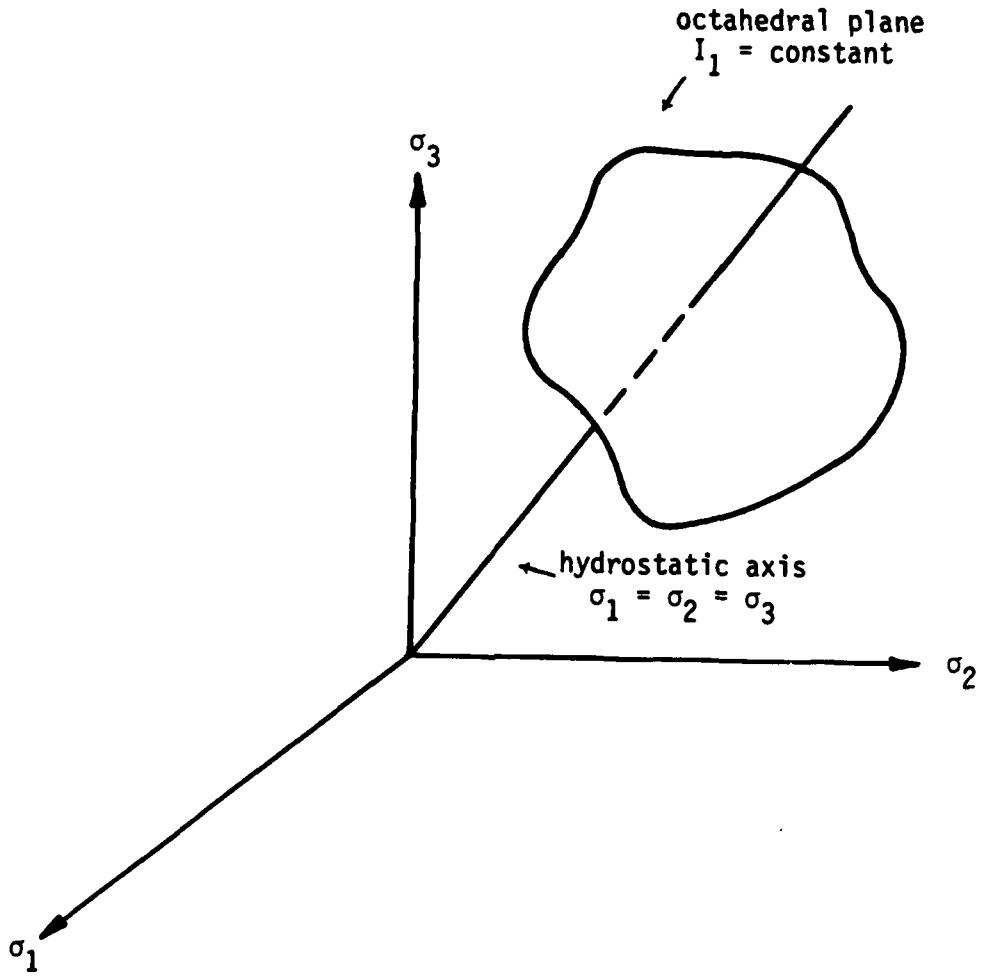

Figure 4.2. Hydrostatic Axis and Octahedral Plane in Principal Stress Space.

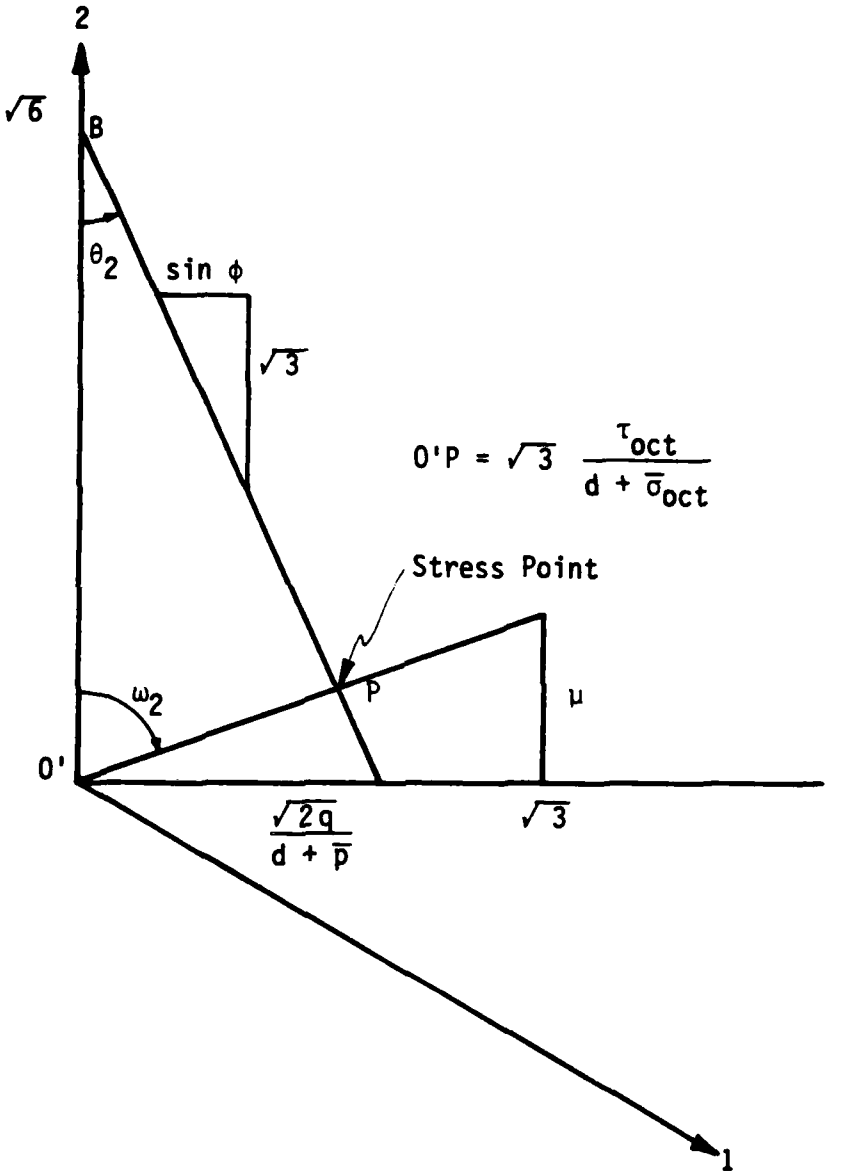

Figure 4.3 Location of a Stress Point in the Octahedral Plane.

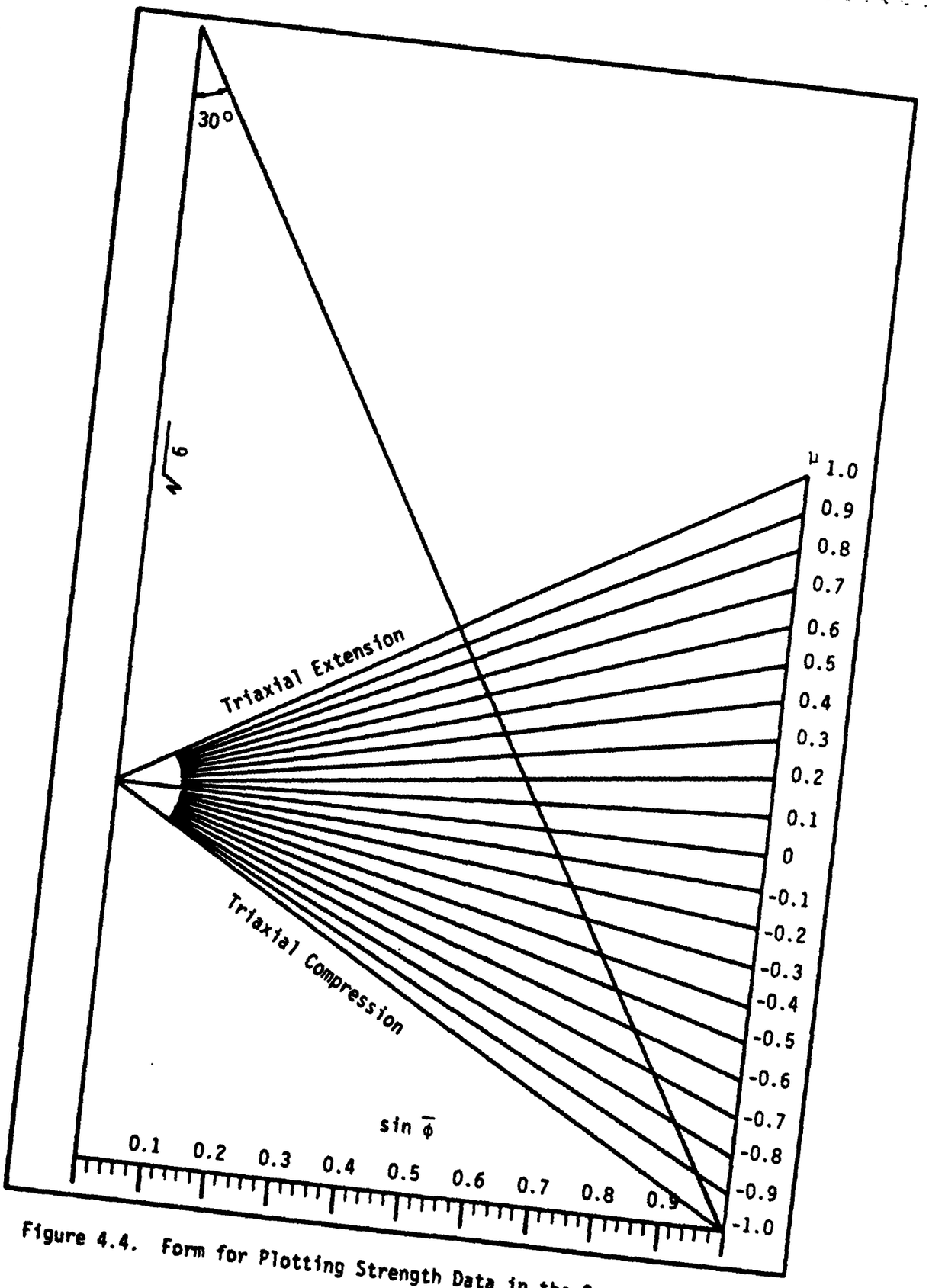

Figure 4.4. Form for Plotting Strength Data in the Octahedral Plane.

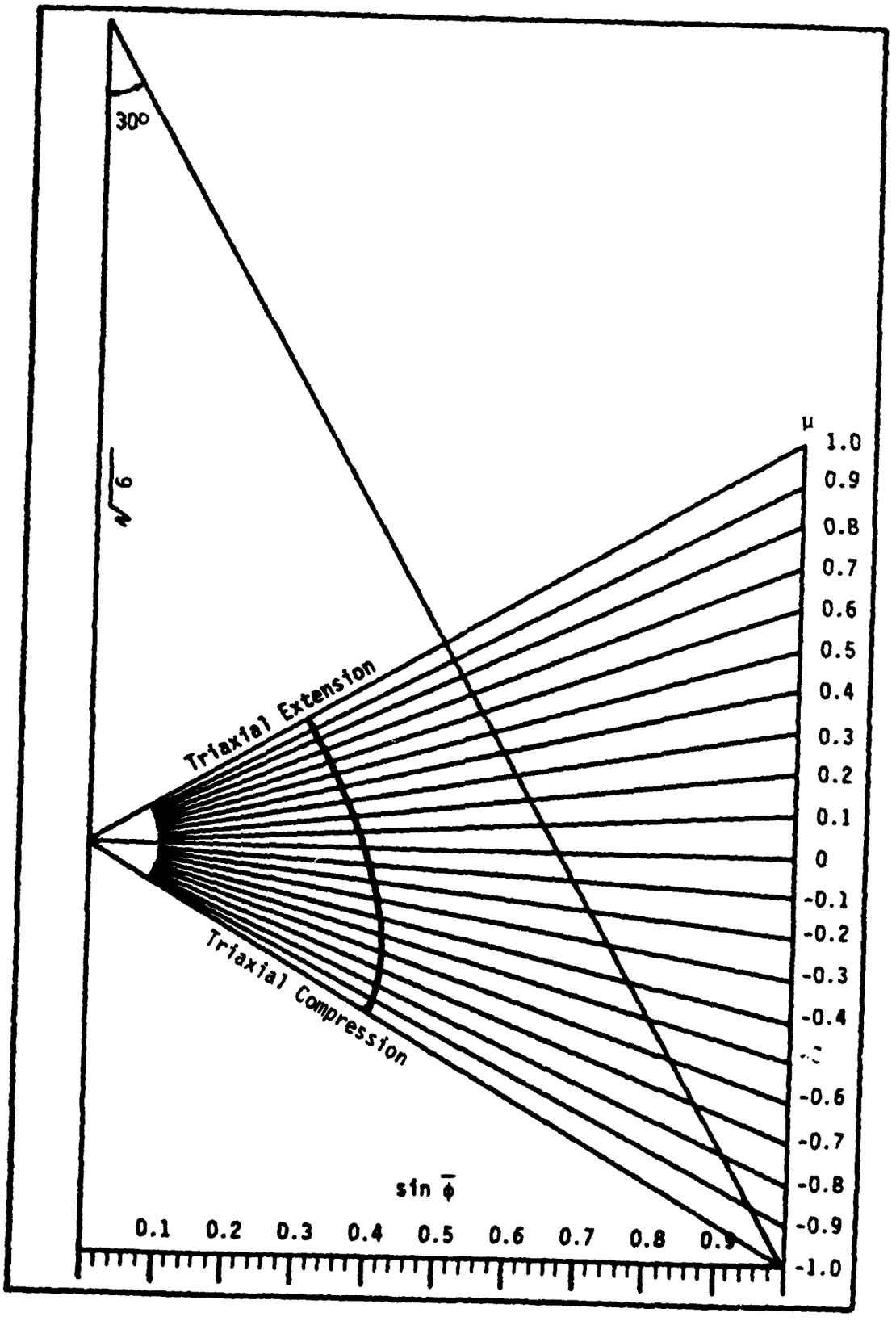

Figure 4.5. Lade Failure Surface Octahedral Cross-Section for ϕ_c = 30 Degrees.

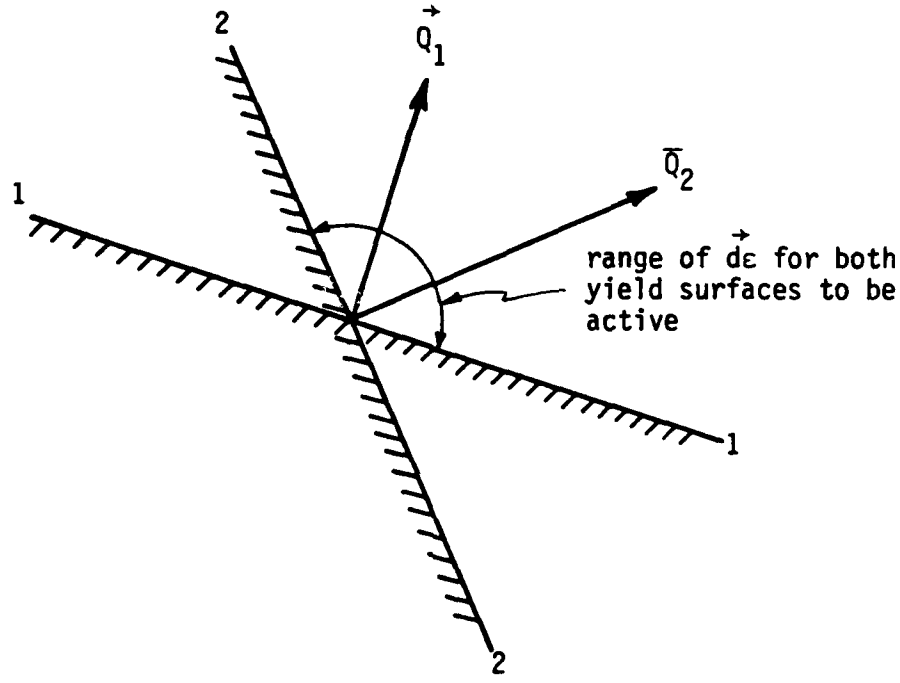

Figure 4.6. Condition for Both Yield Surfaces to be Active.

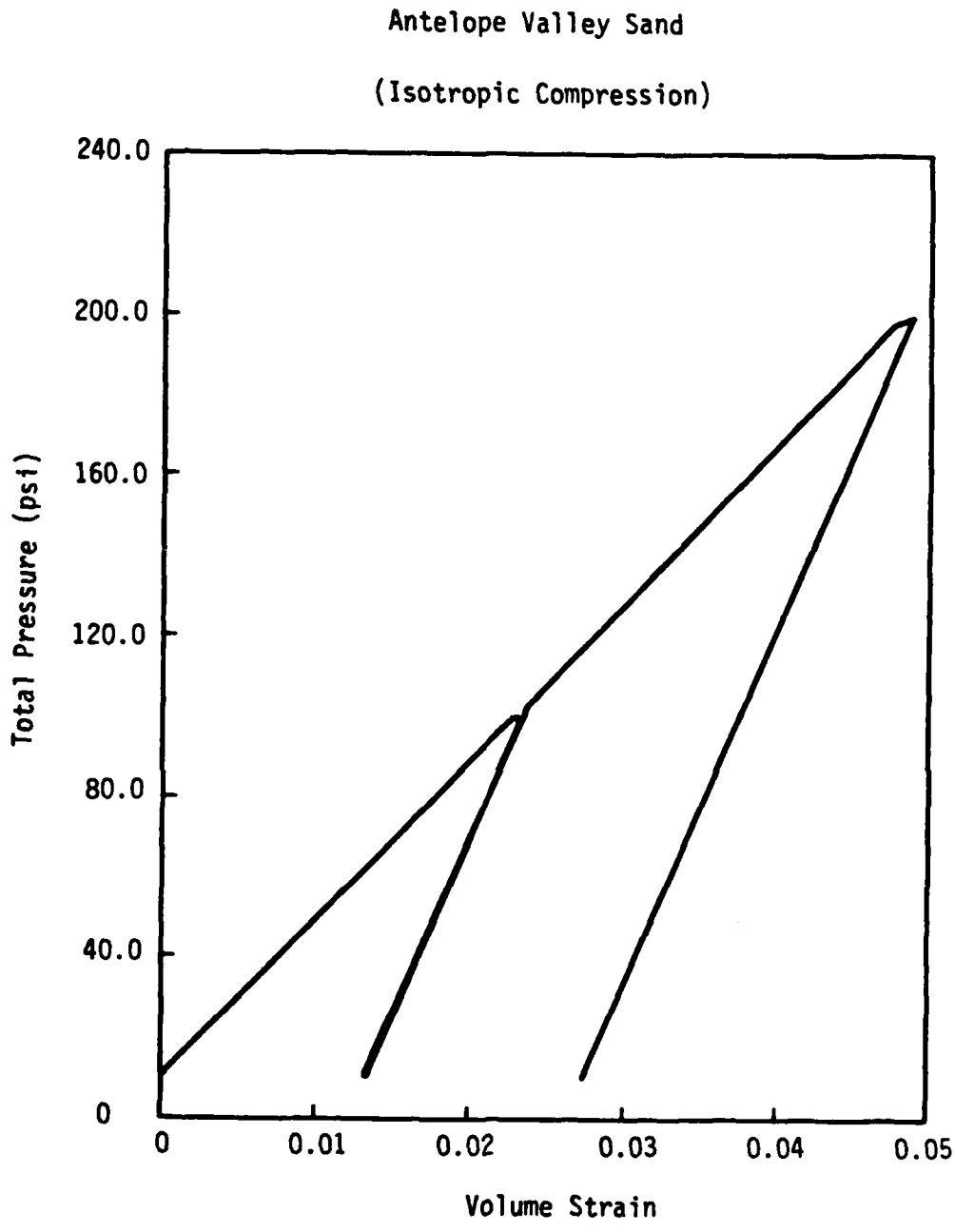

Figure 4.7. Pressure versus Volumetric Strain.

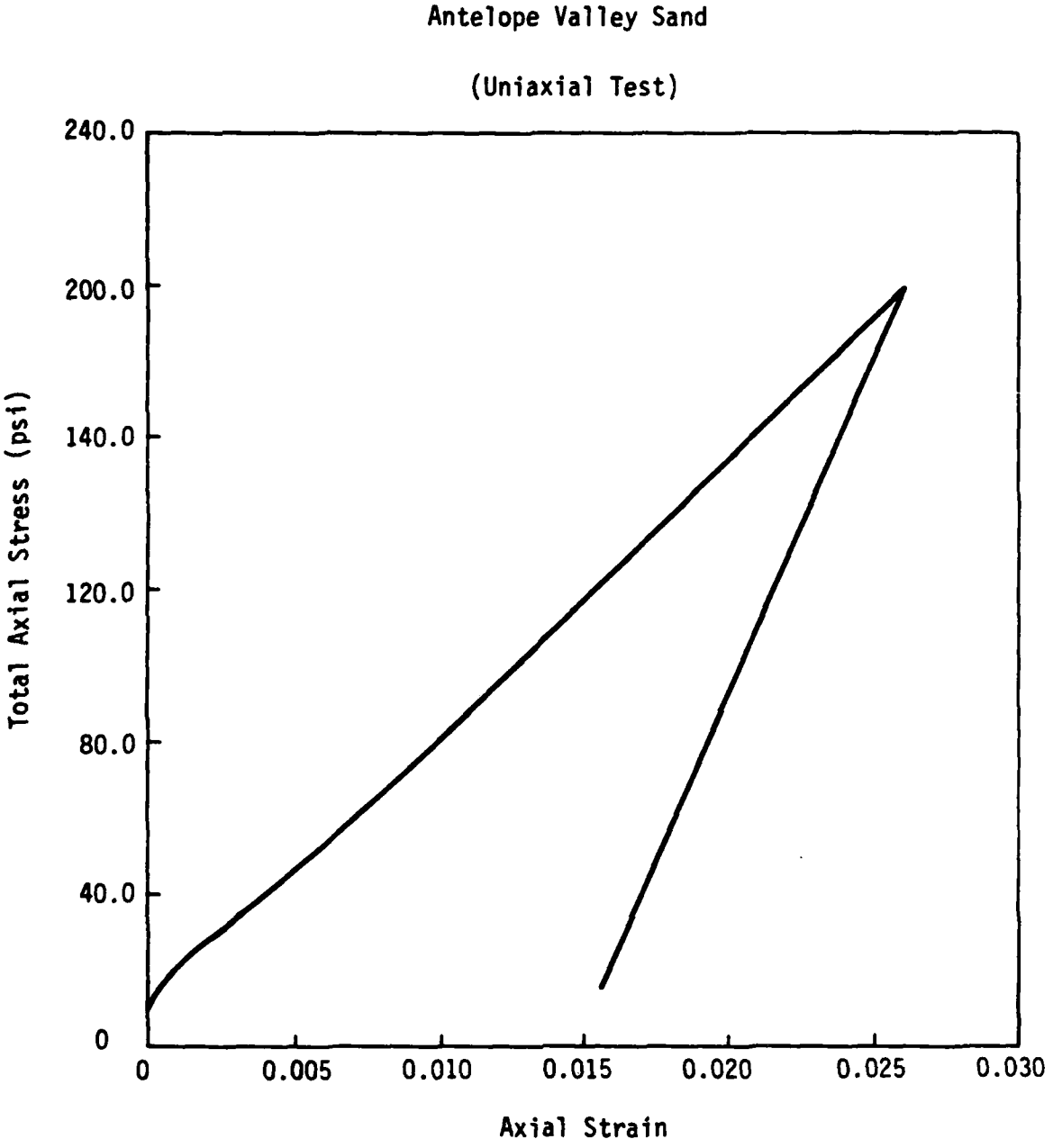

Figure 4.8. Total Axial Stress versus Axial Strain.

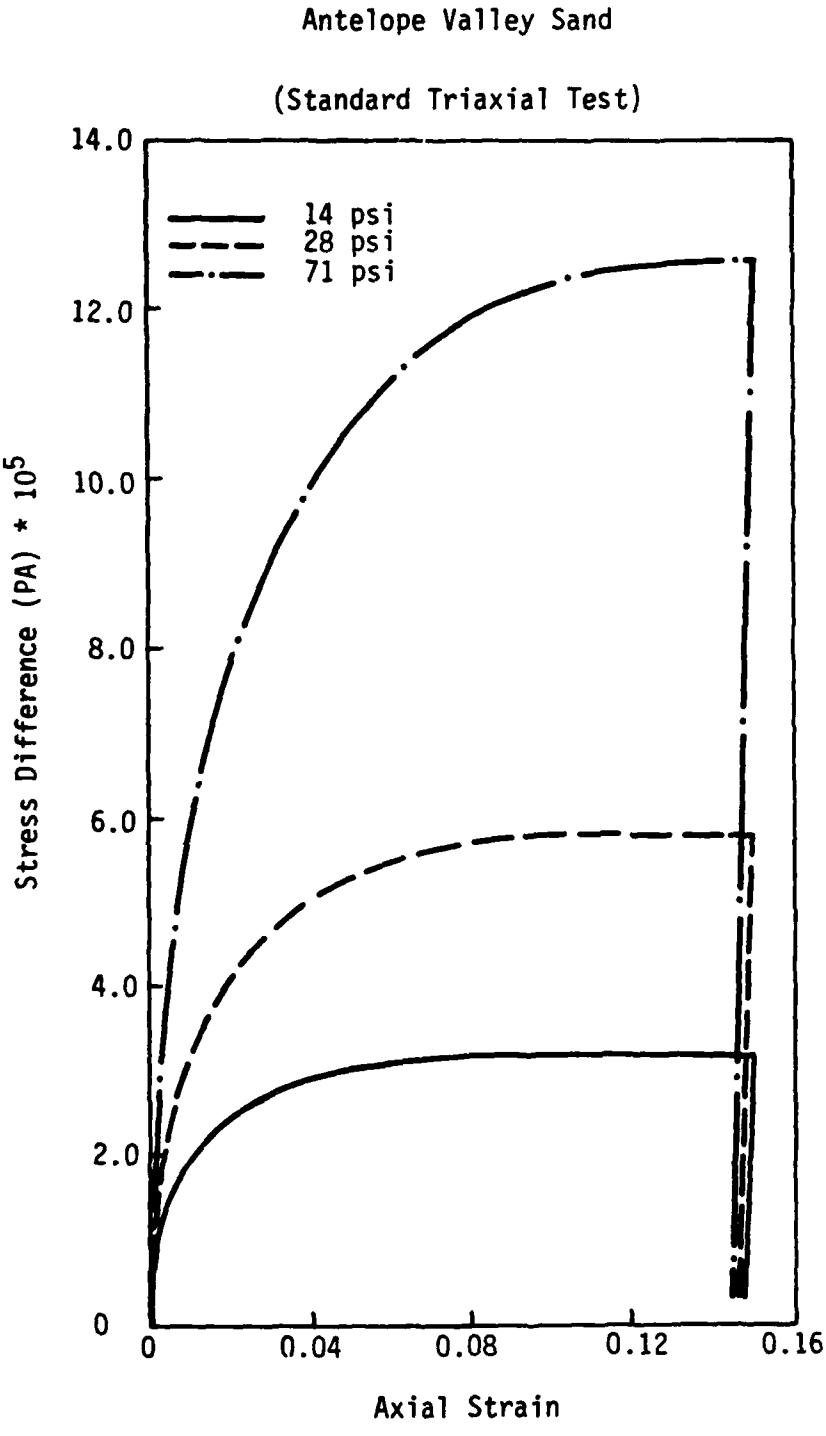

Figure 4.9. Stress Difference versus Axial Strain.

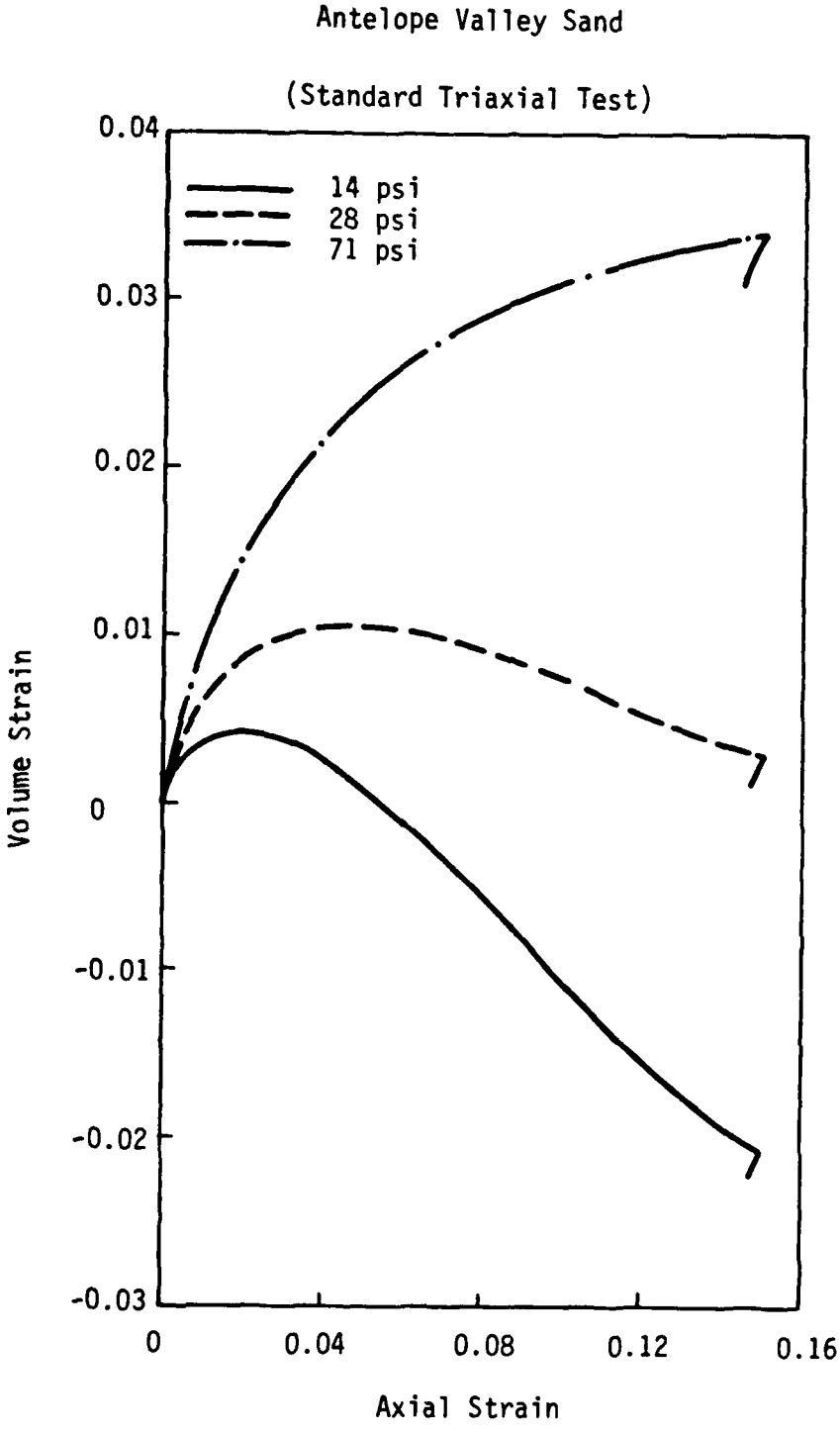

Figure 4.10. Axial Strain versus Volume Strain.

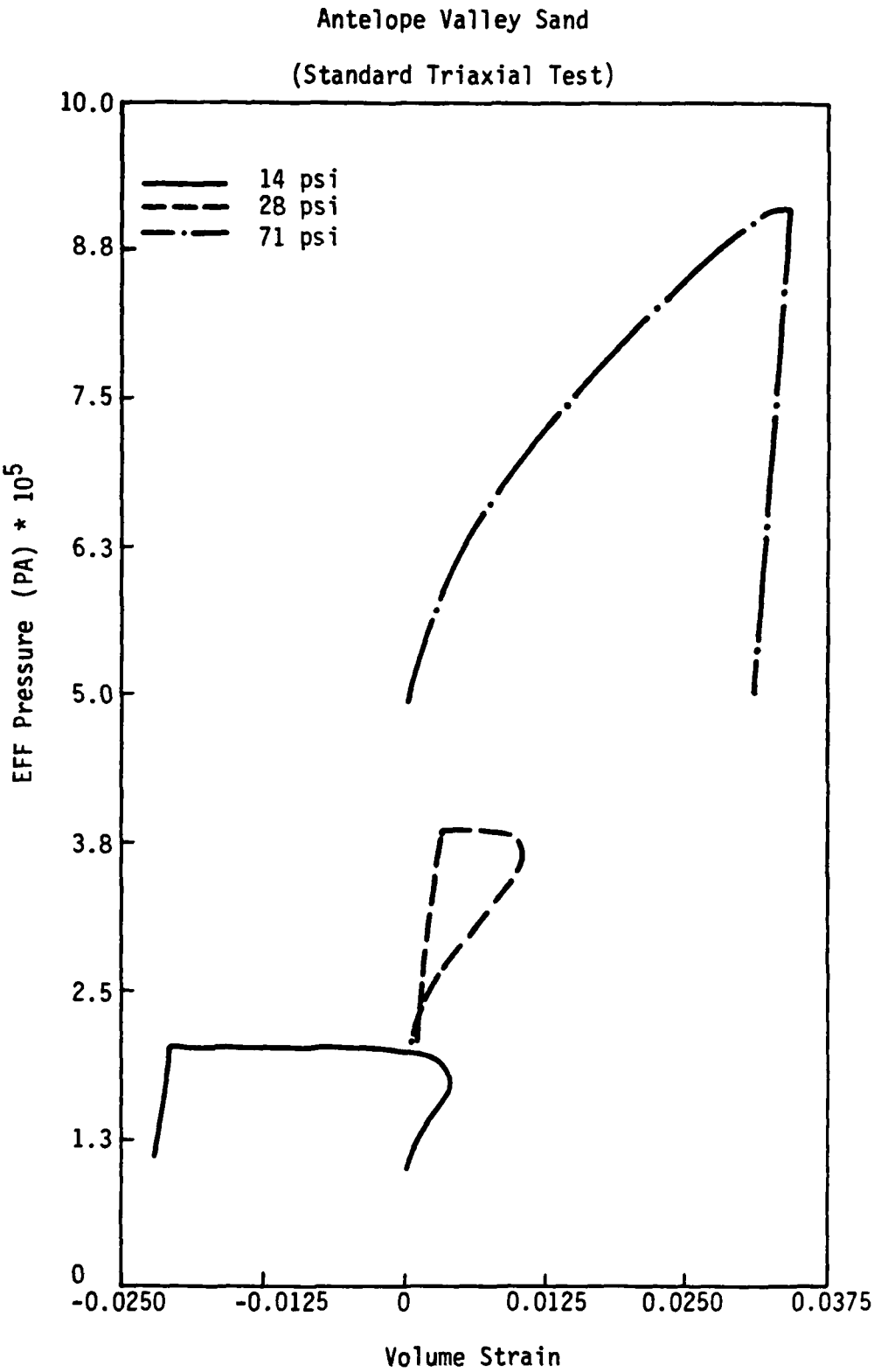

Figure 4.11. Effective Pressure versus Volumetric Strain.

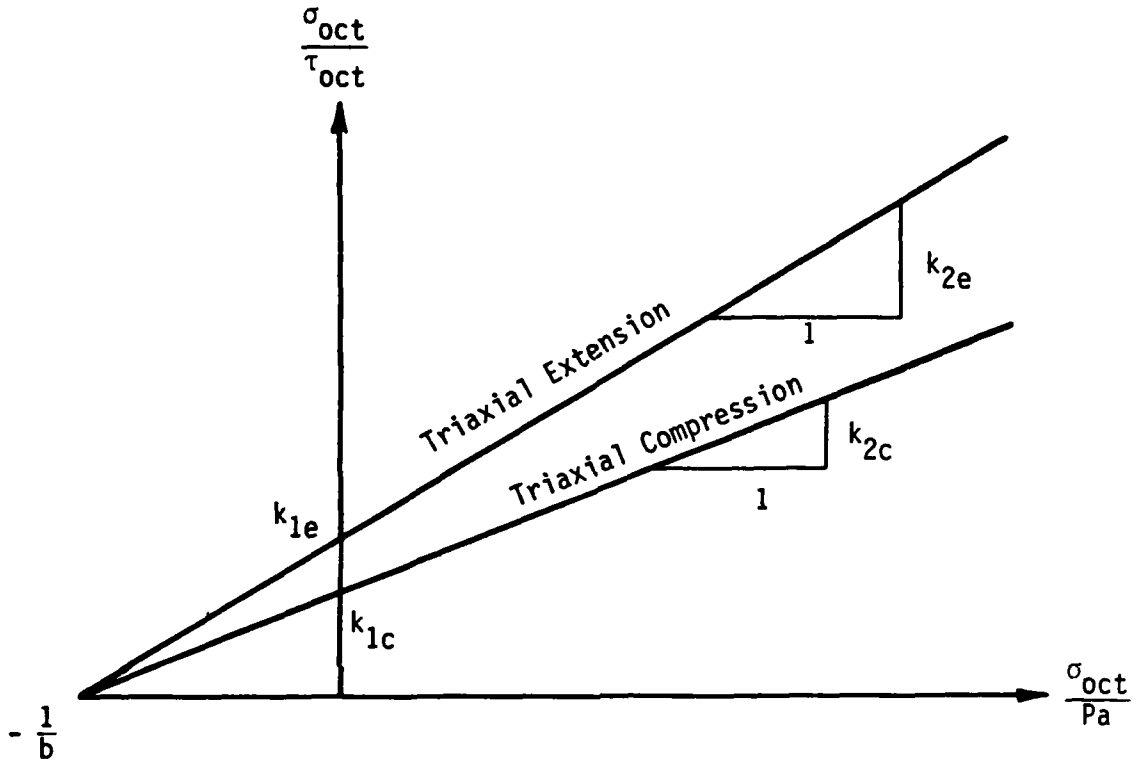

Figure 4.12. Southwell Plots to Determine Yield Criterion Parameters.

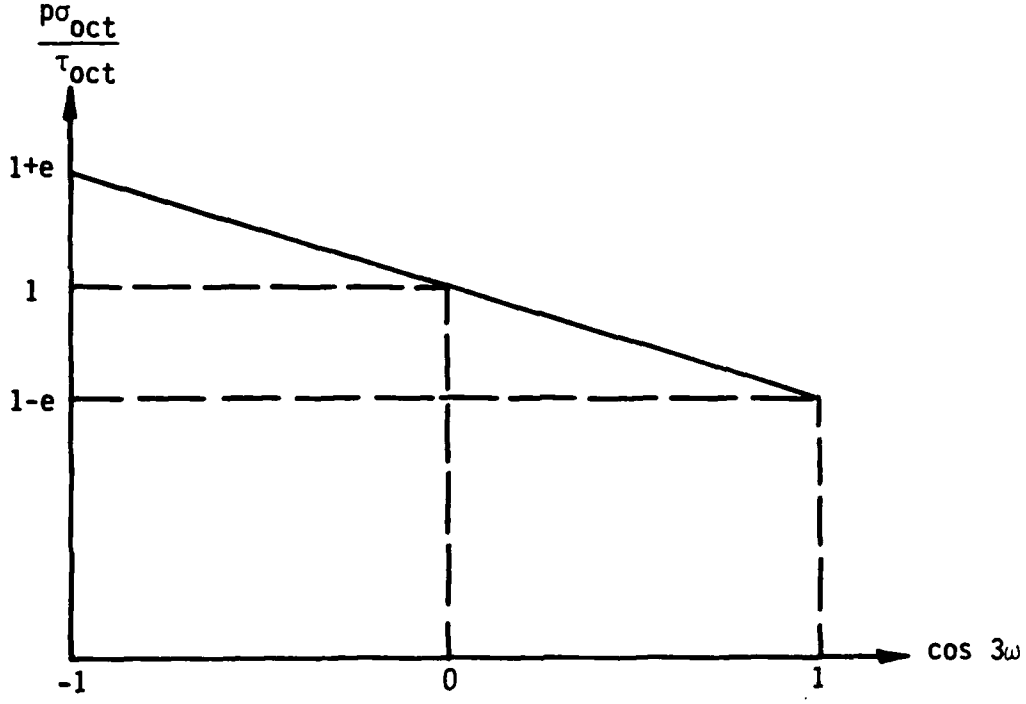

Figure 4.13. Linear Plot for Determining the Octahedral Eccentricity.

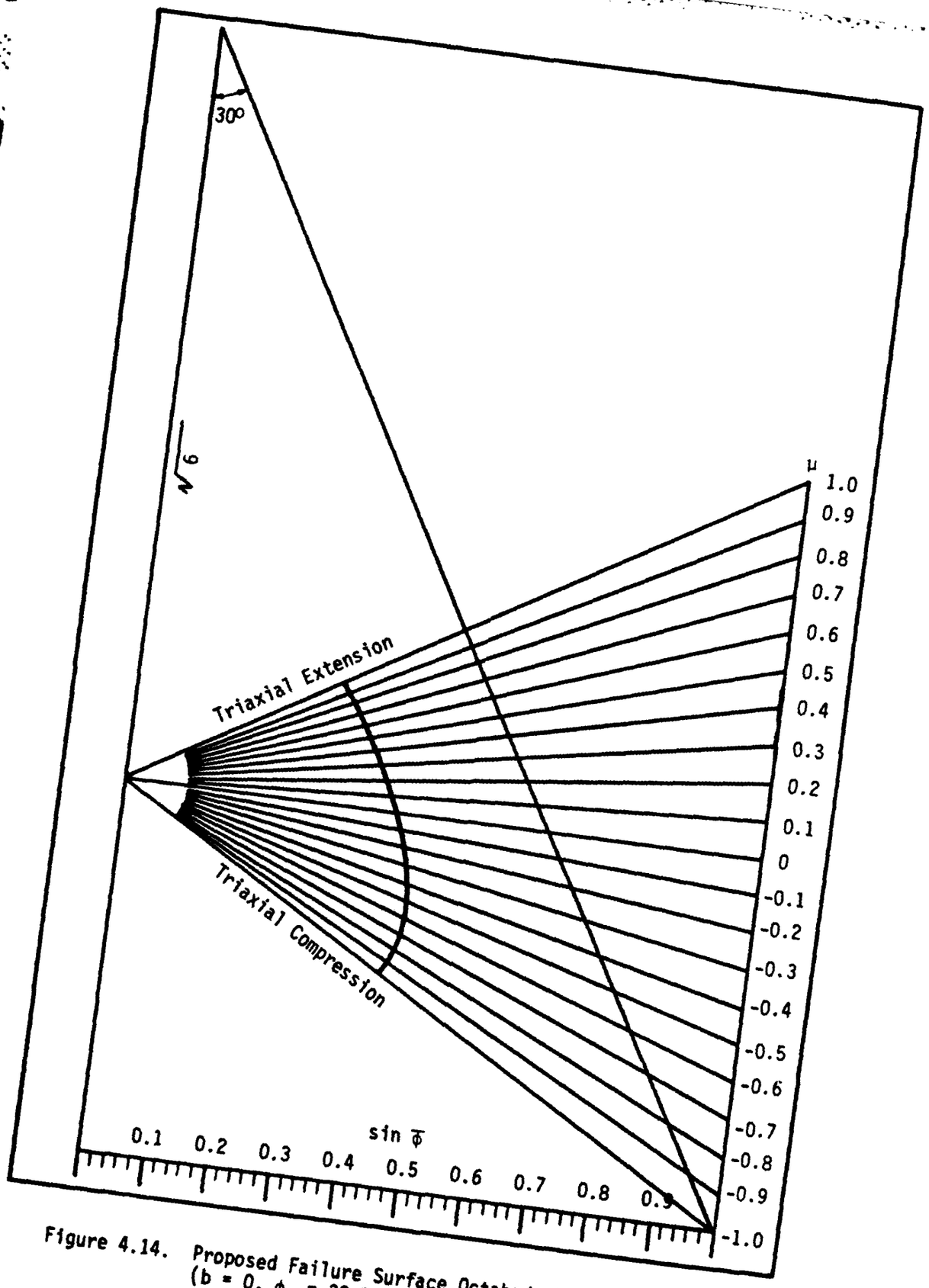

Figure 4.14. Proposed Failure Surface Octahedral Cross-Section for ($b = 0$, $\phi_c = 32$ Degrees; $\phi_e = 35$ Degrees).

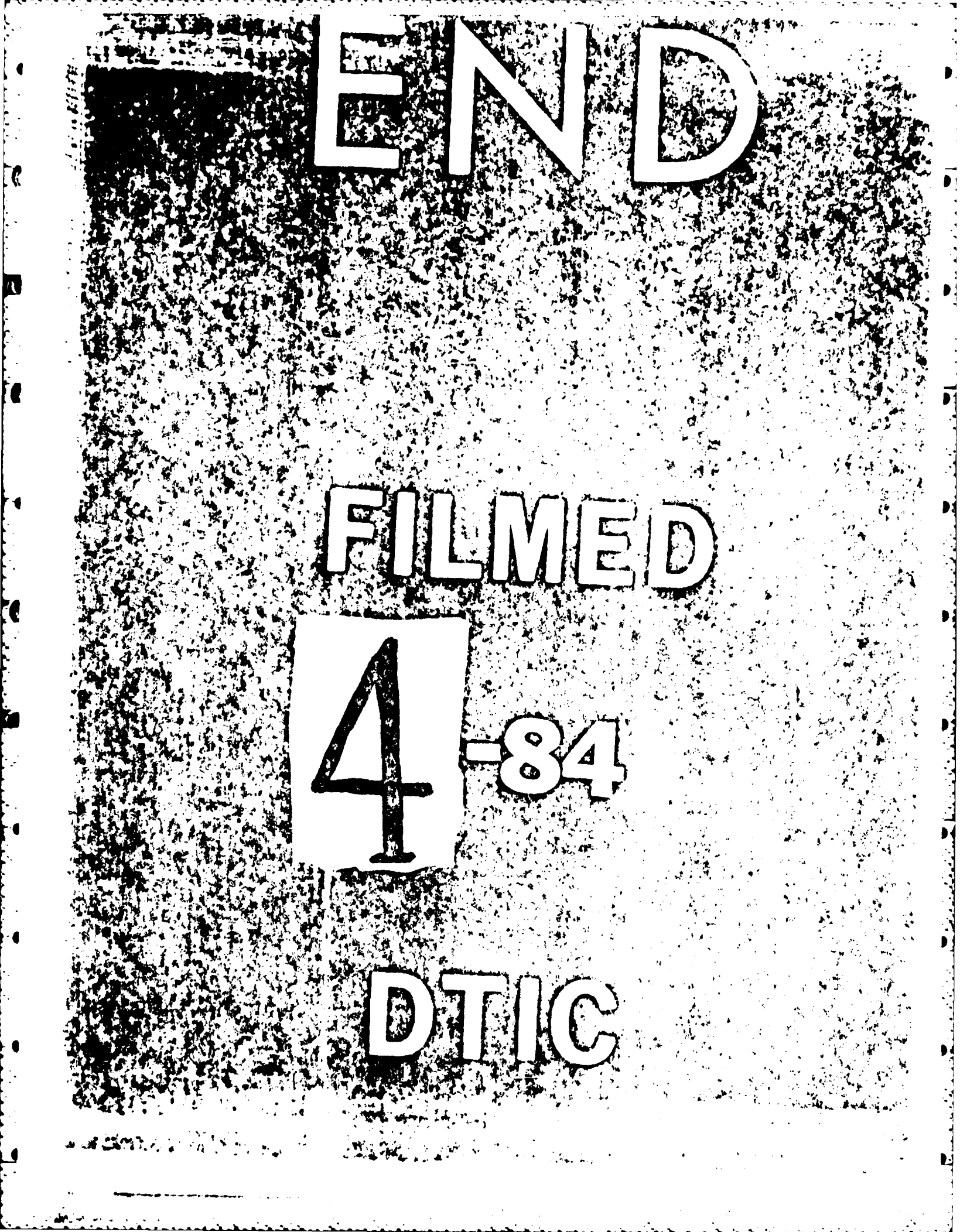
END
FILMED
4-84
DTIC